Cytoskeletal Regulation of Centromere Maintenance and Function in the Mammalian Cell Cycle

Chenshu Liu

Submitted in partial fulfillment of the
requirement for the degree of
Doctor of Philosophy
under the Executive Committee
of the Graduate School of Arts and Sciences

COLUMBIA UNIVERSITY

2016

Abstract

Cytoskeletal Regulation of Centromere Maintenance and Function in the Mammalian Cell Cycle

Chenshu Liu

Equal partitioning of genetic materials of the chromosomes is key to the mitotic cell cycle, as unequal segregation of chromosomes during mitosis leads to aneuploidy, a hall mark of human cancer. Accurate chromosome segregation is directed by the kinetochore, a proteinaceous structure on each sister chromosome that physically connects the chromosome to the spindle microtubules. Kinetochore assembles at the centromere, a specialized chromosome region epigenetically defined by the histone H3 variant centromere protein A (CENP-A) in higher eukaryotes including mammals. In order to maintain centromere identity against CENP-A dilution caused by S phase genome replication, new CENP-A molecules are loaded at preexisting centromeres in G1 phase of the cell cycle. Despite of the several important stages and molecular components identified in CENP-A replenishment, little is known about how new CENP-A proteins become stably incorporated into centromeric nucleosomes. Here by using quantitative imaging, pulse-chase labeling, mutant analysis, cellular fractionation and computational simulations, I have identified the cytoskeleton protein diaphanous formin mDia2 to be essential for the essential for the stable incorporation of newly synthesized CENP-A at the centromere. The novel function of mDia2 depends on its nuclear localization and its actin nucleation activity. Furthermore, mDia2 functions downstream of a small GTPase molecular switch during CENP-A loading, and is responsible for the formation of dynamic and short actin filaments observed in early G1 nuclei. Importantly, the maintenance of centromeric CENP-A levels requires a pool of

polymerizable actin inside the nucleus. Single particle tracking and quantitative analysis revealed that centromere movement in early G1 nuclei is relatively confined over the time scale of initial CENP-A loading, and the subdiffusive behavior was significantly altered upon mDia2 knockdown. Finally, knocking down mDia2 results in prolonged centromere association of Holliday junction recognition protein (HJURP), a chaperone required to undergo timely turnover to allow for new CENP-A loading at the centromere. Our findings suggest that diaphanous formin mDia2 forms a link between the upstream small GTPase signaling and the downstream confined viscoelastic nuclear environment, and therefore regulates the stable assembly of new CENP-A containing nucleosomes to mark centromeres' epigenetic identity (Chapter 2 and 3).

While centromere identity is essential for kinetochore assembly, once kinetochores are assembled, fine-tuned interactions between kinetochores and microtubules become important for a fully functioning mitotic spindle during chromosome segregation. It has been previously found that another diaphanous formin protein mDia3 and its interaction with EB1, a microtubule plus-end tracking protein, are essential for accurate chromosome segregation[1]. In Chapter 4 of this thesis, I found that knocking down mDia3 caused a compositional change at the microtubule plus-end attached to the kinetochores, marked by a loss of EB1 and a gain of CLIP-170 and the dynein light chain protein Tctex-1. Interestingly, this compositional change does not affect the release of cytoplasmic dynein from aligned kinetochores, suggesting a population of Tctex-1 can be recruited to the kinetochores without dynein. During mitosis, Tctex-1 associates with unattached kinetochores and is required for accurate chromosome segregation. Tctex-1 knockdown in cells does not affect the localization and function of dynein at the kinetochore, but produces a prolonged mitotic arrest with a few misaligned chromosomes, which are subsequently

missegregated during anaphase. This function is independent of Tctex-1's association with dynein. The kinetochore localization of Tctex-1 is independent of the ZW10-dynein pathway, but requires the Ndc80 complex. Thus, our findings reveal a dynein independent role of Tctex-1 at the kinetochore to enhance the stability of kinetochore-microtubule attachment.

Together, these work suggest novel regulatory roles of the cytoskeletal systems in the maintenance as well as subsequent functions of the centromere/kinetochore, and provide mechanistic insights into the complex control principles of accurate chromosome segregation. Our findings provide a new model in understanding the epigenetic maintenance of genome integrity, and will have implications with regard to how aberrant cell divisions underlying aneuploidy can be targeted in the treatment of cancer.

Table of Contents

List of Figures

List of Tables

Acknowledgements

First and foremost, I'd like to thank my mentor Dr. Yinghui Mao for his advice and support throughout my years in graduate school. I am truly grateful to the opportunity to have my doctorate training under Dr. Mao's mentorship. My thesis work would have not been possible without the unconditional support and enlightening inputs from Dr. Mao. As a truly great mentor, Dr. Mao has provided me with rigorous training in constructive criticism and synthetic creativity of science, from which I will benefit for my entire career. I'd also like to thank all members of the Mao Lab at Columbia University, past and present, for creating a collegial and stimulating environment where great science can be done. I'd like to thank in particular Sana Ahmad, Christine Kim and Dr. Yige Guo for their outstanding management skills in running the lab; I'd also like to thank fellow graduate student Carmen Taveras for the many productive intra-laboratory collaborations, which had often paved the way for new findings against technical hurdles.

At Columbia, I feel extremely fortunate to have an extraordinary thesis committee throughout my graduate studies. I'd like to thank Drs. Gregg Gundersen, Richard Vallee, Fred Chang and Julie Canman for sharing their expertise and the many insightful discussions we had on particular projects as well as over the spectrum of quantitative cell biology. I am most grateful to the time and efforts each of my committee members has generously contributed in training a young scientist. I am also grateful to the technical inputs and equipment from within the Department of Pathology and Cell Biology at Columbia, especially from the labs of Dr. Gregg Gundersen, Dr. Richard Vallee and Dr. Francesca Bartolini. I'd also like to thank the Integrated Graduate Program at Columbia for having my back over the course of a tenacious graduate career, in particular Dr. Ron Liem and Ms. Zaia Sivo for a wealth of advices on science, career and

beyond; and the present and past co-directors of the program – Drs. Donna Farber, Lori Sussel and Lorraine Symington for the leadership steering a truly exceptional Ph.D. program.

Outside Columbia, I'd like to thank the many collaborators and colleagues who have generously provided important inputs and reagents over the course of my studies – Drs. Ching-Hwa Sung (Weill Cornell), Paul Maddox (UNC-Chapel Hill), Dan Foltz (Northwestern), Dyche Mullins (UCSF), David Odde (U Minnesota), Abby Dernburg (UC Berkeley/HHMI), Jennifer Lippincott-Schwartz (NIH/HHMI), and the late Michael Davidson (National High Magnetic Field Laboratory). I'd also like to thank the training I received from the Physiology Course in 2013 at Woods Hole, MA, and the American Society for Cell Biology for career development opportunities.

Finally, I'd like to thank my family and friends, especially my parents Profs. Ling Xu and Changling Liu who helped ignited my passion for natural science at a very young age and have been a continuing source of encouragement over the years. I am deeply grateful to my beloved wife Ruijun Zhu for the many insightful and enjoyable discussions on science and philosophy, and for being a constant source of inspiration to me. I am also indebted to my friends Yu He (Stanford University) and Yan Wang (Microsoft) for the many fruitful brainstorms on methodologies and for sharing their perspectives in physical and computational sciences. My current understanding of the biological systems would not have been possible without the enduring support from my family and friends.

Chenshu Liu

Manhattan, New York

August 2016

Chapter One *: Introduction to the centromere/kinetochore biology and the cytoskeleton system

*Some contents in this chapter are from the following articles:

Formin-mediated epigenetic maintenance of centromere identity
Liu, C., and Mao, Y. *Small GTPases,* 2016 Jul 22:0. [Epub ahead of print];

Meeting report - New York symposium on quantitative biology of the cell
Liu, C., Taveras, C., Kulukian, A., Ma, R., Ezratty, E., and Mao, Y. *Journal of Cell Science*, 129:1525-1529 (2016)

where the author of this thesis are the first authors.

Introduction

For every cellular life form on earth, one of the most conspicuous phenomena is the ability to go through mitotic cell division cycles in order to proliferate. In mammals, the mitotic cell cycle is an essential constituent of the homeostasis of any proliferative tissue. Key to the mitotic cell cycle is the equal partitioning of genetic information stored in the chromosomes every time the cell divides. Errors in this process could cause aneuploidy, a condition where daughter cells inherit incorrect numbers of chromosomes after mitosis and thus a hallmark of early developmental defects and malignant tumor progression[2].

During the cell cycle, accurate and equal chromosome segregation relies on the highly regulated spatiotemporal dynamics of the chromosomes and their interaction with the cytoskeletal systems. These interactions include the proper interactions between chromosomes and the spindle microtubules at the kinetochores. The kinetochore, a proteinaceous complex assembled at the centromere region of each mitotic chromosome, functions as the sites for microtubule plus end attachment and powers chromosome movement essential for their equal segregation. Because kinetochores are dynamic structures that go through assembly/disassembly in every cell cycle[3], it is important for each kinetochore to remember where assembly occurs on the chromosome every time the cell divides. The centromeric chromatin (the centromere) serves as the landmark for kinetochore assembly, and based on this specialized chromosomal region a functional kinetochore can be built at the right location over many rounds of cell divisions. Instead of the underlying DNA sequences, mammalian centromeric chromatin are determined epigenetically by nucleosomes containing the histone H3 variant centromere protein A (CENP-A). Due to CENP-A dilution as DNA replicates in S-phase, newly synthesized CENP-A proteins

are deposited during early G1-phase of each cell cycle at preexisting centromeres to maintain their identities[4]. A number of molecular pathways required for CENP-A deposition have been identified, however, the stable incorporation of new CENP-A at centromeres and the relationships between multiple pathways underlying different phases of CENP-A loading, remain poorly understood.

In this chapter, I will review the field of centromere/kinetochore biology, with a special focus on the epigenetic determination of centromere identity, as well as the highly regulated kinetochore-microtubule attachment essential for chromosome segregation. I will also give a brief overview on the major cytoskeleton systems that play critical roles in both interphase and mitosis, in order to ensure proper centromere/kinetochore functions underlying accurate chromosome segregation.

The kinetochore and the centromere in dividing cells: an overview

Mitosis starts with the characteristic changes of chromatin/chromosomes in shape and position: prior to nuclear envelop breaks down in prophase, the replicated chromatin fibers condense into chromosomes that is optically resolvable, the condensed chromosomes then move toward the center of the cell in prometaphase, and join each other in collectively forming the metaphase plate. Each sister chromatid is then separated and segregated toward the opposite poles of the mother cell during anaphase, and ultimately end up in each of the two daughter cells in telophase when cytokinesis completes[5,6]. It was first observed and described by Walther Flemming in the late nineteenth century that the condensed chromosomes in mitosis connect to

the spindle fibers (now known as spindle microtubules) at well-defined sites on the chromosomes[7]. These attachment sites on the chromosomes were later coined as 'centromeres' by Cyril Darlington in 1936[5], a term now commonly used when referring to the specialized chromosomal region that joins two sister chromatids of a chromosome, upon which complex protein assemblies are built to attach to spindle microtubules. With early cytogenetics studies where individual metaphase chromosomes spread were stained, centromeres are visibly the 'constriction' sites on a typical, 'X' shaped metaphase chromosome[8]. Being a marker for geneticists in analyzing relative positions of genetic loci along each chromosome[9], the centromere itself remained a challenging problem regarding its form and function for almost a century until a better definition of kinetochore structure was available in the 1960s.

Through thin-section transmission electron microscopy, it has been shown that kinetochores in vertebrate cells assume a trilaminar structure [10-13] – the inner kinetochore, the central kinetochore and the outer kinetochore (**Figure 1.1**). The inner kinetochore makes direct contact with centromeric chromatin, while the 50-60 nm thick outer kinetochore directly attaches to the plus ends of spindle microtubules. The central kinetochore is defined as the region between the dense inner and outer layers. Expansion of the outer layer can be observed under conditions spindle microtubule is depolymerized and is called fibrous corona[3,14]. Across different species, there are two major types of kinetochores determined by the distribution of underlying centromeric chromatin – holocentric and monocentric. Holocentric organisms such as *Caenorhabditis elegans* have diffuse centromeres scattered along the length of the chromosomes[15], whereas monocentric organisms such as yeasts, flies and mammals have one concentrated centromere at one location of a chromosome. Within monocentric organisms, the

budding yeast *Saccharomyces cerevisiae* has only one centromric mark (see next section on centromere for more details) per centromere instead of multiple marks clustered regionally, thus is called 'point' centric organism[16]. Despite the vast diversity of centromere/kinetochore distribution along the chromosomes, the hierarchical configuration of the kinetochore along its inner layer to outer layer axis is more or less similar across species[17,18]. Decades of work have generated a map of molecular architecture as well as assembly hierarchy along the kinetochore's inner-outer axis. For instance, the centromere protein A (CENP-A) assembles into nucleosomes at inner centromere region contacting the inner kinetochore layer; CENP-B, CENP-I, CENP-T and other members of the 'constitutive centromere-associated network' (CCAN) associate with CENP-A nucleosomes and resides from the inner centromere to the inner kinetochore. Motor proteins like cytoplasmic dynein, CENP-E, microtubule associating proteins like the Ndc80 complex, and checkpoint proteins like Bub1, on the other hand distribute in the outer layer of the kinetochore[17]. Recent advances in super resolution microscopy and computer algorithms that can generate localization accuracy at sub-pixel resolution continues to increase the precision of each centromere/kinetochore component's relative position[19]. Interestingly, although physically inner layer components of centromere/kinetochore resides at the basis or outer layer components and suggests linear recruitment(s), the hierarchical relationships during kinetochore assembly (especially at outer kinetochore) could be more complex with feedbacks and cross talks[3]. Nonetheless, it has been widely accepted that inner centromere lays the foundation of kinetochore assembly thus brings up an outstanding question for the whole field: how is centromere determined in the first place?

Centromere determination and centromere protein A (CENP-A)

As a chromosomal region, the centromere is composed of DNA and DNA-binding proteins like histones. A simple minded way to explain centromere determination could be using defined primary DNA sequences to which proteins bind. However, in the vast majority of eukaryotes DNA sequences responsible for nucleating centromeres are not found[13]. In fact, except in the case of the budding yeast *Saccharomyces cerevisiae*, where a precise 125bp-long DNA sequence is both necessary and sufficient for the determination of its point-centromere[20-22], all other organisms from the fission yeast to human, centromere DNA sequences diverge greatly in length (fission yeast ~10kb, fruit fly ~100kb, human ~1Mb), and exhibit no discernable conservation across evolution or even among different chromosomes within the same species[23]. Repetitive sequences (tandem arrays of 'satellite DNA') are commonly found in the DNA sequences underlying centromeres in these organisms, however they are neither necessary nor sufficient for centromere determination. On one hand, 'acquired' functional centromere ('neocentromeres') has been found on certain rearranged chromosomes in the absence of typical centromeric DNA sequences[24]. On the other hand, DNA sequences alone cannot drive the formation of centromeres, evidenced by the well preserved centromere DNA sequences in stable dicentric chromosomes where one centromere is silenced[25]. In contrast to the lack of genetic conservation with regard to DNA-sequences underlying the centromere region, an obvious common theme among the vast majority of eukaryote is the presence of a particular protein at the centromere, the centromere protein A (CENP-A or CENH3).

CENP-A was initially identified by William Earnshaw in 1986 as one of three human chromosomal autoantigens (CENP-A, B, C) using autoimmune sera from scleroderma-spectrum

disease patients[26,27]. Soon afterwards, this 17 kDa protein was shown to copurify with nucleosome core particles including histones, and exhibits histone-like properties as well as distinctive features not related to histone H3 or any other histones[28,29]. CENP-A is a relatively conserved protein used by the vast majority of eukaryotes for centromere determination (including *Schizosaccharomyces pombe*, *Saccharomyces cerevisiae*, *Caenorhabditis elegans*, *Drosophila*, *Xenopus* and *Homo sapiens*[30-32], with the exception of certain species with holocentric chromosomes such as insects in the order *Lepidoptera*[33]), despite of the differences in holocentricity and monocentricity (**Figure 1.2**). Based on the work from multiple groups over the last decade, we now understand that CENP-A is essential for centromere's epigenetic determination and function, in particular the assembly of a functional kinetochore. Depletion of CENP-A in *C.elegans* single cell embryos and human somatic cells both lead to extensive loss of most kinetochore proteins and result in massive chromosome misalignment and missegregation[34,35]. On the other hand, ectopic targeting of clustered CENP-A proteins at chromosome arms using the LacI-LacO systems in both drosophila and human cells demonstrated that regionally concentrated CENP-A is sufficient to drive functional kinetochore assembly, judging by their ability to recruit key centromere/kinetochore components including CENP-C and Ndc80, as well as their ability to attach to spindle microtubules during chromosome segregation[36-38]. Biochemistry and structural biology revealed that CENP-A is a histone H3 variant that specifically participate in the formation of nucleosomes at the centromere region of the chromosomes[13,39]. CENP-A nucleosomes are interspersed with the H3 nucleosomes at the centromere, as revealed with extended chromatin fibers[40]. While H3 nucleosomes can be found in both centromere and non-centromere regions of the chromosome, CENP-A nucleosomes can largely only be found at the centromeres. Similar to canonical histone H3,

CENP-A forms a heterotetramer when co-expressed with the native binding partner histone H4. Despite of the identical stoichiometry of $(CENP\text{-}A:H4)_2$ compared to $(H3:H4)_2$ in the subnucleosomal heterotetramer, CENP-A dramatically differs from H3 in that the interface between CENP-A and H4 is mover 10 fold more rigid than that between H3 and H4, evidenced by a substantially reduced hydrogen/deuterium exchange rate primarily in the α2 region of CENP-A compared to H3 when in complex with H4[41]. Through this unique conformational feature of the nucleosome, CENP-A possibly confers the epigenetic mark to direct centromere/kinetochore assembly.

Recently work in molecular counting have revealed that in human somatic cells, there are about 400 copies of CENP-A molecules (200 CENP-A containing nucleosomes) per centromere at steady state. This number indicates that 1 in 25 nucleosomes at the centromere region is CENP-A containing nucleosome, and the mark of CENP-A at centromere is approximately 50 times enriched compared to the genome in general on the chromosomes[42]. However, as long as there is a finite number of molecules residing at a chromosome locus, serial dilution will occur when that chromosomal locus undergoes continuous rounds of DNA replication in a proliferating cell. Starting with a fixed number of CENP-A molecules per centromere, if the dilution continues to happen, in only 10 rounds of cell divisions the number of CENP-A molecules per centromere will be less than 1 (**Figure 1.3**). Therefore an obvious question is: as a marker molecular that maintains centromere identity, how does CENP-A maintain its own levels at the centromere?

It turns out the cell addresses this problem by replenishing the CENP-A levels per centromeres in every cell cycle. Unlike its canonical counterpart histone H3 which is replenished during DNA replication in S-phase[6], CENP-A loading is uncoupled from DNA replication. Pulse-chase analysis using a cell line stably expressing SNAP tagged CENP-A was able to differentiate the existing copies of 'old' CENP-A at the centromere and the newly synthesized CENP-A molecules, by fluorescently label either the 'old' or the 'new' CENP-A pools with cell permeable fluorescent dye (tetramethylrhodamine for instance). Using this approach, new CENP-A was observed to be loaded onto the centromere after mitosis, during early G1-phase of the cell cycle in mammals[4]. Fluorescent recovery after photobleaching (FRAP) experiments confirmed the time window for loading in early G1, using Drosophila syncytial embryos as well as human cultured cells[43,44]. Over the years, many molecular components constituting the CENP-A loading machineries during G1-phase have been identified through biochemical affinity purifications and cell biology approaches[35,45-50]. Throughout the cell cycle, CENP-A containing nucleosomes at the centromere is redistributed half to half from one centromeric chromatin to two sister chromatids' centromeres after centromeric DNA replication (**Figure 1.4**). The gaps left by the 50% loss of CENP-A nucleosomes per centromere is shown to be temporarily filled up by H3.3 containing nucleosomes as a 'placeholder'[51]. As cell cycle progresses through G2 phase and into mitosis, the two sister chromatids' centromeres are finally segregated into two daughter cells, each containing 50% of the CENP-A levels compared to the unreplicated centromere in the mother cell. Upon mitotic exit, the down regulation of CDK1/CDK2 activity (an inhibitory signal to CENP-A loading machinery) together with Polo kinase 1 (Plk1, a positive 'licensing' signal required to initiate CENP-A loading) being recruited to the centromeres, allows the whole CENP-A loading program to start[52,53]. Upon the cell enters early

G1, the Mis18 complex (composed of Mis18α, Mis18β, and Mis18BP1/KNL2) forms a complex at the 'old' CENP-A labeled centromere[46,53-55], in order to recruit the deposition of newly synthesized CENP-A bound to its specific chaperone Holliday Junction Recognition Protein (HJURP) in a prenucleosomal complex[47,48]. After new CENP-A:HJURP is recruited to the centromere, HJURP utilizes its nucleosome assembly activity to assemble CENP-A into the nucleosomes underlying the centromeres[36,47,48]. Notably, such process of CENP-A loading is actively initiated and can be allowed to happen only at the right time per cell cycle. Therefore, when CENP-A levels are restored at each centromere and the cells go through genome replication to finally reach the next G2/M-phase, the upregulation of CDK1/CDK2 activity will inhibit the assembly of Mis18 complex at the centromere and thus prevent precocious loading of CENP-A in mitosis[52].

Emerging mechanisms contributing to the stable maintenance of centromere identity

Apart from the well-studied process of licensed CENP-A loading, recent findings in the field suggest additional signals and pathways essential for the stable incorporation and maintenance of CENP-A levels at the centromeres inside G1 cell nuclei.

(1) A Rho family small GTPase molecular switch is required for new CENP-A incorporation at centromeres

Rho family small GTPase proteins along with their cognate guanine nucleotide exchange factors (GEFs) and GTPase activating proteins (GAPs) participate in the signaling regulation of membrane and cytoskeleton dynamics[56,57]. Recent studies have suggested nuclear functions of the Rho family small GTPase signaling. Net1, a RhoA specific GEF, and active RhoA have been

found inside the nucleus[58]. Nuclear pool of RhoA is specifically activated in a Net1-dependent manner upon ionizing radiation (IR)[58]. Loss of Ect2 and Net1 has been shown to suppress RhoB activation upon IR-induced DNA damage[59]. Rac1, another Rho family small GTPase protein, has a functional nuclear localization signal (NLS) for nuclear import mediated by karyopherin α2 and is associated with numerous nuclear proteins[60]. Interestingly, recent work demonstrated that nuclear RhoA activity is a function of mechanochemical inputs to the nucleus, as magnetic force applied to nesprin-1 activates RhoA in isolated nuclei[61].

Leptomycin B (LMB) treatment results in a nuclear accumulation of the GTPase activating protein MgcRacGAP concurrent with a decrease in the cytoplasm[62]. The guanine exchange factor Ect2 contains a NLS and is preferentially localized to the nucleus at steady state[63]. Mass spectrometry based proteomics identified MgcRacGAP as a component of the complex associated with Mis18BP1/KNL2, a key player in the licensing step of the CENP-A loading machinery[35,36,46,54,55]. Fluorescently tagged MgcRacGAP exhibits dynamic centromere localization half-way into G1-phase. Knocking down either MgcRacGAP or Ect2 for one cell cycle reduces the total CENP-A levels at the centromere by half, which is consistent with a defect in CENP-A replenishment[64]. As both Ect2 and MgcRacGAP are required for cytokinesis[65], the fact that binuclear cells from failed cytokinesis (following Cytochalasin D or Latrunculin A treatment) have ordinary CENP-A levels suggest that failed cytokinesis itself is not the reason for defective CENP-A replenishment. Importantly, the fact that depleting either MgcRacGAP or Ect2 results in the same CENP-A phenotype suggests defective small GTPase cycling, rather than either protein per se, is the reason underlying CENP-A reduction. Furthermore, depleting Cdc42 or Rac1, but not RhoA, results in a similar phenotype as MgcRacGAP or ECT2 depletion, indicating that

Cdc42 and/or Rac1 are the small GTPases involved in new CENP-A loading/maintenance[64]. Thus, it is proposed that a molecular switch of Rho family small GTPase is essential in regulating epigenetic centromere maintenance by stabilizing newly loaded CENP-A[64]. However, because neither CENP-A nor histone proteins have been shown to be direct effectors downstream of the small GTPase signaling pathways, it remains a unknown what is the molecular effector(s) that connect small GTPase signaling and CENP-A loading. It is difficult to know the functional role for the small GTPase pathway in this process without identifying the downstream effector(s).

(2) Chromatin/chromosome remodeling during CENP-A loading

Apart from MgcRacGAP-dependent small GTPase molecular switch, the stable maintenance of newly loaded CENP-A during the course of G1 phase requires additional chromatin/ chromosome associated proteins. Components of the remodeling and spacing factor (RSF) complex, Rsf-1 and SNF2h are shown to be required for the stable maintenance of CENP-A levels at the centromere upon salt extraction. Rsf-1 exhibits centromere localization in mid-G1, when it also coprecipitates with CENP-A chromatin. In addition, reconstituted and spaced CENP-A nucleosomes can be reconstituted and spaced by puriried RSF complex *in vitro*[49], thus suggests a separate step during G1 CENP-A loading to stably incorporate CENP-A molecules in the centromere chromatin.

RSF complex has ATP-dependent nucleosome remodeling/spacing activity and favors the transcription initiation of chromatin in vitro[49]. Several other chromatin remodeling events linked to active transcription have also been suggested to be important for CENP-A loading. For

instance, recent evidence suggest that while transcriptionally permissive marks such as H3K4me2 or H3K9 acetylation can promote CENP-A maintenance, while elevated levels of heterochromatin (transcriptionally nonpermissive) formation at α–satellite DNA inhibits CENP-A maintenance[66-68]. RNA transcript including long noncoding RNA transcripts have been shown to be required for CENP-A recruitment at the centromeres[69]. In addition, RNA polymerase II has been found at human mitotic centromeres[70], and disruption of transcription initiation or RNA splicing can lead to defective CENP-A maintenance at the centromeres[69,71]. One possibility underlying the involvement of transcriptionally permissive remodeling event during CENP-A loading is the effective exchange of place holder histone H3.3, although direct test of this hypothesis still remains challenging[51,72].

(3) Other centromere proteins promote the stable maintenance of CENP-A

The fact that centromeres are epigenetically defined by CENP-A does not rule out the possibility that other centromere proteins can affect CENP-A loading and maintenance. The recruitment of licensing factors in early G1 onto existing 'old' CENP-A labeled centromeres has created a classic 'chicken-and-egg' problem. In fact, depletion of several centromere proteins can result in severe loss of CENP-A at the centromere. For instance, KNL2 depletion leads to substantial loss of new CENP-A at the centromere[35], while CENP-C depletion reduces the high stability of incorporated 'old' CENP-A at the centromeres[73]. Meanwhile, it has been recently shown that CENP-B, an alphoid repeats binding protein at inner centromere, directly binds to both CENP-A and CENP-C and is required to stabilize CENP-C levels at the centromere[74]. It should be noted that despite the interdependent relationship between CENP-A, B, C, it is still CENP-A that defines the identity of the centromere. Using an induced knock out system[75], it has

been shown that upon CENP-A depletion most kinetochore/centromere proteins will be quantitatively lost, following the serial dilution of residual CENP-A molecules at the centromere. CENP-C, N, P start to diminish after day 5 of induced depletion, while CENP-T, I and Ndc80 complex only start to diminish after day 7 post induced depletion. Interestingly, CENP-B levels at the centromere only starts to decline after day 9 post induced CENP-A depletion. The differed 'diminishing kinetics' among various centromere proteins and the fact that CENP-B being the last one to leave the centromere in the absence of enough CENP-A suggest that CENP-B might have the highest affinity toward CENP-A and only a few remaining CENP-A molecules are enough to ensure the retention of CENP-B. The conclusion that CENP-A is what defines the centromere while CENP-B is not, is also manifested by the lack of CENP-B yet the presence of CENP-A on Y-chromosome centromeres[42].

Taken together, with multiple lines of evidence of emerging mechanisms that regulate CENP-A incorporation and maintenance, it would be important for the field to evaluate the relative contribution of each of the signaling inputs as well as chromatin/chromosome regulators, and how a coordinated function can be achieved among them during the stable maintenance of CENP-A nucleosomes.

The cytoskeleton systems: actin and microtubules

Mammalian cells achieve most of their motile behaviors (e.g. migration and division) using a network of protein filaments inside the cells – the cytoskeleton systems. In higher eukaryotes including mammals, the cytoskeleton systems are composed of four major categories

– actin filaments, microtubules, intermediate filaments and septins[76-79]. Despite structural and functional differences, common features are shared such as GTP/ATP binding and mechanical work through energy coupling. Serving as structural and signaling hubs during dynamic cellular processes, cytoskeleton filaments usually form a vast network through protein protein interactions either on monomers (the building blocks of the filaments) or polymers (the filaments). For the scope of my thesis here, I will only focus on the actin and microtubule cytoskeletons. Actin filaments are polymerized from globular subunits (G-actin) into a two-stranded helical filaments, the filamentous actin (F-actin)[77]. Microtubules are hollow tubes composed of 13 protofilaments, with each protofilaments polymerized from α/β-tubulin-dimer subunits aligned head-to-tail[79]. G-actin binds to ATP while tubulin monomer binds to GTP. Nucleotide hydrolysis activity of the subunits is coupled to the filamentous assembly/polymerization reaction. Due to the subunit structures and the way they are assembled together, polymerized filaments of both actin and microtubules have intrinsic polarities: F-actin grows on the barbed end (as opposed to the pointed end)[80], while microtubules undergoes most of its dynamic events at the plus end (as opposed to the minus end which usually anchors at MTOC such as centrosomes)[79,81]. Nucleotide hydrolysis accompanied with polymerization reactions can result in 'structural plasticity' – in the case of actin "treadmilling" and for microtubules the "dynamic instability" [82-84]. Despite their important functions during numerous cellular processes, it is not well understood how specific spatial and temporal organization are regulated to provide structural support, to generate force, and to serve as integration hubs for signaling.

Filamentous actin in the nucleus

Actin has well documented functions in the cytoplasm such as filopodia and lamellipodia formation, nuclear movement[85] and cytokinesis[86,87]. The role of the actin cytoskeleton inside the nucleus remain controversial and mysterious. It has been debated more than 40 years about the existence, form and function of actin or actin related proteins inside the cell's nucleus[88]. Despite a body of biochemical evidence of the existence of actin, Arp and myosin found in the nuclear fraction[89,90], much of the earlier controversies stemmed from a lack of reliable reagents to achieve direct visualization of polymeric actin inside somatic cell nuclei[88,91]. Recent years have witnessed a tremendous progress in developing tools that can reliably and specifically probe the size, shape and dynamics of endogenous actin polymers inside somatic cell nuclei (**Table 1.1**)[92-97]. However, the potential functions of nuclear actin are just starting to emerge. Apart from the apparently varied forms and functions reported using different probes under differed conditions, it remains elusive how physiological control is achieved to opt between different nucleation pathways, at different nuclear positions at different time during cell cycle. In addition, it is largely unclear how the physical properties of short actin filaments could participate in the regulation of molecular events inside the nucleus.

Microtubule dynamics and the dynein motor

Like the actin cytoskeleton, it is always curious how the complex behaviors of microtubules are manifested at different scales – how self-assembly/disassembly can happen specifically in response to differed signaling cues, can bias one over the other in nearby cellular compartments, and can come up with organizational diversity as a function of time, such as the thin fiber in interphase while thick bundled kinetochore fibers during mitosis. Kinetochore

microtubules are essential for connecting mitotic chromosomes to the spindle apparatus in order to execute the accurate segregation of the genome. Many microtubule associate proteins (MAPs) are essential for the function of microtubule cytoskeleton, among them is the cytoplasmic dynein complex[98]. Dynein is a multi-component motor protein complex with the core part being dimerized heavy chains including the motor domains that directly walk on the microtubules toward the minus end[99]. The functions of dynein motor complex at the kinetochore has been well studied during mitotic chromosome alignment and segregation[100,101], and have been shown to be essential for force generation and stable kinetochore-microtubule attachment, as well as for the timely removal of spindle assembly checkpoint proteins from bioriented kinetochores[101-107]. However, the exact roles of dynein accessory proteins, including light chains that bind to the heavy chains, during mitosis is less well understood.

During mitosis, many motor and non-motor proteins can localize to the outer layer of kinetochores that in direct contact with microtubule plus ends. Although there is much support for the KMN network (KNL1, Mis12, and Ndc80 complexes) serving as the core microtubule binding apparatus at the kinetochore [108,109], it is quite clear that many other kinetochore- and microtubule-associated proteins play important roles in maintaining the stable connection between kinetochores and dynamic microtubule plus ends. For instance, depletion of the Ska1/RAMA complex [110-113] or a formin mDia3 [114,115] results in chromosome misalignment phenotypes in mammalian cultured cells. Meanwhile, the fact that cells depleted of motor proteins such as dynein or CENP-E still have quite a few chromosomes aligned at the metaphase plate, indicates that force-generating motors are not the only mechanisms underlying chromosome alignment in prometaphase[100,116-120]. Emerging evidence suggest a more complex

interaction network of microtubule plus-end tracking proteins in fine tuning the structural and signaling dynamics at the kinetochore/microtubule interface[121-123]. Therefore it remains an open question how do different molecular-modules coordinate their interactions with microtubule plus-ends in achieving regulated kinetochore-microtubule attachment?

The diaphanous formin proteins

For both actin and microtubule cytoskeleton, initial nucleation is the rate limiting step in filament growth. While microtubule utilize gamma-tubulin and MTOC to help nucleation, actin nucleation depends on upstream signaling (such as small GTPase signaling) activated Arp2/3 complex and formin proteins to nucleate branched and unbranched filaments, respectively[77,124].

Among many formin families, the diaphanous formin family of proteins are well-established regulators of both actin and microtubule dynamics[125,126] and function as effectors of the small GTPase signaling in diverse aspects of the cell cycle. Diaphanous formins assume an auto-inhibited state resulted from an intra-molecular interaction between the DID and DAD domains. Upon small Rho GTPase binding at the N-terminus, the auto-inhibition of mDia formins is released to expose the formin homology domain (FH2) responsible for actin polymerization and microtubule stabilization[124]. A short-version of mDia proteins consisting of formin homology domains without regulatory regions required for auto-inhibition (**Figure 1.5**) is constitutively active even in the absence of small GTPase binding[127].

Three members of the diaphanous formin family, mDia1-3, have conserved domain structures and a similar mode of action but different choices of upstream GTPase signaling pathways[115,127-135] (**Figure 1.5**). While important kinetochore functions have been discovered for

the diaphasnous formin mDia3[1,136], its family member mDia2 is the one that has been shown to shuttle from cytoplasm to nucleoplasm evidenced by nuclear accumulation upon LMB treatment[137] and clear nuclear distribution in early G1 cells (**Figure 1.5**). Notably, mDia2 has been shown to be required for nuclear actin assembly during serum stimulation[94]. Meanwhile, mDia2 has been shown to be the effector of either Rac or Cdc42[130-132], two small GTPases downstream of the MgcRacGAP-based molecular swtich whose depletion results in a centromeric CENP-A reduction phenotype[64]. Based on recent proteomic discoveries of many chromatin-related proteins associated with the FH1FH2 domain of mDia2 but not mDia1 or 3[138], it is intriguing to ask: is mDia2 the effector of the small GTPase signaling pathway that directly acts on stable CENP-A loading/maintenance?

Quantitative approaches in understanding dynamic processes

Recent years have witnessed profound progress in the transition of cell biology toward a more quantitative science. Quantitative imaging has come a long way in generating multidimensional and high throughput datasets that characterize complex cellular behaviors. Despite many measurements, an integrated quantitative understanding often times remains challenging due to intrinsic complexity or technical hurdles against precise measurement (e.g. photo toxicity, masked localization due to protein overexpression, etc.). In addition to quantitative experimental measurements, quantitative modeling of complex biological systems is a powerful tool to bridge our knowledge of microscopic molecular processes with macroscopic observations. Building mathematical models, both deterministic and probabilistic, is not only a key to recapitulate and explain experimental findings, but also a critical step in guiding future experiments by generating testable predictions[139]. In this thesis, I will present a combination of

multiple quantitative approaches in understanding the complex cytoskeletal control of centromere and kinetochore functions during mammalian cell cycle.

Figures

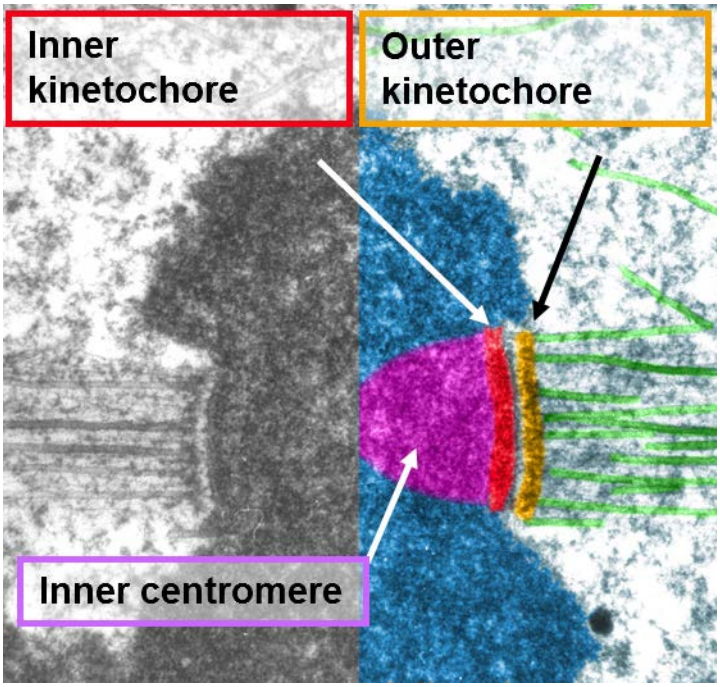

Figure 1.1. The laminar structure of the kinetochore

Adapted from Cleveland, Mao and Sullivan (2003), electron micrograph showing a biorientad mitotic chromosome composed of two sister chromatids, attached by microtubules from two opposite poles. Microtubules (pseudo-colored in green) contact with the outer kinetochore layer (yellow), while the inner kinetochore layer (red) is in a continuum with the inner centromere chromatin (magenta). The non-centromere chromosome for the sister chromatid on the right is pseudo-colored in blue.

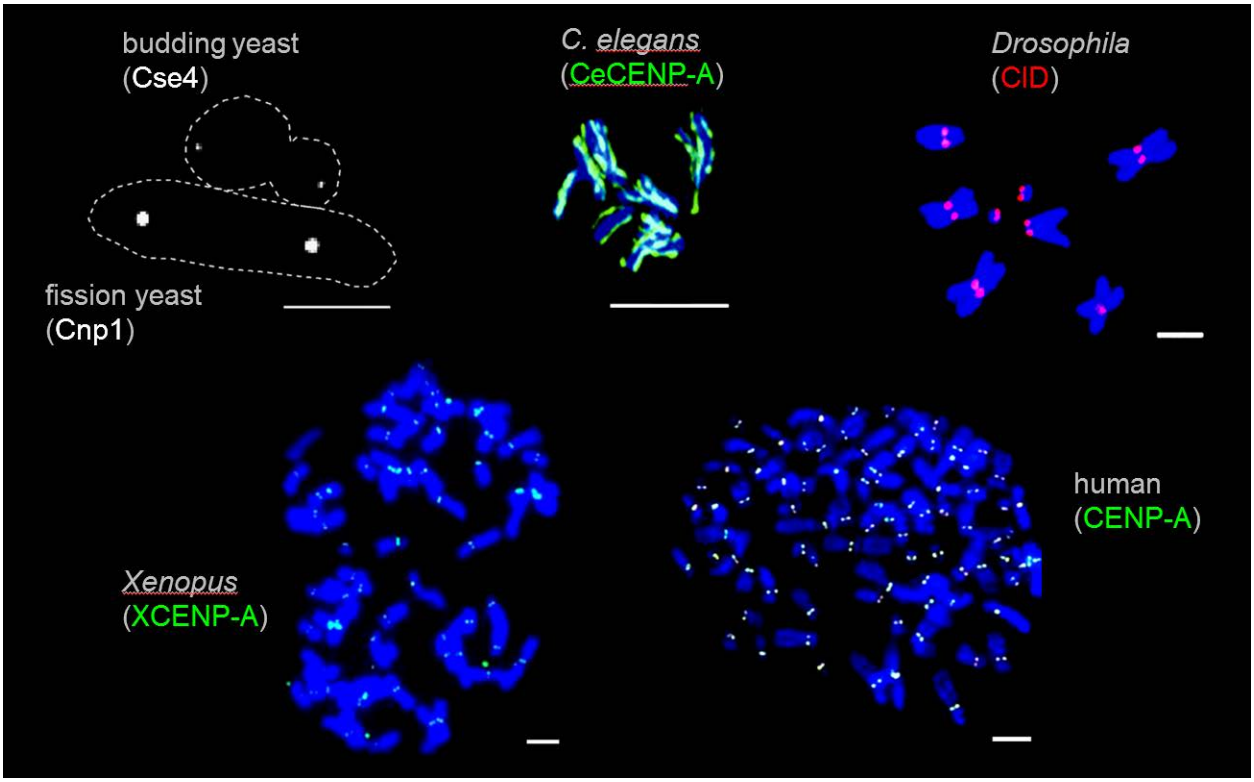

Figure 1.2. Centromere protein A (CENP-A) is widely used to mark the identity of centromeres in eukaryotes

Eukaryotes including including *S. pombe*, *S. serevisiae*, *C. elegans*, *Drosophila*, *Xenopus* and *Homo sapiens* all use CENP-A to mark their centromeres. The names of CENP-A in individual species (for instance, 'CID' in *Drosophila*) are color coded according to the color of CENP-A staining in the corresponding images. Adapted from images obtain for respective species (see text for references). Scale bars: 5 μm.

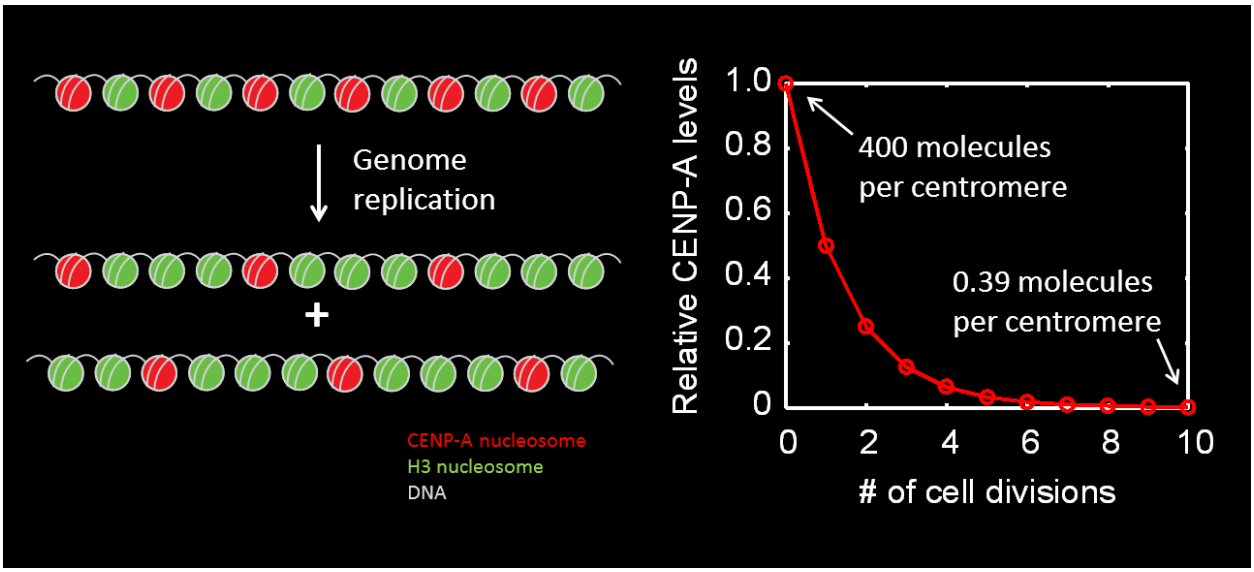

Figure 1.3. Centromeric CENP-A are diluted as chromosomes replicate

(Left) Schematic showing the one half reduction of CENP-A nucleosomes' numbers per centromere during centromeric DNA replication in S-phase, resulting in a scenario of 'serial dilution' if no replenishment is available. (Right) Counting of CENP-A's number per centromere upon continued serial dilution, modeled with exponential decay function. Reference number of CENP-A copy number at steady state is based on Bodor et al., 2014.

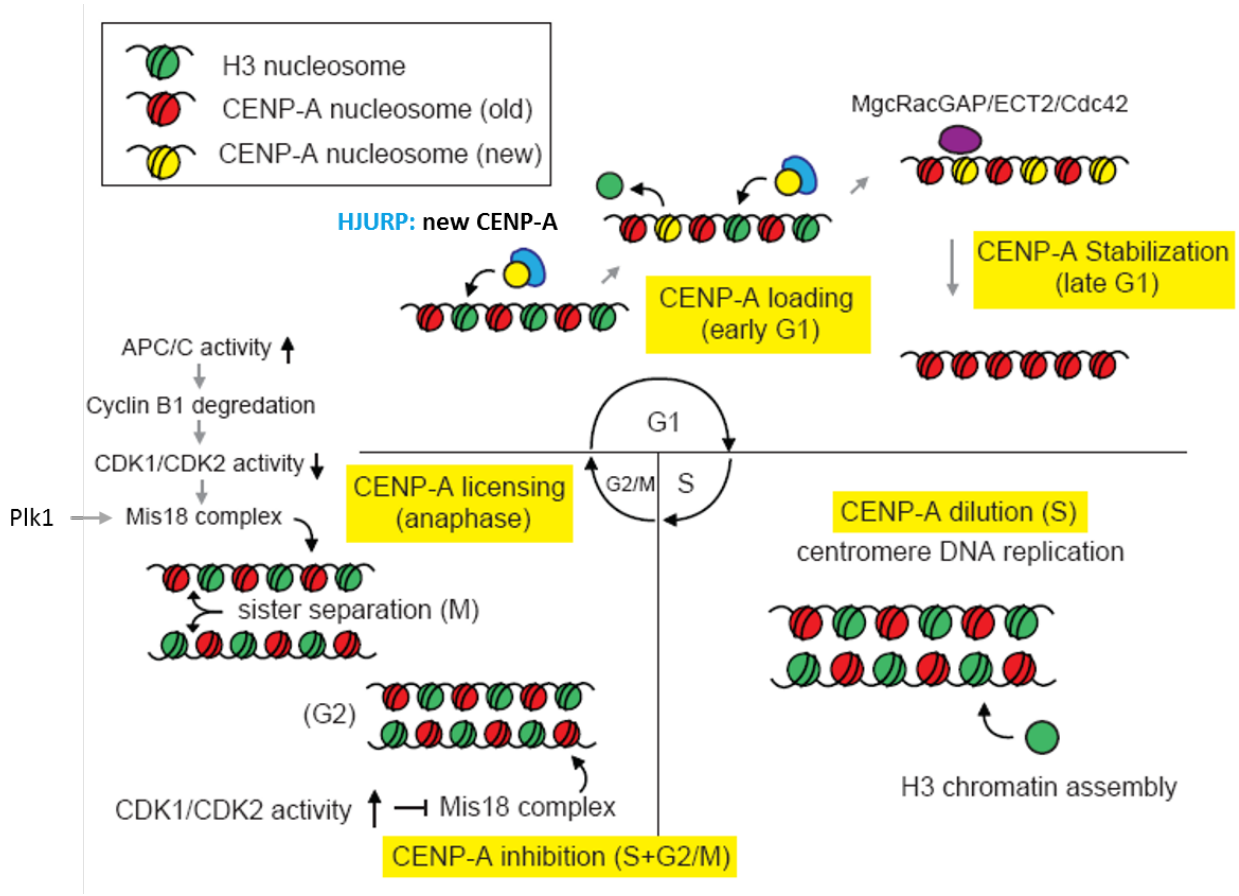

Figure 1.4. The CENP-A cycle.

As the epigenetic mark of centromere identity, centromeric CENP-A proteins are replenished during the G1-phase of cell cycle in a highly regulated manner. CENP-A loading occurs only once per cell cycle at preexisting centromeres marked by the old CENP-A molecules inherited from previous centromere prior to DNA replication. See the text for more details.

A

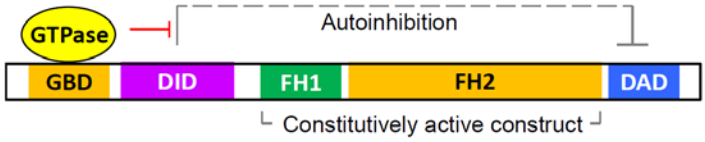

B

mDia formin	Upstream small GTPase	Nuclear accumulation upon LMB treatment	mDia localization in G1 HeLa cell	DNA Tubulin	References (on GTPases)
mDia1 (DIAPH1)	Rho	No	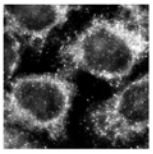	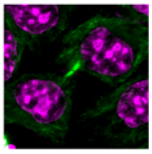	Watanabe et al., EMBOJ, 1997 Watanabe et al., NCB, 1999 Lammers et al., JBC, 2008
mDia2 (DIAPH3)	Rho Rac Cdc42	Yes	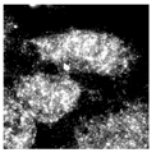	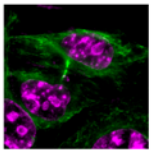	Alberts et al., JBC, 1998 Wallar et al., Exp Cell Res 2007 Lammers et al., JBC, 2008 Ji et al., NCB 2008 Peng et al., Curr Biol, 2003
mDia3 (DIAPH2)	Rho Rac Cdc42	No	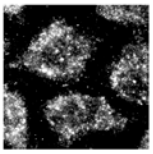	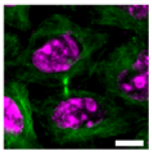	Lammers et al., JBC, 2008 Yasuda et al., Nature, 2004

Figure 1.5. Diaphanous formins are effectors of the small GTPase signaling.

(A) Schematic diagram of the general structure and the mode of action of diaphanous formin proteins. GBD – GTPase binding domain; DID – Dia interacting domain; FH – Formin homology domain; DAD – Dia auto-inhibition domain. Small GTPase binding releases the auto-inhibitory interaction between the DID and the DAD domains. The FH1FH2 alone can be used as a constitutively active construct that functions without the GTPase signaling.

(B) Comparison between the three members of diaphanous subfamily formins, with emphasis on cognate the upstream small GTPase signaling and the subcellular localization. Scale bar, 10 µm.

Chapter Two *: Diaphanous formin mDia2 regulates CENP-A levels at centromeres

*This chapter is reproduced from:

Diaphanous formin mDia2 regulates CENP-A levels at centromeres
Liu, C., and Mao, Y.
The Journal of Cell Biology, Vol.213 No.4 415–424 (2016)

Highlighted by *JCB*'s Biobytes, May 23, 2016

Where the author of this thesis is the first author.

Abstract

Centromeres of higher eukaryotes are epigenetically defined by CENP-A, a centromere-specific histone H3 variant. The incorporation of new CENP-A into centromeres to maintain the epigenetic marker following genome replication in S phase occurs in G1 phase; however, how new CENP-A is loaded and stabilized remains poorly understood. Here, we identify the formin mDia2 as essential for stable replenishment of new CENP-A at centromeres. Quantitative imaging, pulse-chase analysis and high-resolution ratiometric live cell studies demonstrate that mDia2 and its nuclear localization are required to maintain CENP-A levels at centromeres. Depletion of mDia2 results in a prolonged centromere association of HJURP, the chaperone required for CENP-A loading. A constitutively active form of mDia2 rescues the defect in new CENP-A loading caused by depletion of MgcRacGAP, a component of the small GTPase pathway essential for CENP-A maintenance. Thus, the formin mDia2 functions downstream of the MgcRacGAP-dependent pathway in regulating assembly of new CENP-A containing nucleosomes at centromeres.

Introduction

Epigenetic landscape of the chromosome is well inherited independent of underlying DNA sequences. In mammals, centromeres, the fundamental unit for chromosome segregation during mitosis, are defined epigenetically by nucleosomes containing the histone H3 variant CENP-A [140-142]. In order to maintain centromere identity against CENP-A dilution as DNA replicates and cell divides, newly synthesized CENP-A proteins are deposited at centromeres during early G1 of each cell cycle [143]. This process is initiated by Plk1-mediated [53] centromeric recruitment of the Mis18 complex at anaphase onset [144-146] and involves the recruitment of HJURP [147,148], the CENP-A chaperone.

The incorporation of new CENP-A at centromeres remain poorly understood. A small GTPase molecular switch has been shown to stabilize newly incorporated CENP-A. Depletion of Cdc42 or Rac1 in human cells leads to a decrease of CENP-A level at centromeres [64]. The downstream effector(s) of the small GTPase activity remains unidentified. Mammalian Diaphanous-related (mDia) formins nucleate and assemble unbranched actin structures downstream of Rho family GTPase signaling [149]. Recent studies have revealed potential nuclear roles for mDia formins [150,151]. Among mDia formin proteins (mDia1-3), only mDia2 can shuttle between the cytoplasm and the nucleus [150,152]. By affinity purification and mass spectrometry analysis, histones and topoisomerases have been identified as binding partners of mDia2, but neither mDia1 nor mDia3 [153].

Using quantitative imaging, we now provide direct evidence that the formin mDia2 is a novel cytoskeleton protein required for maintaining CENP-A levels at centromeres. As a constitutively active form of mDia2 rescues centromeric CENP-A levels caused by depletion of MgcRacGAP, a component of the small GTPase pathway essential for CENP-A maintenance, we

additionally uncover mDia2 as the downstream effector of the GTPase pathway for epigenetic centromere maintenance.

Results and discussion

Diaphanous formin mDia2 is essential to maintain CENP-A levels at centromeres

To test if the formin mDia2 is required for CENP-A level maintenance at centromeres, mDia2 protein levels were reduced in human cells (0.47 ± 0.11 relative to control, $p < 0.0001$) by the transfection of small interfering RNA (siRNA) duplexes targeting mDia2 for 48 hr (**Figure 2.1A**). The mDia2 depletion resulted in a decreased level, but not elimination, of CENP-A at centromeres (**Figure 2.1B**) without affecting total CENP-A protein levels (**Figure 2.1A**) compared to control cells (transfected with GAPDH siRNA). Significantly, the loss of CENP-A at centromeres could be rescued by the co-expression of a siRNA-resistant full-length mDia2 (**Figure 2.1B**), excluding the possibility of an off-target effect from mDia2 siRNA. CENP-A levels at centromeres from large numbers of cells were quantified using an automatic image-analysis algorithm (**Figure S2.1**; see Materials and Methods), designed in this study, without human bias. This confirmed the partial reduction in CENP-A levels at centromeres in mDia2-depeleted cells (**Figure 2.1C**). The decrease of CENP-A level was not caused by loss of centromere numbers in individual cells, judging by counting the immunostaining of CENP-B (**Figure 2.1D**), which localizes to centromeres independently of CENP-A [154]. In contrast to mDia2, knockdown of mDia3, a formin protein that has been shown to associate with kinetochores and to be important for kinetochore-microtubule attachment [114,115], did not result in loss of CENP-A at centromeres (**Figure 2.1, B and C**). These results support a role for the formin mDia2 in CENP-A level maintenance at centromeres.

To exclude the possibility that the CENP-A loss in mDia2-depleted cells could be due to cell-cycle-dependent transcriptional regulation of CENP-A, YFP-CENP-A levels were measured in fixed cells stably expressing a yellow fluorescent protein (YFP)-tagged CENP-A. Despite that the YFP-CENP-A fusion is controlled by the 5' LTR of the virus [148], a similar CENP-A loss at centromeres was observed upon mDia2 depletion (**Figure 2.1, E and F**). Reduced CENP-A levels in mDia2-depleted cells is reminiscent of the depletion of the CENP-A chaperon HJURP (**Figure 2.1, E and F**). These results are consistent with a role for mDia2 in regulating CENP-A levels at centromeres.

The mDia2 protein is specifically required for loading of new CENP-A

To determine if mDia2 is required for cell-cycle-dependent incorporation of new CENP-A into centromeres of duplicated sister chromatids after mitotic exit into G1, YFP-CENP-A levels at individual centromeres were followed by high-resolution ratiometric live-cell imaging designed in this study (for imaging and quantification analysis see **Figure S2.2**, Materials and Methods). In control cells, the increase of centromeric YFP-CENP-A levels began shortly after anaphase onset and continued for several hours (**Figure 2.2, A and B, and Video 1 and 2**), which is consistent with previous observations [64,143]. By contrast, the increase of YFP-CENP-A levels at centromeres in mDia2 depleted cells could not be maintained despite an initial slight increase within 2 hours after anaphase onset (**Figure 2.2, A and B; Video 1 and 2**). The defective increase of YFP-CENP-A in mDia2 depleted cells is also manifested with a significantly shorter apparent half-time (**Figure S2.2, B and C**), consistent with attempted yet failed loading events. These results clearly demonstrate that mDia2 is essential for replenishing CENP-A levels during early G1 phase, when new CENP-A is loaded onto centromeres marked with pre-existing CENP-A.

Whereas cell-cycle distribution was not significantly altered upon depletion of mDia2 (**Figure S2.2G**), live-cell imaging analysis showed reduced levels of CENP-A recruitment at centromeres upon mDia2 depletion. Cells with fully loaded CENP-A at centromeres inherits 50% "old" CENP-A during S phase and recruit 50% "new" CENP-A at early G1. To test which population of CENP-A was affected by mDia2 depletion, "old" and "new" CENP-A levels were analyzed by the SNAP-tag pulse-chase method [64,143]. The "old" inherited CENP-A was pulse-labeled (15 min) with a fluorescent mark, whereas all additional CENP-A ("new") was chased with a non-fluorescent label (**Figure 2.2C**). This analysis revealed that mDia2 depletion resulted in 37% reduction of total CENP-A levels, but unchanged levels of "old" CENP-A in comparison to control cells (**Figure 2.2, D-F**). Thus, the formin mDia2 functions in the recruitment of "new" CENP-A onto centromeres in G1 cells.

The formin mDia2 is a downstream effector of the MgcRacGAP-dependent small GTPase pathway required to maintain CENP-A levels at centromeres

The mDia2 protein contains functional nuclear localization (**Figure 2.3A**) and nuclear export signals, and shuttles between the nucleus and the cytoplasm through importin-α/β- and CRM1-mediated nuclear transport mechanisms [152,155]. Depletion of mDia2 did not change CENP-A distributions between cytoplasm and nucleus, though resulted in less CENP-A bound to chromatins, as expected (**Figures 2.3B and S2.3A**). Full-length mEmerald-mDia2 proteins were accumulated in nucleus upon treatment with leptomycin B (LMB) to block CRM1. By contrast, the K35A/R36A mutation within the NLS signal abolished nuclear accumulation of mEmerald-

mDia2 upon LMB treatment (**Figure 2.3C**). Replacing endogenous mDia2 with this mutant resulted in significantly reduced levels of CENP-A at centromeres (**Figure 2.3, D and E**), demonstrating that the nuclear function of mDia2 is required for its role in CENP-A maintenance.

A small GTPase switch including MgcRacGAP, a Rho family GTPase activating protein, is involved in CENP-A maintenance at centromeres [64]. The mDia formin proteins are auto-inhibited through an intramolecular interaction between N-terminal GBD-DID domains and C-terminal DAD domain [128]. The auto-inhibition is relieved upon the binding of the small GTPase at the GBD domain [134]. The mDia2 construct lacking the regulatory GBD and DAD domains (FH1FH2-mDia2), but not FH1FH2-mDia2 constructs with actin assembly-defective point mutations (K853A, I704A, and W630A) [156], was able to restore CENP-A levels at centromeres as well as the full-length mDia2 in cells depleted of endogenous mDia2 (**Figure 2.4, A and B**). Although lacking the known NLS signal, the EGFP-fused FH1FH2-mDia2 localized to the nucleus in G1 cells (**Figure 2.4C**). Further, the constitutively active form of mDia2 was very efficient in restoring CENP-A levels at centromeres in MgcRacGAP-depleted cells (**Figure 2.4D**). This is consistent with the formin mDia2 as a downstream effector of the MgcRacGAP-dependent GTPase pathway to play a role in centromeric CENP-A maintenance.

Depletion of mDia2 results in a prolonged centromere association of HJURP

New CENP-A loading at G1 centromeres requires the CENP-A histone chaperone HJURP, which also has the CENP-A nucleosome assembly activity [157]. A subset of early G1 cells has HJURP colocalized to centromeres [148]. To test whether depletion of mDia2 affects the dynamics

of HJURP at centromeres, we examined the HJURP centromere localization in early G1 cells expressing the EGFP-HJURP fusion upon releasing from thymidine arrest (**Figure 2.5A**). This revealed that mDia2 depletion did not affect the intensity of HJURP at centromeres (**Figure 2.5, B and C**), but the percentage of HJURP positive cells upon depleting mDia2 was almost doubled compared to control cells (**Figure 2.5D**). These results indicate a prolonged attempting of new CENP-A nucleosome assembly by HJURP in the absence of mDia2. Stochastic simulation demonstrated that prolonged HJURP dwelling (i.e. reduced HJRUP turnover) not only suffices to cause a higher percentage of HJURP positive cells as observed experimentally, but also contributes to the inability of CENP-A accumulation on centromeres, which is in good quantitative agreement with ratiometric live cell measurement over time (**Figure S2.3, B-E**). These results are consistent with a role of mDia2 in regulating CENP-A levels at centromeres and indicate that this function is at least in part through the regulation of the timely turnover of HJURP at centromeres (**Figure 2.5E**).

A novel nuclear function of formin mDia2 in centromere epigenetic regulation

Centromeres are epigenetically marked by the conserved histone H3 variant CENP-A. Each sister centromere inherits one half the number of CENP-A molecules upon DNA duplication. In order to maintain centromere identity, new CENP-A is added to double the number of CENP-A molecules at centromeres during G1. Loading of new CENP-A molecules into centromeres includes the following steps (**Figure 2.5E, left panel**): (1) the assembly of licensing factors, the Mis18 complex, at anaphase onset [144-146], (2) new CENP-A deposition and nucleosome assembly by the CENP-A chaperone HJURP at early G1 [157], and (3) a maintenance step involving a small GTPase molecular switch [64]. Here, our results reveal a critical role for the formin mDia2 in

regulating epigenetic maintenance of centromere identity. Quantitative imaging and high resolution ratiometric live cell studies have demonstrated that knockdown of mDia2 results in reduced levels of CENP-A at centromeres. In contrast, depletion of mDia2 does not affect the recruitment of H2A.Z, another histone variant in human cells (**Figure S2.3, F and G**).

The formin mDia2 is not likely to play a role in centromere licensing or the recruitment of centromere components, as we have not been able to detect mDia2 centromere localization at any point in the cell cycle. This is further supported by the normal level of HJURP associated with centromeres in mDia2-depleted cells. By contrast, the increased percentage of HJURP positive cells upon mDia2 depletion indicates a role of mDia2 in regulating nucleosome assembly for new CENP-A incorporation (**Figure 2.5E, right panel)**. Expressing a constitutively active form of mDia2 is able to rescue the CENP-A deposition defect caused by knockdown of MgcRacGAP, a phenotype that is consistent with the formin mDia2 being the downstream effector of the MgcRacGAP-dependent GTPase pathway during the maintenance step to stabilize newly incorporated CENP-A. The formin mDia2 could be involved in this process by, at least, two different mechanisms: (1) assisting chromatin-remodeling for new CENP-A incorporation, as the FH2 region of mDia formins has been shown to interact with CENP-A using a *yeast* two-hybrid assay [115]; and (2) altering mobility or organization of chromatin. The latter possibility will require mDia2-mediated nuclear actin activity. Recent studies have demonstrated nuclear actin network assembly mediated by formin proteins in regulating the MAL/SRF (megakaryocytic acuteleukemia/serum response factor) transcription function [150] and in DNA damage response [151]. Although it has been shown that latrunculin A or cytochalasin D treatment does not affect CENP-A levels at centromeres [64], actin in nucleus could form short oligomers or other forms of structures

that are less sensitive to drug treatment than actin polymers [158-161]. It will be important to understand whether actin dynamics is important for epigenetic centromere maintenance in future studies.

Materials and Methods

siRNA sequences, constructs and antibodies

The siRNAs used in this study include:

GAPDH (NM_002046.4, UGGUUUACAUGUUCCAAUA);

DIAPH3/mDia2 (AB244756.1, CUCCGGCACAAUUCAGUUCAA);

DIAPH2/mDia3 (BC117414, CACCGTCTCAATGACATTCGA);

HJURP (NM_018410.4, CUACUGGGCUCAACUGCAAU).

The constructs used in this study include: H2B-YFP, H2B-RFP [148], FL-mEmerald-mDia2, FL-ΔNLS-mEmerald-mDia2, pEGFP-FH1FH2mDia2-WT, pEGFP-FH1FH2mDia2-K853A, pEGFP-FH1FH2mDia2-I704A, pEGFP-FH1FH2mDia2-W630A, pmCherry-C1 (Clontech Cat.# 632524), MgcRacGAP MISSION shRNA plasmid (Sigma, NM_013277.3-2165s21c1, NM_013277.2-456s1c1). The pEGFP-FH1FH2mDia2 based constructs were gifts from Francesca Bartolini. The construct of mEmerald-mDia2-C-14 was a gift from Michael Davidson (Addgene plasmid # 54158). Site directed mutagenesis was performed to generate the K35AR36A mutant, using QuikChange Lightning following manufacturer's instructions.

Primary antibodies used in this study include: rabbit anti mDia2 [162], rabbit anti mDia3 (LS-C19007, Lifespan), mouse anti CENP-A (Ab13939, Abcam), mouse anti tubulin (T6199, Sigma), rabbit anti HJURP (Ab100800, Abcam; Foltz et al., 2009), chicken anti GFP (Ab16901, Millipore), rabbit anti CENP-B (Ab25734, Abcam), mouse anti HA (MMS-101P, COVANCE), rabbit anti MgcRacGAP (Ab61192, Abcam), and rabbit anti H2A.Z (Ab4174, Abcam).

Cell culture, transfection, and drug treatment

HeLa cells were used for most of the quantitative imaging experiments in this study. A HeLa cell line stably expressing YFP-CENP-A was used for high-resolution ratiometric live cell imaging. A HeLa cell line stably expressing GFP-HJURP (gift from Dan Foltz) was used for fixed cell imaging in Figure 5. Cells were maintained in DME medium supplemented with 10% FBS (complete growth medium) at 37°C in 5% CO_2. The transfection of siRNAs was performed with Hiperfect (Qiagen) following the manufacturer's protocol. For co-transfection experiments, siRNAs were transfected with at least 20-fold molar excess to marker plasmids encoding fluorescent proteins. Control cells were transfected with GAPDH siRNA. All knockdowns were confirmed by immunoblotting analysis. Cells were fixed for immunostaining or imaged 48 hours after transfection. Thymidine synchronization (also detailed in 'SNAP-tag pulse chase assay' below) was performed with 2 mM thymidine in complete growth medium for at least 17 hr, washed twice in pre-warmed PBS, and released into complete medium supplemented with 24 μM deoxycytidine (for 9 hr if followed by another round of thymidine arrest). Nocodazole was used at 100 ng/ml. Leptomycin B (LMB, provided in methanol: water = 7:3) was used at 20 nM (final concentration) for 1 hr. All drugs were purchased form Sigma-Aldrich.

Quantitative fixed cell imaging and data analysis using 'INCA' method

For immunofluorescence and fixed cell imaging, cells grown on poly-D-lysine coated coverslips were washed in PBS (pre-warmed at 37°C), fixed in cold MeOH at -20°C for 5 min, and then permeablized with 0.1% Triton-X-100 in PBS for 1 min. After being re-hydrated in PBS

briefly, fixed cells were blocked in 5% BSA in PBS at 4°C overnight. Coverslips were subjected to primary antibodies diluted in PBS and Alexa Fluor® 488, DyLight™594 or Cy™5 conjugated secondary antibodies, both at room temperature for 1 hr. DAPI (16.67 ng/ml) was used to stain DNA/nuclei. Coverslips were mounted using antifade reagent (ProLong Gold; Molecular Probes). Images were acquired at room temperature using an inverted microscope (IX81; Olympus) with a 60×, N.A. 1.42 Plan Apochromat oil immersion objective (Olympus), a monochrome charge-coupled device camera (Sensicam QE; Cooke Corporation) at 1×1 binning, which are all controlled by the SlideBook software (3i and Olympus). 10 optical sections 0.5 μm apart spanning 5 μm were acquired for each field. All images in each experiment along with appropriate controls were collected on the same day with identical exposure time. Representative images presented in figures are scaled identically across groups. Cells stably expressing YFP-CENP-A were fixed following a slightly different protocol to preserve YFP's fluorescence: cells were washed in PBS (pre-warmed at 37°C), fixed in freshly prepared EM grade paraformaldehyde (PFA, 4% diluted in PBS; 16% stock from Electron Microscopy Sciences, Cat # 15710-S) at room temperature for 10 min, washed in PBS twice (5 min each), and then permeablized with 0.1% Triton-X-100 in PBS for 1 min. The subsequent block and staining steps are the same as the general protocol.

Inspired by a previous study [64], we developed an image analysis technique by measuring the integrated CENP-A intensity per nucleus: the Integrated Nuclear CENP-A (INCA) measurement, a custom-written software using MATLAB (MathWorks, R2013a). All 16-bit uncompressed raw images processed only by maximum Z-projection were fed into MATLAB for an automatic and unbiased measurement. Briefly, raw images were subjected to band-pass filtering (**Figure S2.1A**) which eliminates noise by applying a narrow kernel and removes

background with a wide kernel (kernel sizes were fixed throughout the study). Resultant DAPI images were subjected to Otsu thresholding [163] and watershed algorithm [164] to generate binary nuclear masks, which were subsequently applied to the cognate CENP-A images. The integrated fluorescence intensities on CENP-A images within the nuclear masks were eventually measured in order to reflect the 'loading capacity' of all centromeric CENP-A in that particular nucleus/cell. To confirm quantification obtained using the 'INCA' method, a more labor-intensive traditional method measuring the integrated intensity of single centromeres (with ROIs slightly larger than each single centromere) was performed using ImageJ (NIH) and yielded the same results as the 'INCA' method (**Figure S2.1B**). The 'INCA' method returned the integrated intensity value for every single nucleus. In order to compare the intensity values of nuclei between experiments, the measurements of each experiment were normalized against that of the control group in that dataset, therefore allowing cross-dataset comparison [64]. Imaging experiment with or without co-transfection markers were both carried out and analyzed using 'INCA' method with the same conclusions.

High resolution ratiometric live cell imaging

HeLa cells stably expressing YFP-CENP-A[148] were plated onto Poly-D-Lysine coated 35 mm glass-bottom dishes (MatTek Corporation) and maintained in CO_2 independent medium supplemented with 4 mM L-glutamine and 10% FBS, with an environmentally controlled chamber at 37°C during imaging. Images were acquired every 20 min for a total duration of about 13 hrs, with 11 z-sections spanning 10 μm (1 μm apart each optical section) being acquired at each time point. Exposure time was kept constant throughout the duration of live imaging (200ms for YFP after being optimized against photobleaching). All Live imaging were performed using a

motorized inverted microscope (IX81; Olympus) with a 60×, N.A. 1.42 Plan Apochromat oil immersion objective (Olympus) and a interline transfer cooled CCD camera (ORCA-R2 C10600-10B; HAMAMATSU Photonics) at 1×1 binning, which were controlled by the MetaMorph software (Molecular Devices, LLC).

For live imaging data, due to a much lower signal-to-noise ratio than fixed samples, a different quantification method was developed based on a previous study [64]. Essentially, intensity measurement was performed for individual cells upon mitotic exit and during G1. Only cells staying in focus were subjected to measurement (mCherry-C1 was used as a cotransfection marker to identify siRNA transfected cells). Measurements were performed on maximum z-projections with all 16-bit depth preserved. Ratiometric analysis was performed by normalizing the time course of each cell's centromeric CENP-A intensities with a 'reference frame', which represents the averaged centromeric CENP-A level for that particular cell before CENP-A loading occurs. Due to resolution constraints (i.e. more than one centromeres are inevitably overlapped during anaphase/ telophase), in order to ensure it is the single centromeres' intensity that were measured, the reference frame (against which the 'loading curve' was normalized) were selected to be late prometaphase or early metaphase, where single sister centromere can be identified and measured to obtain an internal reference intensity before any new CENP-A loading has occurred. During the course of telophase/G1 phase, only well separated single centromeres, whose intensity distributions are circular-symmetric on z-projection images, were randomly selected and measured using ImageJ (NIH). Because pixel intensities on each centromere approximately follow 2D-Gaussian distribution, local maxima were considered as a reasonable measurement of CENP-A levels per centromere. The measurements were followed by normalization: each data point

throughout the time course was normalized against the host cell's mean measurement in the 'reference frame'. After normalization, data were plotted as mean ± SD. For visual comparison, representative maximum z-projection images were demonstrated, with linear intensity transformation function (ITF) being applied [165] and identical dynamic range/ LUT being used for all images of each cell throughout the time course.

Regarding photobleaching, our protocol for long term live cell imaging has been optimized such that only minimal photobleach occurred by 10 hours after imaging started (**Figure S2.2, D-F, and Video S3**).

SNAP-tag pulse chase assay

The SNAP-tag pulse chase assay was performed based on published protocols [64,143]. Essentially, HeLa cells stably expressing CENP-A-SNAP-3×HA were synchronized using double thymidine block (2 mM thymidine, 17 hr each) with 9 hr release in between (in medium supplemented with 24 μM deoxycytidine). During the second round of thymidine arrest, siRNAs were transfected to allow for about 48 hr knockdown time before fixation whereas only one round of CENP-A deposition during the immediate next G1 was affected. Upon releasing from the 2nd round of thymidine block, cells were pulse-labeled with TMR-Star, a fluorescent SNAP substrate (3 μM), for 15 min, followed with complete washes and block. Cells were fixed and stained for total CENP-A (anti HA tag). Quantitative imaging and image processing were performed as detailed above using the 'INCA' method.

Cell Fractionation

Cell fractionation analysis was carried out using an adapted protocol based on established methods [150,166,167]. Briefly, cells (5×10^6) were harvested and washed with cold PBS. Cell pellet was resuspended in 500 μl 1x hypotonic buffer [20 mM Tris-HCl (pH 7.4), 10 mM NaCl, 3 mM $MgCl_2$, 1 mM PMSF, and 1x protease inhibitor cocktail (Roche)] by pipetting several times, followed by 15 min incubation on ice to allow for swelling. 25 μl of 40% NP40 was added into the system prior to vortexing for 10 sec. The homogenate was then centrifuged (3000 rpm 10 min at 4℃) to separate the cytoplasmic fraction (supernatant) from the nuclear pellet. Nuclear pellet was re-washed with hypotonic buffer (without NP40) and centrifuged, and was then resuspended in 50 μl relatively low-salt extraction buffer [10 mM Tris (pH 7.4), 2 mM Na_3VO_4, 100 mM NaCl, 1% Triton-X-100, 1 mM EDTA, 10% glycerol, 1 mM EGTA, 0.1% SDS, 1 mM NaF, 0.5% deoxycholate, 20 mM $Na_4P_2O_7$, 1 mM PMSF, 1x protease inhibitor cocktail] and incubated on ice for 30 min, with vortexing every 10 min. The mixture was then centrifuged for 30 min at 14000 g in 4℃. Supernatant is nucleoplasm and pellet is chromatin-associated materials. For immunoblotting, tubulin was used as the cytoplasmic marker [150], RNA Pol II as the nucleoplasmic marker [167], while histone H4K20me2 as the chromatin-associated marker [166].

Immunoblotting analysis

Immunoblotting was carried out as previously described [168]. Briefly, cells were lysed in RIPA buffer [50 mM Tris-HCl (pH 7.5), 150 mM NaCl, 1% NP-40, 0.1% SDS, 0.5% Na-Deoxycholate Acid] and then denatured using SDS sample buffer. Cell lysates were subsequently subjected to 10% SDS-PAGE followed by membrane transfer (Immobilon-P, Millipore; Towbin transfer buffer, pH 8.3). Immunoblots on the membrane were blocked with 5% nonfat milk dissolved in Tris-buffered saline with tween (TBST) [20 mM Tris−HCl (pH 7.4), 150 mM NaCl, 0.05% Tween] and then probed with primary antibodies diluted in TBST. Primary antibodies were visualized using Alexa Fluor®680 conjugated secondary antibodies (Life technologies) together with the LI-COR imaging system (LI-COR Biosciences).

Cell cycle analysis

Control HeLa cells or mDia2 knockdown cells (confluent) were trypsinized from 6-well plate, fixed with MeOH (-20°C), and stained with DAPI. The BD LSRII Cell Analyzer was used for FACS experiments. The FlowJo was used for FACS data analysis with Gaussian fitting based on univariate cell cycle model [169].

Statistical analysis and plotting

All statistical analyses were performed with GraphPad Prism 5 (GraphPad) using unpaired, two tailed t-test between groups unless noted otherwise (e.g. z-test with MATLAB to compare two sample proportions). All plots were prepared in MATLAB (MathWorks, R2013a), Prism (GraphPad), Origin 8.6 (OriginLab) or Excel (Microsoft). Control groups and mDia2-depleted groups in all experiments were pooled together after normalization and presented.

Stochastic simulation of HJURP turnover at centromeres

To test if extended dwelling time of HJURP molecules on centromere can contribute to the change in the observed percentage of HJURP positive cells, we applied the Gillespie next reaction algorithm to numerically simulate the stochastic association/ dissociation events of HJURP molecules on the centromere [170]. Parameters were chosen based on reported numbers (k_{on}, k_{off}, etc., see **Table 2.1**) or realistic assumptions when no parameters are available (numbers of docking site per centromere). Briefly, a realistic number of "docking sites" (30, which is smaller than the total number of CENP-A nucleosomes per centromere) were assigned for each single centromere and there is no HJURP associated on any docking site at the beginning. Each round of simulation starts with generating a series of random numbers (Random Probability, P_{rand}) for each time step (t_i) and compare the $P_{rand}(t_i)$ with the actual probability of either association (P_{on}) event or dissociation event (P_{off}) given the current docking site status is either unoccupied or occupied respectively at time t_i. P_{on} and P_{off} are calculated following equations (1) and (2), where k_{off} (dissociation rate constant, min^{-1}) and k_{on}* (pseudo-association rate constant, min^{-1}) are derived from parameters listed in **Table 2.1**.

$$P_{on} = 1 - e^{-(k_{on^*}) * t_i} \qquad (1)$$

$$P_{off} = 1 - e^{-(k_{off}) * t_i} \qquad (2)$$

If $P_{on}(t_i) > P_{rand}(t_i)$, it suggests compared to random probability the association event is more likely to happen given an unoccupied docking site. One molecule of HJURP will jump on the docking site. If $P_{off}(t_i) > P_{rand}(t_i)$, it suggests compared to random probability the dissociation event is more likely to happen given an occupied docking site. One molecule of HJURP will jump off and leave the docking site available for the next round of possible association event.

In the case of incomplete/ failed incorporation, the increased level of CENP-A as a result of HJURP association will be removed following HJURP dissociation, giving rise to unsuccessful association and the inability of new CENP-A nucleosomes to build up. Meanwhile, k_{off} is lowered by half compared to ordinary conditions to manifest on altered HJURP dwelling time and thus turnover rate (**Figure S2.3A**).

Extended dwelling time shouldn't affect the number of dwelling events per docking site per centromere. In order to estimate the total numbers of time steps in case of lowered k_{off} and failed incorporation to get similar numbers of dwelling events, we plotted the number of dwelling event per docking site with empirical increment of time steps. It turns out that 3500 time steps under this circumstance is the minimum requirement to achieve similar numbers of total dwelling event per docking site ($p = 0.0923$). Total dwelling time per docking site therefore has the mean value of 333.384 min as compared to 185.06 min under ordinary conditions. Δt is therefore 2.4721 hr longer under the condition of 'failed incorporation + lower k_{off}'.

Next, in order to assess the influence of temporal changes on the percentage of observable HJURP positive cells, we initiated another matrix to simulate thousands of cells' collective behavior. It is assumed that a cell shares the same temporal property of the docking site regarding HJURP's presence on its centromeres. Instructed by experimental observations and practical experiences (**Table 2.1**), here we assumed 50% cells are synchronized around the G1/S boundary upon being released from single round of thymidine arrest. The exact position of each cell's time

line at the start of simulation (upon thymidine release) is stochastically distributed within a normal time window (μ= 0, SD = 2). As a reference, a cell starts right at G1/S boundary (0 hr) will proceed for 9 hrs to start having HJURP on its centromeres. After 3 hrs for this cell to be a 'HJURP positive' cell, HJURP will stop being associated with centromeres, therefore making 12 hrs the last time point for it to be a 'HJURP positive' cell (**Figure S2.3C**). 'Green point' and 'red point' will be used hereafter to name the start and end of HJURP association respectively. Despite of the intrinsic uncertainties associated with cell synchronization, all cells are fixed 11 hrs after thymidine release for imaging (invariant observational point). Consequently, all cells with their 'red point' before the observational point, and all cells with their 'green point' after the observational point, will not be documented as 'HJURP positive' cells. The percentage of 'HJURP positive' cells can then be calculated based on these criteria (**Figure S2.3D**).

In order to test if the number of HJURP molecules per centromere is altered at any given time during the period of being an 'HJURP positive' cell, 10 random position inside the 'HJURP positive' time window were chosen (per simulation) to count how many docking site are occupied at that particular time point. The number of occupied docking site on that centromere reflects the number of HJURP molecules per centromere at that time. This process is repeated three times for plotting the simulated HJURP level per centromere (**Figure S2.3D**).

Finally, to visualize the time dependent 'loading' of CENP-A nucleosomes on the centromere, results from stochastic simulations described above were summed up over time to create 'loading curves' of the accumulated number of CENP-A nucleosomes per centromere.

Ordinary conditions and conditions with 'failed incorporation + lower k_{off}' were processed respectively and plotted to compare with experimental measurements (**Figure S2.3E**).

Online supplemental material

Fig. S2.1 shows the Integrated Nuclear CENP-A (INCA) measurement method developed in this study. Fig. S2.2 shows the method used for quantifying high resolution ratiometric live cell imaging data and details of nonlinear regression. Fig. S2.3 shows the stochastic simulation of HJURP turnover at G1 centromeres. Video S1 shows live cell imaging movies of a control cell and an mDia2 knockdown cell stably expressing YFP-CENP-A going through G1 phase. Video S2 shows the ratiometric live cells imaging of YFP-CENP-A signals in a control cell and an mDia2 knockdown cell. Video S3 shows a representative cell expressing YFP-CENP-A arrested in G1/S phase (in the presence of thymidine) imaged every 20 min for 10 hrs for photobleaching test. Online supplemental materials can be found at:
http://www.jcb.org/cgi/content/full/jcb.201512034/DC1

Acknowledgements

We thank all members of the Mao laboratory for stimulating discussion. We thank Gregg Gundersen and Francesca Bartolini for insight on the project. We thank Richard Vallee for inputs on the project and equipment for live cell imaging. We thank Dan Foltz, Michael Davidson, and Dyche Mullins for reagents. We are grateful to the training C.L. received from the Physiology Course (2013) in Marine Biological Laboratory (Woods Hole, MA), in particular computational programming from David Odde and Melissa Gardner. This work has been supported by grants from the National Institute of Health (GM89768) to Y.M.

Abbreviations

CENP-A, Centromere protein A; FH, formin-homology domain; HJURP, holiday junction recognition protein; MgcRacGAP, male germ cell Rac GTPase-activating protein;

Figures

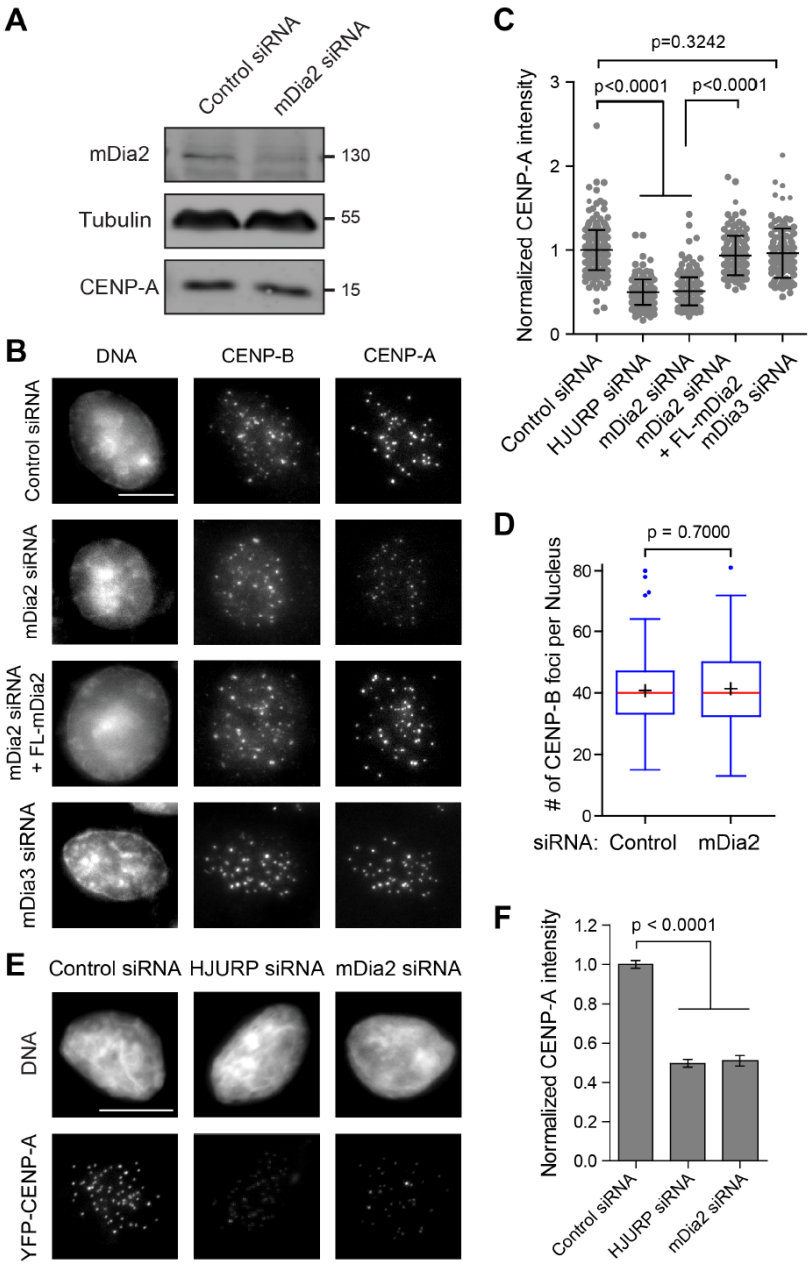

Figure 2.1. The formin mDia2 is required to maintain CENP-A levels at centromeres.

(**A**) Depletion of mDia2 does not affect CENP-A protein level. Immunoblotting analysis of HeLa cell lysates 48 hr post transfection with control (GAPDH) and mDia2 siRNAs.

(**B**) Immunofluorescence detection of CENP-A and CENP-B in HeLa cells 48 hr post transfection with the indicated siRNAs and the full length mEmerald-tagged mDia2 (FL-mDia2) expression

vector (DNA - DAPI). Transfected cells were identified by co-transfected fluorescence markers. Scale bar, 10 μm.

(**C**) Scatter plot showing the distribution of normalized CENP-A integrated intensity per nucleus (mean ± SD overlaid with scatter plot) with the 'INCA' method (**Figure S1**). Control: n = 292, HJURP siRNA: n = 196, mDia2 siRNA: n = 260, mDia2 siRNA + FL-mDia2: n = 136, and mDia3 siRNA: n = 117 from three independent experiments. The p-value was computed using two tailed *t*-test.

(**D**) Depletion of mDia2 does not affect centromere numbers. Whisker-Tukey boxplots show the number of CENP-B foci. The boxes span 25-75 percentile of the data, while the center bar denotes median and the '+' marks mean. Control: n = 168 and mDia2 siRNA: n = 125 from three independent experiments. The p-value was computed using two tailed *t*-test.

(**E**) Depletion of mDia2 results in reduced levels of YFP-CENP-A at centromeres. Immunofluorescence images showing YFP-CENP-A in HeLa cells stably expressing YFP-CENP-A 48 hr post transfection with indicated siRNAs (DNA - DAPI). Scale bar, 10 μm.

(**F**) Quantification showing the mean levels of normalized integrated YFP-CENP-A intensity per nucleus (means ± 95% confidence intervals). Control (GAPDH siRNA): n = 456, HJURP siRNA: n= 250, and mDia2 siRNA: n = 158 cells from three independent experiments. The p-value was computed using two tailed *t*-test.

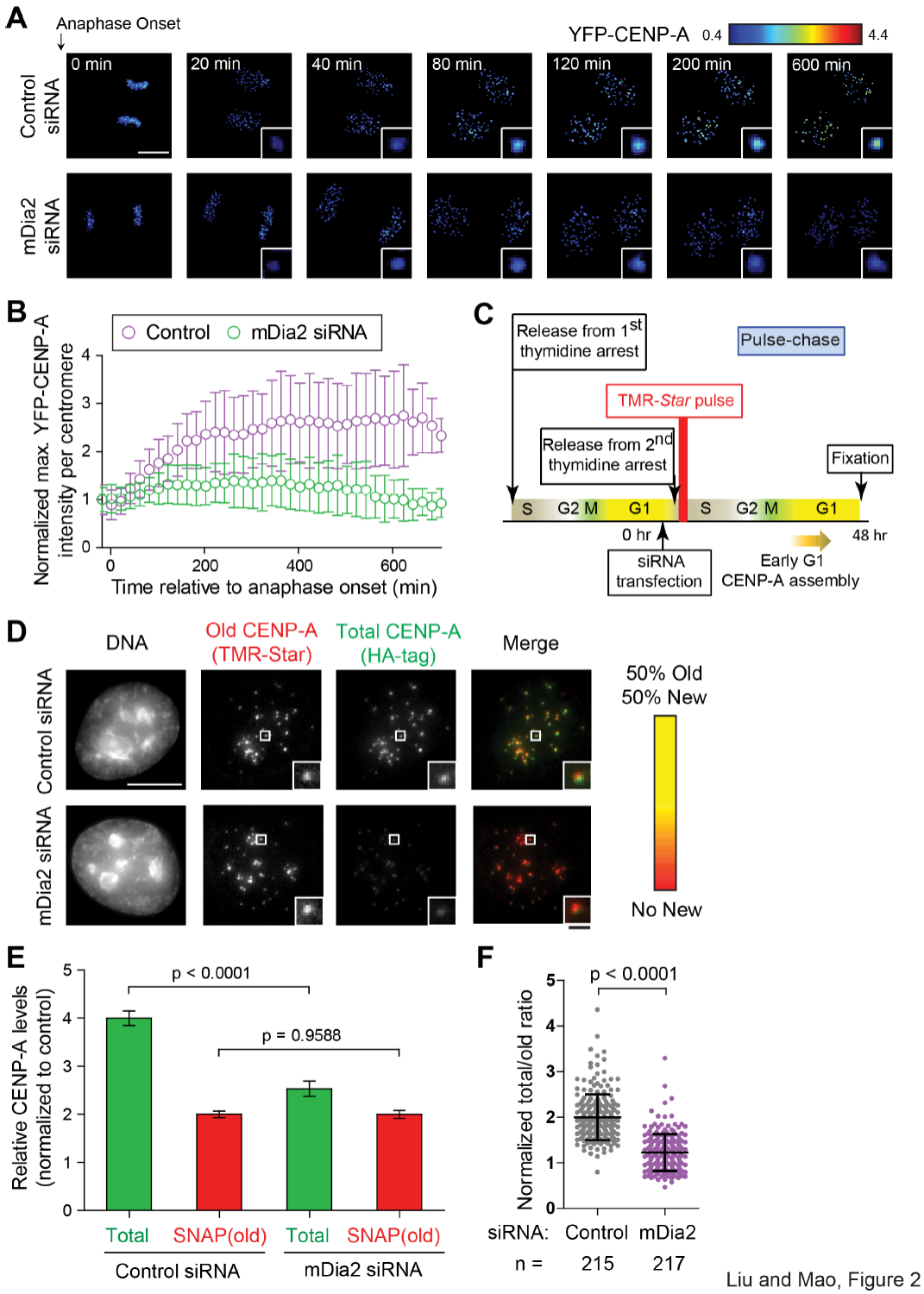

Figure 2.2. The mDia2 protein is required for loading new CENP-A during G1.

(A) High resolution ratiometric live cell imaging showing defective YFP-CENP-A loading upon mDia2 knockdown. Pseudo-colored live imaging stills following cells through the 10 hour time window after anaphase onset. Identical lookup table (LUT, linear and covering the full range of data) was used over time. Scale bar: 10 µm (insets are 3× magnified).

(B) Quantification of centromeric YFP-CENP-A levels during G1 phase (plotted as mean ± SD). Control: n = 4,100 centromeres from 12 G1 pairs and mDia2 siRNA: n = 4,310 centromeres from 13 G1-pairs were measured from three independent transfections (See Materials and Methods and Figure S2 for more details).

(C) Scheme for the SNAP pulse chase labeling to distinguish existing centromeric CENP-A protein (old) from newly synthesized CENP-A loaded onto centromeres (new).

(D) Immunofluorescence analysis showing old CENP-A labeled by TMR-Star and total CENP-A stained with anti-HA antibody. In merge: red - TMR-Star and green - HA-tag. Scale bar, 10 μm (1 μm in 4× magnified insets).

(E) Quantification of SNAP-tag-labelled CENP-A (old, red) and total CENP-A (total, green) (means ± 95% confidence intervals). The p-value was computed using two tailed t-test.

(F) Quantification showing the normalized ratio between total CENP-A and old CENP-A (mean ± SD overlaid with scatter plot). Control: n = 215 and mDia2 siRNA: n = 217 cells from three independent experiments. The p-value was computed using two tailed t-test.

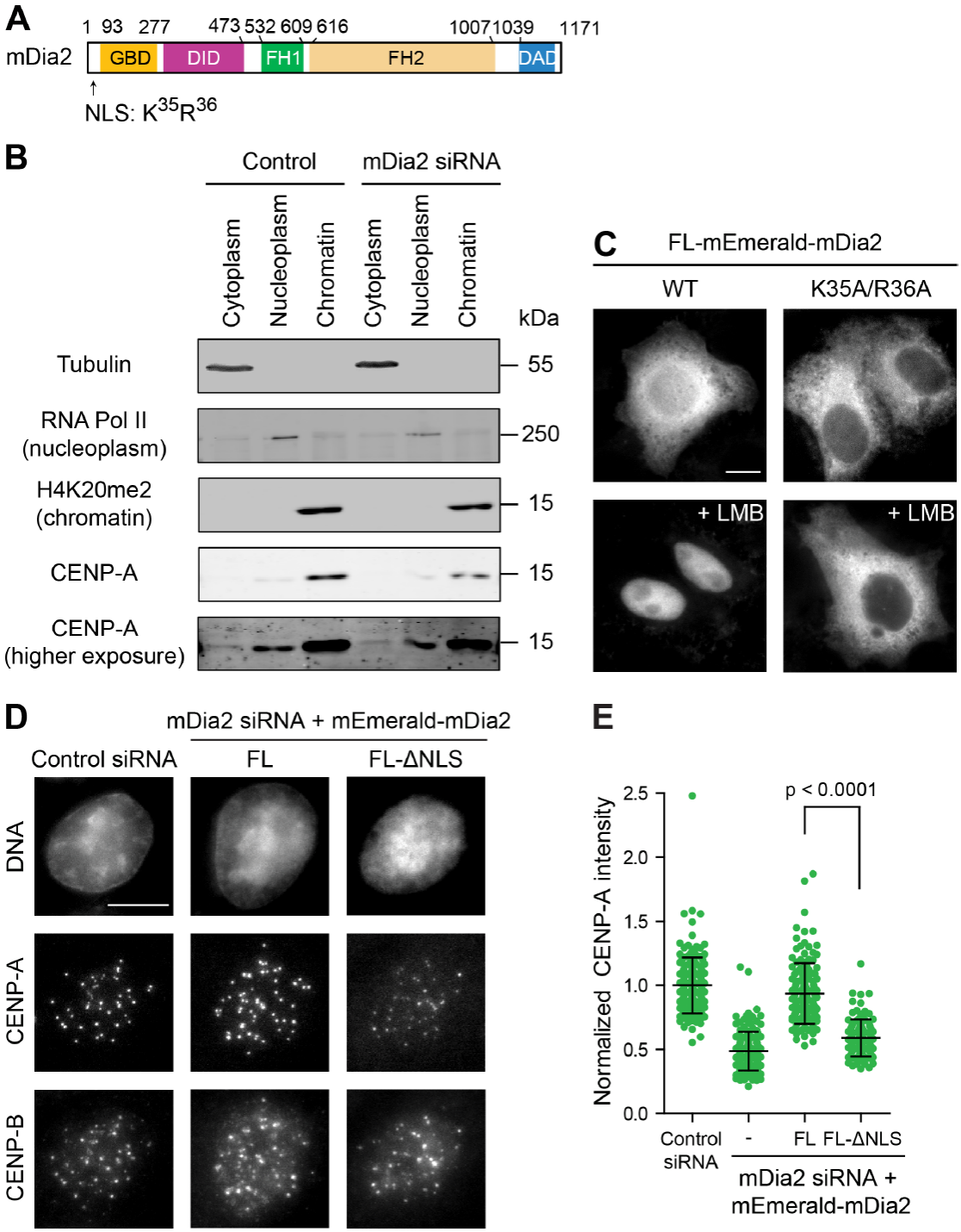

Figure 2.3. Nuclear mDia2 is required for CENP-A levels at centromeres.

(A) The mDia2 protein structure showing the relative positions of GBD, DID, FH1, FH2 and DAD domains as well as the position of nuclear localization signal (NLS).

(B) Depletion of mDia2 does not affect CENP-A distribution in cytoplasm and nucleus. Cellular fractionation and immunoblotting analysis showing the distribution of CENP-A proteins in cytoplasm, nucleoplasm and insoluble materials associated with the chromatin marked by tubulin, RNA polymerase II and H4K20me2, respectively. A higher exposure of CENP-A blot was shown for its cytoplasmic distribution.

(C) Cells expressing wild-type mDia2 or the mDia2K35A/R36A mutant (with a defective NLS) fused with mEmerald were treated with or without LMB (20 nM for 60 min) before fixation and imaging mEmerald. Scale bar, 5μm.

(D) Immunofluorescence detection of CENP-A and CENP-B in HeLa cells 48 hr post transfection with the indicated siRNAs and the full length mDia2 (FL-mDia2) or mDia2 ΔNLS mutant expression vectors (DNA - DAPI). Scale bar, 5 μm.

(E) Quantification showing the normalized CENP-A integrated intensity per nucleus (mean ± SD overlaid with scatter plot). The p-value was computed using two tailed t-test. Control: n = 174, mDia2 siRNA: n = 149, mDia2 siRNA + FL-mDia2: n = 136, mDia2 siRNA + FL-ΔNLS: n = 103.

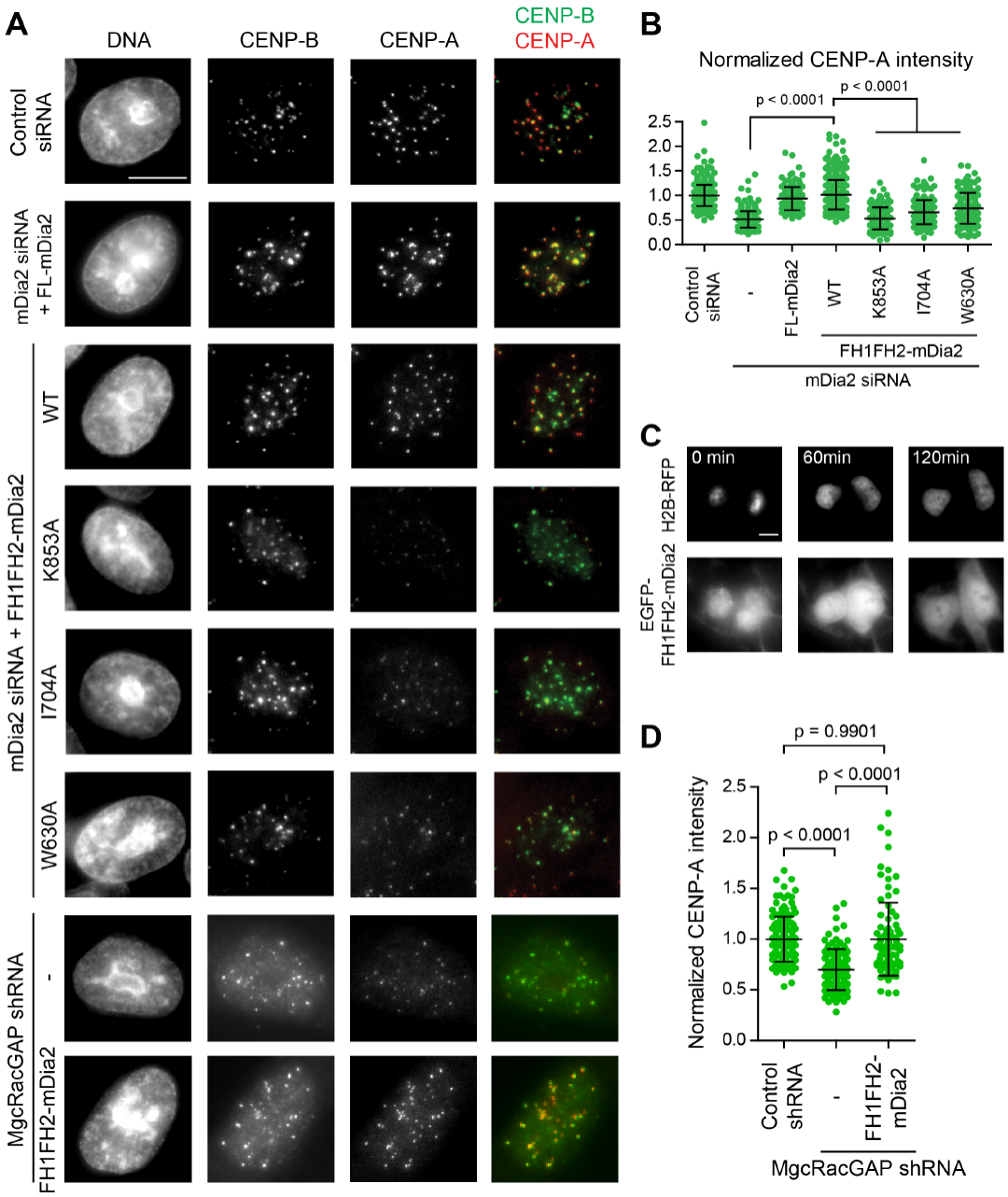

Figure 2.4. The formin mDia2 is a downstream effector of the MgcRacGAP-dependent GTPase pathway to regulate epigenetic centromere maintenance.

(**A**) HeLa cells were transfected with indicated siRNAs along with expression vectors. Cells 48 hr post transfection were fixed and stained with DAPI (DNA), CENP-B and CENP-A. Transfected cells were identified by fluorescence markers. Scale bar, 10 µm.

(**B and D**) Quantifications of normalized CENP-A integrated intensity per nucleus plotted as means ± SD overlaid with scatter plot. The p-value was computed using two tailed *t*-test. Control: n = 425, mDia2 siRNA: n = 260, mDia2 siRNA + FL-mDia2: n = 136, mDia2 siRNA + WT-FH1FH2-mDia2: n = 383, mDia2 siRNA + K853A-FH1FH2-mDia2: n = 151, mDia2 siRNA +

I704A-FH1FH2-mDia2: n = 158, mDia2 siRNA + W630A-FH1FH2-mDia2: n = 128, MgcRacGAP shRNA: n = 117, MgcRacGAP shRNA + WT-FH1FH2-mDia2: n = 88 from at least three independent experiments.

(**C**) Live cell imaging stills showing EGFP-FH1FH2-mDia2 nuclear localization during G1 phase upon anaphase onset (0 min). Scale bar, 10 μm.

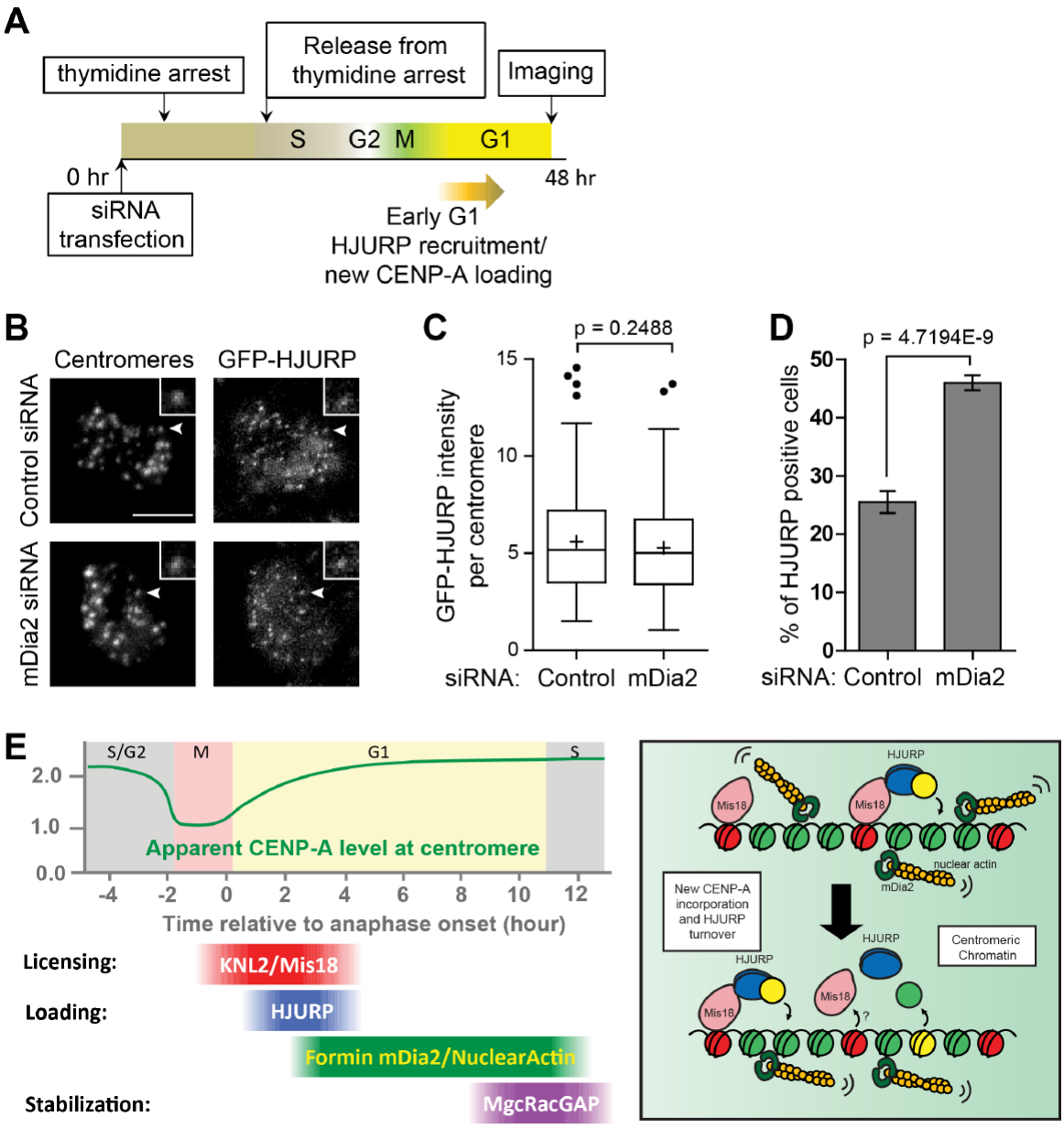

Figure 2.5. Depletion of mDia2 produces a prolonged HJURP localization at centromeres.

(A) Scheme for the siRNA transfection and the thymidine arrest to examine centromere localization of HJURP in early G1 cells.

(B) Immunofluorescence images of GFP-HJURP. Centromeres were identified using ACA antibodies. Scale bar, 5 μm (insets are 2× magnified).

(C) Whisker-Tukey boxplots show the relative intensity of GFP-HJURP foci at centromeres. The boxes span 25-75 percentile of the samples, while the center bar denotes median and the '+'

marks mean. Control: n = 174 centromeres from 26 cells and mDia2 siRNA: n = 183 centromeres from 20 cells. The p-value was computed using two tailed t-test.

(D) Mean percentage of GFP-HJURP centromere-positive cells with error bars showing standard deviations from three experiments (Control: n = 594 cells and mDia2 siRNA: n = 277 cells). The p-value was computed using two tailed z-test.

(E) Model of mDia2 regulating CENP-A loading. Left panel: time line of the epigenetic inheritance of CENP-A over cell cycle. Right panel: schematic model showing mDia2 to be important for HJURP-mediated CENP-A chromatin assembly and timely HJURP turnover.

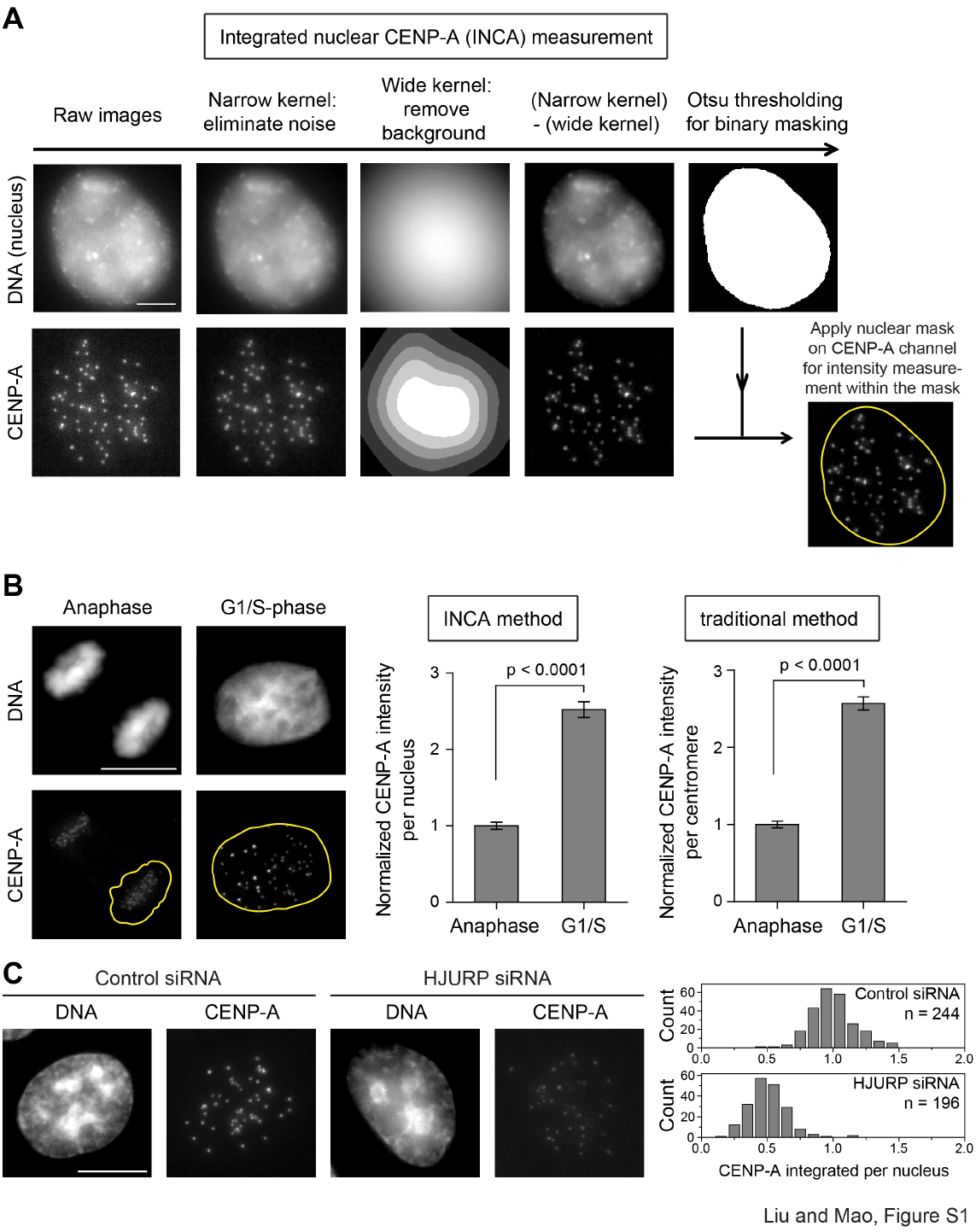

Figure S2.1. The Integrated Nuclear CENP-A (INCA) measurement.

(A) Automatic routine of the 'INCA' method based on a previous study (Lagana et al., 2010) with minor modifications. See Experimental Procedures for more details. Scale bar, 5 μm.

(B) A proof-of-principle application of the INCA method showing consistent conclusions with the traditional method when comparing centromeric CENP-A levels between anaphase and G1/S

phase cells (representative images with nuclear masks outlined in yellow). Quantification of the normalized CENP-A integrated intensity following the INCA method (means ± 95% confidence intervals). Anaphase: n = 156 and G1/S: n = 138 G1/S cells from three independent experiments. CENP-A levels are approximately doubled in G1/S compared to anaphase. This result is consistent with the quantification using the traditional method (means ± 95% confidence intervals). Anaphase daughter cells: n = 423 and G1/S cells: n = 529 single centromeres randomly measured from the same cells used in the INCA measurement. Scale bar, 10 μm. The p-value was computed using two tailed t-test.

(C) Another proof-of-principle application of the INCA method showing reduced CENP-A levels in cells depleted of HJURP. Histograms showing normalized CENP-A integrated intensity plotted from control (n = 244) and HJURP siRNA (n = 196) cells (from three independent experiments and $p < 0.0001$ by two tailed t-test). Scale bar, 10 μm.

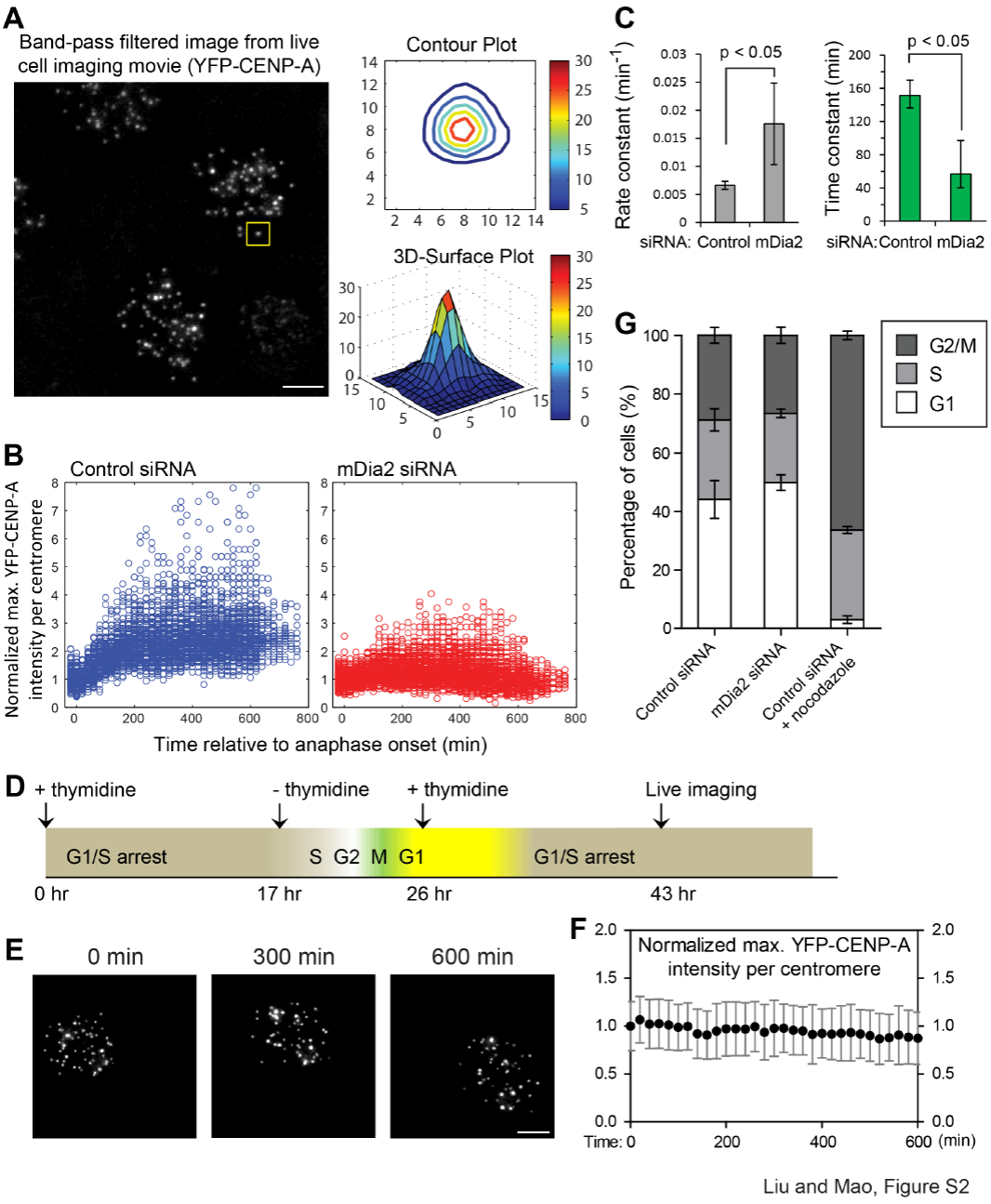

Liu and Mao, Figure S2

Figure S2.2. The method used for quantifying high resolution ratiometric live cell imaging data and details of nonlinear regression.

(A) YFP-CENP-A signals approximately follow Gaussian distribution at centromeres, making it reasonable to use local maxima for the measurement of centromeric CENP-A levels. Scale bar, 5 μm.

(B) Raw scatter plots of ratiometric CENP-A levels on individual centromeres, which were used for plotting mean ± SD in Figure 2B, in control cells and mDia2 siRNA treated cells.

(C) Bar graphs comparing the "apparent" rate constant and time constant between control cells and mDia2 siRNA treated cells. Apparent rate and time constants were computed from nonlinear regression using one phase association model. In total n = 4,100 centromeres from 12 G1 pairs for control and n = 4,310 centromeres from 13 G1-pairs for mDia2 siRNA cells were analyzed and plotted (means ± 95% confidence intervals).

(D) Scheme of thymidine synchronization and live imaging of G1/S cells with fully loaded CENP-A levels. This was designed to test for photobleaching over long term live cell imaging.

(E) Representative frames from live imaging movie of YFP-CENP-A in arrested G1/S cells. Imaging setup was identical as that used in Figure 2 and images were scaled on the same dynamic range over time. Scale bar, 5 μm.

(F) Quantification of centromeric YFP-CENP-A levels over time (plotted as mean ± SD). For every time point, 100 centromeres in 10 cells were measured from 2 repeated experiments (See Materials and Methods for more details).

(G) Depletion of mDia2 does not affect cell cycle. Quantification of the percentage of cells within each cell cycle stage (mean ± SD, n = 30,000 cells per treatment from three independent experiments). The univariate model was used for FACS data analysis(Watson JV et al., 1987). The p-value was computed by two tailed t-test. G1 (Control vs mDia2 siRNA) $p = 0.2254$, G1 (Control vs Control + nocodazole) $p = 0.0004$, S (Control vs mDia2 siRNA) $p = 0.2007$, S (Control vs Control + nocodazole) $p = 0.2031$, G2/M (Control vs mDia2 siRNA) $p = 0.3782$, G2/M (Control vs Control + nocodazole) $p < 0.0001$.

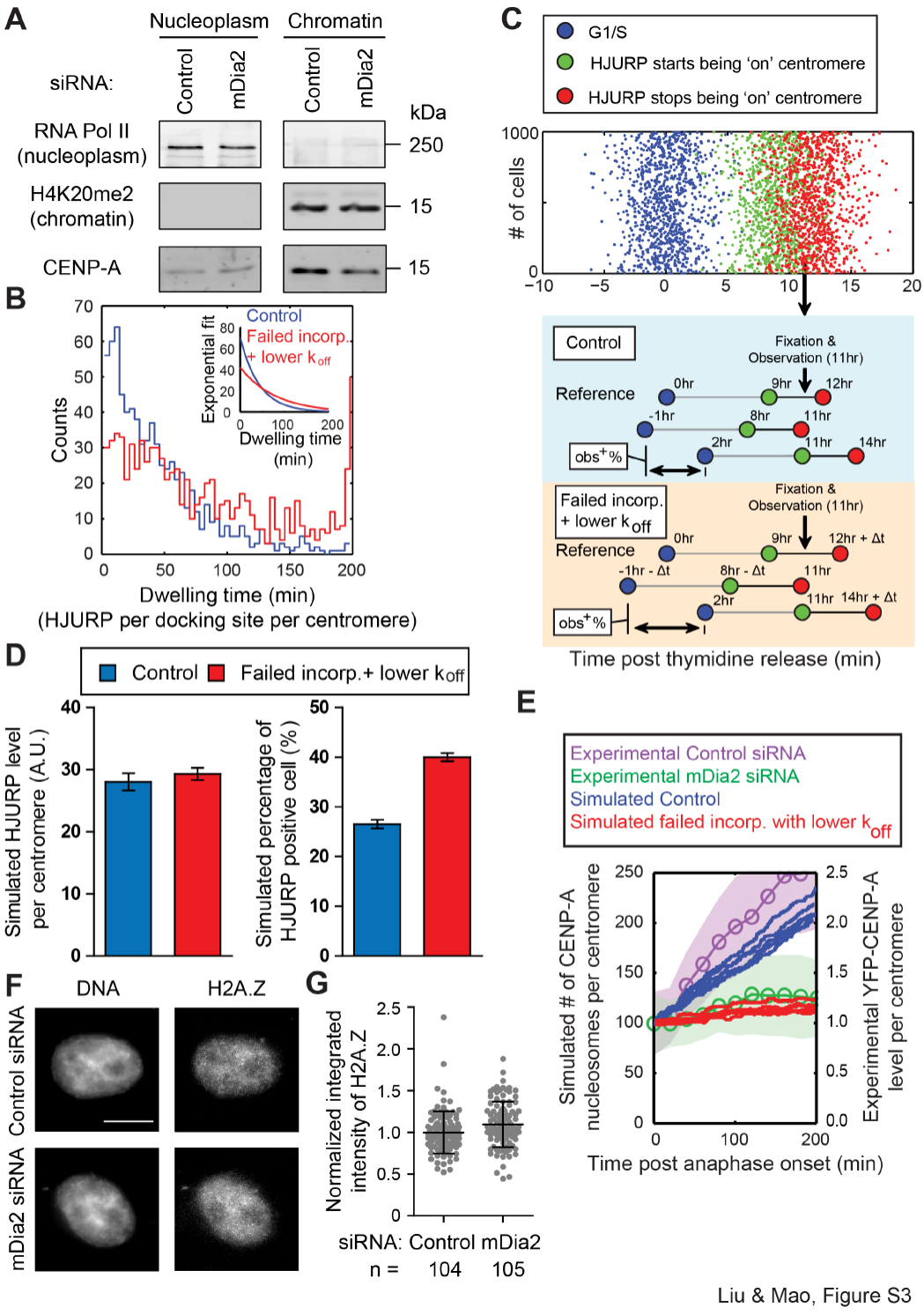

Figure S2.3. Stochastic simulation of HJURP turnover at G1 centromeres.

(A) Pair-wise immunoblots showing relative levels of nucleoplasmic and chromatin-bound CENP-A proteins in control cells and cells depleted of mDia2.

(B) Histograms of the distribution of single dwelling events per docking site per centromere. Exponential fits were given as inset. For control and perturbed conditions: n = 761 and n = 855, respectively (pooled from 3 simulations).

(C) Scatter dot plot of key 'points' of time lines from synchronized cell (a control condition's plot is given for demonstrative purpose). Blue points are the starts of each simulated time line. 'Green point' and 'red point' represent the start and end of HJURP association, respectively. The duration for each cell to be documented as 'HJURP positive' cell is the distance between cognitive green and red points, represented by the black bars in the schematics. All cells with their 'red point' before the observational point (arrow, 'Fixation & Observation'), and all cells with their 'green point' after the observational point, will not be documented as 'HJURP positive' cells. The percentage of observed 'HJURP positive' cells (obs + %) can then be calculated based on these criteria. See Materials and Methods for more details.

(D) Left panel: simulated HJURP levels per centromere (mean ± SD). Data were plotted using measurements from 10 random positions inside the 'HJURP positive' time window per simulation, 3 simulations in total. Right panel: simulated percentages of 'HJURP positive' cells in control or perturbed populations with one round of thymidine synchronization (mean ± SD). Percentage values were calculated from 40 independent simulations, 2000 cells each.

(E) Simulated 'loading curves' of the number of CENP-A nucleosomes per centromere overlaid with experimental measurements shown in Figure 2. For each condition, 6 representative simulation traces were plotted. For experimental data, mean ± SD were shown.

(F) Immunofluorescence detection of histone H2A.Z 48 hr post transfection of indicated siRNAs (DNA - DAPI). Transfected cells were identified by fluorescence co-transfection markers. Scale bar, 10 μm.

(G) Quantification showing the distribution of normalized H2A.Z integrated intensity per nucleus (mean ± SD overlaid with scatter plots). Control: n = 104, mDia2 siRNA: n = 105 cells from two independent experiments.

Chapter Three: Diaphanous formin mDia2 bridges small GTPase signaling with nuclear environment to regulate stable CENP-A loading at the centromere

Abstract

The epigenetic determination of centromeric chromatin in higher eukaryotes depends on CENP-A, a centromere-specific histone H3 variant. Due to quantitative dilution of CENP-A during chromatin replication, new CENP-A assembles into centromeres at G1 phase to maintain the epigenetic mark. The stable incorporation of new CENP-A at the centromere is not well understood. We have discovered that a cytoskeletal regulator, diaphanous formin mDia2, is essential in maintaining CENP-A levels at the centromeres. Using quantitative imaging, here we determined the temporal requirement for the MgcRacGAP-dependent small GTPase signaling during CENP-A loading, and show that endogenous mDia2 acts downstream of the MgcRacGAP-dependent small GTPase pathway to ensure stable loading of CENP-A in early G1-phase. This function of mDia2 requires its actin nucleation activity, and dynamic actin filaments observed in early G1 nuclei depend on mDia2. Indeed, in the absence of nuclear actin pool, a polymerizable actin protein reintroduced into the nucleus, but not its non-polymerizable counterpart, could restore centromeric CENP-A levels. Particle tracking of centromere movement in early G1 nuclei revealed subdiffusive motion, a characteristic behavior significantly impaired in the absence of mDia2. Thus our findings suggest the nuclear diaphanous formin mDia2 forms a link between upstream small GTPase signaling and the downstream nuclear environment in order to promote the stable assembly of new CENP-A nucleosomes at the moving centromeres.

Introduction

Epigenetic inheritance of chromosomal landscapes in eukaryotes is often regulated by signaling inputs as well as nuclear environment[171-176]. As a fundamental landscape essential for accurate partitioning of chromosomal materials during mitotic cell division, centromeres are defined epigenetically by the histone H3 variant centromere protein A (CENP-A) containing nucleosomes[13]. In order to ensure stable inheritance of centromere identity over generations of cell divisions, the centromere marker CENP-A manages to replenish its own levels at each centromere in every cell cycle to compensate for the quantitative dilution caused by centromeric chromatin replication[4]. A number of important signaling pathways have been identified underlying the initiation and execution of recruiting newly synthesized CENP-A molecules to the centromeres[46-48,52-54]. Nevertheless, a complete understanding is pending regarding how new CENP-A become stably incorporated into the centromeric nucleosomes.

Recent work have identified a small Rho GTPase signaling pathway essential for stable maintenance of CENP-A levels at the centromeres. Depletion of the GAP, MgcRacGAP, as well as its downstream small GTPases Cdc42 and Rac1, results in 50% reduction of centromeric CENP-A levels[50]. We recently found that the mammalian diaphanous formin mDia2 – a cytoskeleton regulator and well-studied small GTPase effector – is also required for new CENP-A loading at G1 centromeres[177], thus positioning itself as a potential effector of the MgcRacGAP-dependent molecular switch in stabilizing newly loaded CENP-A[178]. However, it remains to be tested whether and when endogenous mDia2 acts downstream of the MgcRacGAP signaling pathway in regulating the stable incorporation of new CENP-A at centromeric

nucleosomes. It has also been recently reported that formin proteins, well known for their ability to regulate the actin and microtubule cytoskeletons in the cytoplasm[124], could have unappreciated novel functions inside the nucleus. The diaphanous formin mDia2 for instance can translocate from the cytoplasm to the nucleus[94,137] and bind to a growing list of nuclear proteins including histones and topoisomerases with its FH2 domain, characteristics not shared by the other members of the diaphanous family[138]. Inside the nucleus, diaphanous formin mDia2 can nucleate filamentous actin polymers. The roles of actin filaments regulating the dynamics environment inside somatic cells' nuclei are beginning to emerge, with newly identified functions in the repair of double-strand DNA breaks[97], interactions with chromatin remodeling complexes[179,180], and crosstalk with important epigenetic enzymes[181]. It is therefore intriguing to ask whether and how nuclear actin polymerized by mDia2 could directly contribute to CENP-A assembly at centromeric chromatin.

Using quantitative imaging and epistatic analysis, here we provide temporal evidence that endogenous diaphanous formin mDia2 functions downstream of the MgcRacGAP-dependent small GTPase signaling pathway in early G1. By polymerizing filamentous nuclear actin, mDia2 is required for the relatively confined centromere movement when the stable incorporation of new CENP-A molecules occur. Combined evidence from our study indicates a unique role of mDia2 in bridging upstream small GTPase signaling and downstream nuclear environment during stable CENP-A loading at the moving centromeres in early G1 phase.

Results

Endogenous mDia2 acts downstream of the MgcRacGAP-dependent GTPase signaling pathway to ensure ordinary CENP-A levels at centromeres

To test whether endogenous mDia2 functions downstream of the MgcRacGAP-depdent small Rho GTPase molecular switch, we introduced exogenous fragment of the Dia autoinhibition domain (DAD) of mDia2 into cells depleted of MgcRacGAP. DAD fragment can bind to the Dia interacting domain (DID) of endogenous mDia2 with high affinity, thus ectopically opens up the otherwise auto-inhibited endogenous mDia2 due to a lack of small Rho GTPase binding to the GTPase binding domain (GBD) at the N-terminus (**Figure 3.1A**)[182,183]. A point mutation (L1168G) was introduced to the NES-like motif of DAD such that this fragment shifts its cytosolic distribution into the nucleus[94,137]. Another point mutation (M1141A) at the core of DAD abolishes its interaction with DID[184], thus the combination of L1168G and M1141A serves as an 'incactive' control (**Figure 3.1B**). As expected, centromeric CENP-A levels were significantly reduced upon knocking down MgcRacGAP. Importantly, the decrease of CENP-A levels can be rescued by co-expressing DAD-L1168G, but not the DAD-L1168G-inactive fragment (**Figure 3.1 C and D**). Because the DAD fragment per se is not necessary for restoring centromeric CENP-A levels upon depleting endogenous mDia2[177], the results here strongly suggest an epistatic relationship between upstream small GTPase signaling and downstream endogenous mDia2 in maintaining CENP-A levels at the centromeres.

MgcRacGAP is required for apparent CENP-A loading in early G1

The epistasis between MgcRacGAP and endogenous mDia2 prompted us to examine more closely of the temporal requirement of the MgcRacGAP-dependent small GTPase pathway during CENP-A replenishment. Despite an apparent centromere enrichment of MgcRacGAP toward the end of G1[50], depleting MgcRacGAP caused a defective CENP-A loading in live cells going through early G1 phase. High resolution ratiometric live cell imaging demonstrated that, in the absence of MgcRacGAP, the increase of YFP-CENP-A levels at individual centromeres cannot be maintained despite an initial slight increase within 2 h after anaphase onset (**Figure 3.2 A and B; Movie S1**). Non-linear regression using a first-order reaction model predicted substantially lower plateau (maximum) loading amount as well as higher rate constant, consistent with attempted yet failed loading behaviors (**Figure 3.2C**). These data are in agreement with the phenotype caused by mDia2 depletion, thus by revealing the temporal requirement of the MgcRacGAP-dependent small GTPase pathway, support the epistatic relationship between MgcRacGAP and mDia2 in early G1-phase.

Short and dynamic actin filaments in G1 nuclei require mDia2

To understand how mDia2 regulates CENP-A loading in early G1, we went on to test if actin polymerization activity in full length mDia2 is required for its function in stable CENP-A assembly. Similar to the point mutation for actin nucleation activity in the constitutively active mDia2-FH1FH2 fragment[126,177], K853A mutation in full length mDia2 failed to restore the decreased CENP-A levels at centromeres upon depleting endogenous mDia2 (**Figure S3.1**). Next, to examine if there are nuclear actin polymers inside G1 nucleus during CENP-A loading, an utrophin-based nuclear actin probe, Utr230-EN[96], was transiently expressed in synchronized HeLa cells transfected with mDia2 or GAPDH (control) siRNA (**Figure 3.3A**). Live cell

imaging revealed that about 40% of control G1 cells showed dynamic and short nuclear actin filaments as measured by the utrophin probe, with a typical "nuclear puncta" pattern. In contrast, the percentage of cells with nuclear puncta pattern was significantly reduced upon mDia2 depletion (**Figure 3.3 B and C; Movie S2**). This result confirms the existence of short and dynamic nuclear actin in early G1 cells, dependent on mDia2.

Actin polymerization inside the nucleus is important for stable maintenance of CENP-A levels at the centromeres

To further test the possibility that filamentous nuclear actin polymerized by nuclear mDia2 directly participates in the regulation of stable CENP-A incorporation, we set out altering the pool of actin inside the nucleus. Importin 9 has been shown to be the essential importin responsible for shuttling actin monomers into the nucleus[93]. Depleting IPO9 depletes the pool of actin proteins inside the nucleus, but doesn't change the total amount of YFP-CENP-A or untagged CENP-A proteins, nor does it alter the relative distribution of CENP-A proteins in the cytoplasm or nucleoplasm upon cellular fractionation (**Figure 3.4B, S3.2A**), therefore ruling out potential side effects on the expression or distribution of new CENP-A proteins (**Figure 3.4 A and B**). Given this opportunity to evaluate only the 'loading' machineries of CENP-A at centromeres, we expressed NLS-tagged actin constructs that accumulate in the nucleus independent of IPO9[97], and asked the question: is actin polymerization important for CENP-A level maintenance at the centromeres (**Figure 3.4C**)? Significantly, the wild type, polymerizable actin tagged with NLS can restore the reduced CENP-A levels upon IPO9 depletion; however, the nonpolymerizable[185], R62D mutant of actin cannot rescue the phenotype (**Figure 3.4 D and E**), suggesting that actin polymerization inside the nucleus is essential for the stable maintenance of CENP-A levels at centromeres. Moreover, a meshwork of filamentous actin filaments at close

proximity to centromeres were observed in cells expressing the wild type NLS-actin, but not the R62D-actin (**Figure S3.2B**).

Centromere movement is relatively confined during new CENP-A loading time

Dynamic and short nuclear actin filaments can potentially regulate nuclear events by providing mechanical inputs that either actively transport cargos or help organize nuclear contents. Upon telomere damage, it has been shown that telomere movement is enhanced, which is likely to facilitate DNA repair[186-188]. To test whether mDia2-mediated nuclear actin polymers affects centromere movement during the time new CENP-A is being loaded, single particle tracking of centromere movement was performed in early G1 nuclei by imaging HeLa cells stably expressing YFP-CENP-A at relatively high sampling frequency (**Figure 3.5A** and **Movie S3**). Trajectories of these loci displayed relatively confined movement (**Figure 3.5B**), with anomalous diffusion over the time range of initial CENP-A loading in early G1, about 25 - 200 min post anaphase onset (**Figure S3.3C**). The confined centromere motion, however, is significantly impaired upon mDia2 knockdown (**Figures 3.5A, 3.5B, S3.3**), with an increase in relative apparent diffusion coefficient by 22.1% (**Figure 3.5D**). In particular, long range centromere movements over the scale of several microns were occasionally observed in mDia2 knockdowns but not in control cells (**Figure S3.4; Movie S3**). Thus, the formin mDia2 is required for the relatively confined movement of centromeres at the time scale of CENP-A loading in early G1. Furthermore, intensity profiling of individual tracks showed that the relative YFP-CENP-A loading ratio in control cells were 27.4% higher than that in mDia2 knockdown cells (**Figure 3.5, C and D**), supporting the earlier observations that the mDia2 protein is essential for new CENP-A deposition.

Long term depletion of nuclear mDia2 generates chromosomal phenotype consistent with centromere dysfunction

Although the CENP-A loss upon depleting mDia2, MgcRacGAP or IPO9 only go as much as 50% reduction after approximately one round of cell cycle, it has been demonstrated that continued failure in CENP-A replenishment will ultimately lead to substantial loss of centromere identity and kinetochore function – reasons sufficient to cause errors in mitotic chromosome segregation. Due to serial dilution of residual cetromeric CENP-A, such continued failure could take as long as 5 consecutive days to show chromosomal phenotypes[75]. To test the long term consequences of defective CENP-A loading upon mDia2 depletion, we performed co-transfection to strategically replace endogenous mDia2 with either wild type or full length ΔNLS mutant of mDia2 (**Figure 3.6A**). Importantly, the full length ΔNLS-mDia2 construct did not cause higher index of binuclear cells than the wild type mDia2 construct, indicating that cytokinesis failure was not a major issue in our long term replacement (**Figure S3.5**)[162]. After 5 days, mitotic cells were well synchronized to score the metaphase chromosome alignment. Remarkably, the percentage of fully aligned chromosomes in wild type mDia2 expressing cells was indistinguishable from control group, while that in the ΔNLS-mDia2 expressing cells was significantly lower. Meanwhile, interphase nuclear morphology was compared between the two groups and cells expressing ΔNLS-mDia2 have significantly higher percentage of micronuclei. Thus, a significantly higher indices of misaligned chromosomes in metaphase and micronuclei in interphase following long term depletion of nuclear portion of mDia2 are consistent with centromere dysfunction caused by the loss of centromere identity.

Discussion

Faithful transmission of chromosomes during cell division requires the stable maintenance of centromeres, whose identity are epigenetically defined by a finite number of CENP-A-containing nucleosomes at each centromere[42]. Genome replication in S-phase and subsequent chromosome segregation in mitosis reduce the copy numbers of existing CENP-A-containing nucleosomes by half, thus the epigenetic landmark at each centromere needs to reload itself every time the cell goes from mitosis to the next G1-phase. Loading of new CENP-A at G1 centromeres requires release from inhibition signals from CDK[52], initiation signals from Plk[53], assembly of licensing factors at anaphase onset[35,46], recruitment of new CENP-A molecules for nucleosome assembly by its chaperone HJURP[36], and presumably a maintenance step using a small Rho GTPase molecular switch whose downstream effector remained to be tested. Notably, it has been suggested that the GAP responsible for the molecular switch, MgcRacGAP, only starts to have obvious centromere localization until late G1 (the earliest as 6 hours post anaphase onset)[50]. By contrast, mDia2, a candidate effector cytoskeletal regulator of the MgcRacGAP-dependent pathway, has been shown to be important for loading of new CENP-A in early G1 (around 2 hours post anaphase onset)[177]. To address this obvious discrepancy, we performed ectopic induction of endogenous mDia2 in the background of MgcRacGAP depletion, as well as direct live imaging for YFP-CENP-A loading kinetics in the absence of MgcRacGAP. Importantly, our results strongly support an epistatic relationship between MgcRacGAP and mDia2, and revealed that the requirement for MgcRacGAP in YFP-CENP-A loading already occurs in early G1 (around 2 hour post anaphase onset). One possibility is that low levels of MgcRacGAP already resides at early G1 centromere before its fluorescence signal becomes apparently detectable to regulate the small Rho GTPase signaling, which then communicates to downstream mDia2 to ensure stable incorporation of new CENP-A. Accordingly, centromeric

localization of MgcRacGAP at later G1 could potentially represent a separate step whose exact function remains to be identified.

In addition to the connections to upstream signaling pathways, our data also provided evidence that mDia2 mediated nuclear actin polymerization could be important to the nuclear environment during stable CENP-A loading at the moving centromeres in early G1 phase. It has been demonstrated recently that nuclear actin polymers are required for efficient clearance of DNA double-strand breaks (DSB), through an mDia1/2-independent but Formin-2 (FMN2) dependent mechanism[97]. Apart from the differed families of formin proteins in these processes, the polymerized nuclear actin we observed in G1 cells have different morphology than those observed upon DNA damage. On the one hand, this underlines the diversified use of nucleators for actin polymerization involved in differed chromosomal pathways; on the other hand, because it has been suggested that CENP-A can be recruited to double-strand DNA breaks[189], it might be interesting to test potential links between centromere maintenance and DSB repair, especially with regard to nuclear actin.

The functional roles of filamentous actin inside the nucleus are just beginning to emerge. Broadly speaking, it has been debated whether actin polymerization inside the nucleus functions by simply depleting the monomer pool, or by contrast, actually does mechanical work with the polymerized filaments. The first hypothesis is supported by the observation that actin polymerization inside the nucleus release the inhibitory effect of monomeric actin on MAL (megakaryocytic acute leukemia protein), a cofactor for the transcriptional factor SRF (serum

response factor)[94,95]. However, monomer removal seemed not to be the reason behind the role of nuclear actin polymerization in CENP-A loading. If monomer removal is the main function of G1-actin filaments formation concurrent with CENP-A loading, depleting IPO9 (by which both monomeric and polymeric actin are removed) would not phenocopy filament inhibition (by depleting mDia2), with regard to CENP-A levels at the centromere. Meanwhile, the fact that the NLS-tagged polymerizable actin, but not its nonpolymerizable counterpart, restored CENP-A levels strongly suggests it is the filament specific functions that participate in regulating stable CENP-A maintenance. It didn't escape our notice that mDia2 depletion could cause indirect transcriptional effects through the SRF pathway, and this will be discussed further in Chapter five of the thesis.

Short and dynamic nuclear actin filaments can potentially regulate nuclear processes through two major mechanisms: (a) modulating the mobility or organization of chromatin; (b) delivering other assembly factors essential for CENP-A loading, or sequestering inhibitory factors that would otherwise suppress CENP-A loading. These two scenarios are not mutually exclusive. While a sequestering role is consistent with a lack of obvious colocalization of either mDia2 or nuclear actin filaments at the centromeres, further biochemical experiments are needed to examine potential interactomes of mDia2 as well as filamentous nuclear actin in G1 nuclei. A role in delivering assembly factors is inconsistent with the fact that at least the recruitment of HJURP at G1 centromeres is not affected upon mDia2 depletion[177]. Finally, a role in regulating the movement or spatial organization of chromosmes/chromatin is supported by the apparent change in the sub-diffusive motion of centromeres upon mDia2 knockdown, correlated with defective CENP-A loading. The sub-diffusive motion itself is consistent with the hypothesized

local reaction chambers that greatly enhance chemical efficiency[190]. Physically, this phenomenon is consistent with relatively stable chromosome territories[191] and the fractal globule model[192] under ordinary conditions. Indeed, we have observed several long range centromere movements in mDia2 depleted cells. Whether this reflects global rearrangement of chromosome territories in mDia2 knockdown cells remains to be investigated in the future.

Given our combined results, we suggest that nuclear actin polymerized by formin mDia2 contributes to the physical confinement of early G1 centromeres which is pivotal to ensure the chemical reactivity of stable CENP-A loading. The diaphanous formin mDia2, in turn, serves as a link between upstream small GTPase signaling and the downstream viscoelastic nuclear environment to regulate the stable marking of centromere's epigenetic identity (**Figure S3.6**).

Materials and methods

Constructs, siRNA sequences and antibodies

The construct of GFP-myc-DAD[182,184] was used as the template to make all DAD constructs in this study. NLS-flag-tagged actin[185] were kind gift from the Grosse Lab (University of Marburg) and was used as template to make the constructs used in this study. Utr230-EGFP-NLS was a kind gift from Dyche Mullins (UCSF). Full length K853A-mDia2 was generated based on the full length WT-mDia2 (plasmid 54158, Addgene), a kind gift from Michael Davidson. Site directed mutagenesis was performed to generate the mutants, using QuikChange Lightning following manufacturer's instructions. The shRNA against MgcRacGAP was MISSION shRNA plasmid DNA from Sigma (clone NM_013277.2-456s1c1). The siRNA oligos used in this study were the same as those described before, except siRNA against IPO9 (s31299, SilencerSelect siRNA from ThermoFisher). Primary antibodies used in this study include: rabbit anti mDia2 (Watanabe et al., 2008), mouse anti CENP-A (Ab13939, Abcam), mouse anti tubulin (T6199, Sigma), chicken anti GFP (Ab16901, Millipore), rabbit anti MgcRacGAP (Ab61192, Abcam), rabbit anti Flag (F7425, Sigma), rabbit anti IPO9 (Ab124710, Abcam), and rabbit anti H4K20me2 (Ab9052, Abcam).

Cell culture, transfection, and drug treatment

HeLa cells were used for most of the quantitative imaging experiments in this study. A HeLa cell line stably expressing YFP-CENP-A was used for high-resolution ratiometric live cell imaging. Cells were maintained in DME medium supplemented with 10% FBS (complete growth medium) at 37°C in 5% CO2. The transfection of siRNAs was performed with Hiperfect

(Qiagen) or DharmaFECT DUO (Dharmacon) following the manufacturers' protocols. For co-transfection experiments, siRNAs were transfected with at least 20-fold molar excess to marker plasmids encoding fluorescent proteins. Control cells were transfected with GAPDH siRNA. All knockdowns were confirmed by immunoblotting analysis. Cells were fixed for immunostaining or imaged 48 hours after transfection. Thymidine synchronization was performed with 2 mM thymidine in complete growth medium for at least 17 hr, washed twice in pre-warmed PBS, and released into complete medium supplemented with 24 μM deoxycytidine (for 9 hr before entering mitosis). Monastrol was used at 100 μM, MG132 was used at 10 μM. All drugs were purchased form Sigma-Aldrich.

Quantitative fixed cell imaging and automated image analysis

Immunofluorescence and fixed cell imaging, as well as quantitative image processing using the INCA method were performed as previously described[177].

High resolution ratiometric live cell imaging and automated image analysis

Live cell imaging was performed as previously described[177]. Quantitative analysis of single centromereic YFP-CENP-A movies were conducted in MATLAB using custom code, with part of the measurement dependent on the mixed-model Gaussian fit in μ–track (Gaudenz Danuser Lab and Khuloud Jaqaman Lab, UTSW)[193]. Briefly, single centromeric foci of fluorescence were automatically detected and processed for local maxima measurement as a reasonable estimate for YFP-CENP-A level at each centromere. All centromeric foci' intensity were then normalized against the 'unloaded' frame's intensity and averaged for every time point in one

single cell, in order to generate a time-lapse averaged intensity profile for each cell (Figure 2B). Multiple cells' time-lapse intensity traces were finally pooled for statistical analysis.

Cell fractionation and immunoblotting analysis

Cell fractionation and immunoblotting analysis were performed as previously described[177], except that cellular fractionation only separated the cytoplasmic fraction and the nuclear pellet.

Live imaging of centromere movement, single-particle tracking and analysis

With the same wide-field microscopy setup as described before, HeLa cells stably expressing YFP-CENP-A were imaged from metaphase to early G1 every 5 min, across 11 z-sections 1 μm apart at every time point[194]. Maximum z-projections were generated for each time point in the movie, based on which single-particle tracking and analysis was performed, using primarily the MATLAB based software μ–Track (Jaqaman et al., 2008). Only cells that survived at the end of movie and those without obvious nuclear rotation are included in our analysis. The frame at 25 min post anaphase onset, when most cells have their centromeres spread out well enough while largely remaining unloaded of CENP-A, was considered the beginning of each track. Approximately 36 frames spanning the 25 min to 200 min window were subjected to Gaussian mixture-model fitting to detect the coordinates of centromeres at sub-pixel resolution. Coordinates of centromeres at each frame were then subjected to drifting correction, following the equations below, for any given centromere at time point (i):

$$X_i' = X_i - \frac{\sum_1^N X_i}{N}$$

$$X_i' = X_i - \frac{\sum_1^N X_i}{N}$$

Where *N* is the total number of centromeres at time point *i*, X_i and Y_i are raw coordinates per centromere at time point *i*, X_i' and Y_i' are updated coordinates corrected for global drifting. This way global long-range movement of the whole cell is eliminated so that only the motion inside the nucleus relative to the cell is reflected as a change of coordinates. Reverse tracking was performed using the adjusted coordinates with default parameters in μ–track. Trajectory analysis was performed upon the resultant tracks using μ–track[193,195] with tracks whose lengths are at least 20 frames (Figure S3B), following the principles below:

$$\mu_{v,l}(\Delta n) = \frac{1}{M_l - \Delta n} \sum_{n=0}^{M_l-\Delta n-1} |x_l(n+\Delta n) - x_l(n)|^v$$

Where $x_l(n)$ is the position vector on trajectory l at time $n\Delta t$ for n = 0, 1, 2, 3 …, M_l-1. M_l is the total number of positions in the trajectory l . Δt is the true time interval between frames. $\mu_{v,l}(\Delta n)$ is the moment of order *v* for a given shift spanning *n* frames, consistent with a time shift δt = ΔnΔt. Euclidean distance is denoted by |…|. In particular, the condition where v = 2 is Mean Square Displacement (MSD). Because each moment is dependent on the time shift following a power law,

$$m_n(\delta t) \propto \delta t^{\gamma v}$$

The scaling coefficient was then computed with least-square linear regression of log(m_n) as a function of log(δt). A similar MSD analysis was also conducted[196] which led to the same conclusions (data not shown). Notably, in the ensemble MSD curve (Figure S5C), only the first

25% of the curve were subjected to least-square linear fit[197]. (Figure S3A). Relative apparent diffusion coefficients were computed using μ–track, in arbitrary unit.

To quantify the change of intensity over time for each track, relative YFP-CENP-A loading ratio was defined as follows, in order to reflect the levels of CENP-A loading during an early time window of G1:

$$LR = \frac{\sum_{90\ min}^{140\ min} I(t)}{N \cdot Med}$$

Where *LR* is the YFP-CENP-A relative loading ratio, *I(t)* is the intensity at time point (t) post anaphase onset, *N* is the total number of frames with intensity information between 90 min and 140 min, '*Med*' is the median value of all tracks' intensity values within the first two frames (25min, 30min). The range 90-140 min was empirically chosen so that the maximum initial loading capacity is captured prior to inevitable fluorescent quench near the end of the movies. We understand that this algorithm may underestimate the actual loading ratio, yet nevertheless believe this is the best way to stringently reveal any differences in loading capacity in early G1. '*Med*' was determined to be a robust point estimate of common intensity of all tracks prior to most CENP-A loading (this estimate is necessary as not all tracks were detectable in the first two frames, making it otherwise impossible to compute the ratio).

Visualizing nuclear actin short filaments with Utr230-EN probe in G1 cells

Schematic procedure is summarized in **Figure 3A**. Briefly, cells were co-transfected with siRNA and mCherry vector (co-transfection marker) 48 hr prior to imaging, following aforementioned general transfection procedures. Upon releasing from the thymidine arrest (–about 12 hr prior to

imaging), cells were transfected with Utr230-EN using the DharmaFECT Duo transfection reagent following manufacturer's instructions. Live imaging was performed as described above for "high resolution retiometric live cell imaging", with some minor modifications: only single Z-section was imaged, and the movie was taken every 2 sec. An additional 1.6x optical magnifier was used. Cells containing both mCherry (indicator of siRNA transfection) and Utr230-EN were documented as short movies and categorized based on the patterns of spatiotemporal dynamics of the Utr230-EN probe. Three categories of patterns were observed: nuclear punctate, nuclear diffusive and cytoplasmic aggregate. The nuclear punctate pattern distinguishes itself from nuclear diffusive pattern by multiple small fast-moving particles inside the nucleoplasm (**Movie S2**).

Statistical analysis and plotting

All statistical analyses were performed with GraphPad Prism 5 (GraphPad) using unpaired, two tailed t-test between groups unless noted otherwise (e.g. z-test with MATLAB to compare two sample proportions). All plots were prepared in Prism (GraphPad) or MATLAB (MathWorks, R2015b). Control groups and mDia2-depleted groups in all experiments were pooled together after normalization and presented.

Acknowledgements

We thank all members of the Mao laboratory for stimulating discussion. We thank Francesca Bartolini for insight on the project. We thank Richard Vallee, Fred Chang, Julie Canman and Abby Dernburg (UC Berkeley) for inputs on the project and Dyche Mullins (UCSF) for reagents. We are also grateful to Yu He (Stanford), Yan Wang (Microsoft) and David Odde (U Minnesota) for insightful discussions on physics and computational sciences. This work has been supported by grants from the National Institute of Health (GM89768) to Y.M.

Abbreviations

CENP-A, Centromere protein A; DAD, Dia autoinhibition domain; DID, Dia interacting domain; GBD, GTPase binding domain; FH, formin-homology domain; MgcRacGAP, male germ cell Rac GTPase-activating protein; NLS, nuclear localization signal; NES, nuclear exporting signal; INCA, integrated CENP-A intensity per nucleus.

Figures

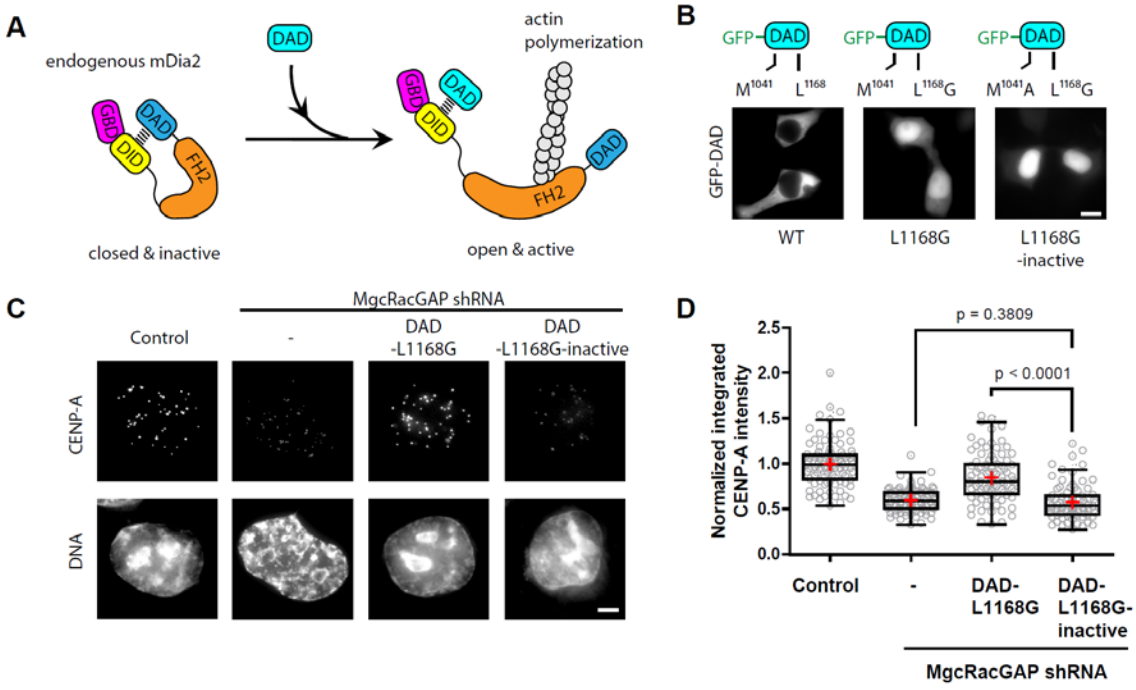

Figure 3.1. Ectopic activation of endogenous mDia2 restores centromeric CENP-A levels in the absence of MgcRacGAP

(A) Schematics showing that exogenous Dia autoinhibition domain (DAD) fragment of mDia2 can bind to the Dia interacting domain (DID) of endogenous mDia2 and enable its actin polymerization activity even in the absence of Rho GTPase binding to the GTPase binding domain (GBD) of endogenous mDia2.

(B) Engineered DAD localization in the nucleus. Wild type DAD fragment is excluded from the nucleus and a point mutation, L1168G, in a NES-like motif caused its nuclear accumulation. M1041A is a mutation in the core region that makes the DAD fragment unable to stimulate endogenous mDia2 activation. Scale bar, 10 µm.

(C) Ectopic induction of endogenous mDia2 with DAD-L1168G rescues reduced CENP-A levels caused by MgcRacGAP depletion. Representative immunofluorescence images showing CENP-A levels at centromeres. DNA are stained with DAPI. Scale bar, 5 µm.

(D) Quantification of the normalized CENP-A integrated intensity per nucleus using Whisker-Tukey boxplots overlaid with scatterplots. The boxes span the 25th to 75th percentile of the data, whereas the center bar denotes the median and the + marks the mean. n = 95 (Control), 96 (MgcRacGAP shRNA), 91 (MgcRacGAP shRNA + DAD-L1168G), 82 (MgcRacGAP + DAD-L1168A-inactive) cells. The p-values were computed using two-tailed *t* test.

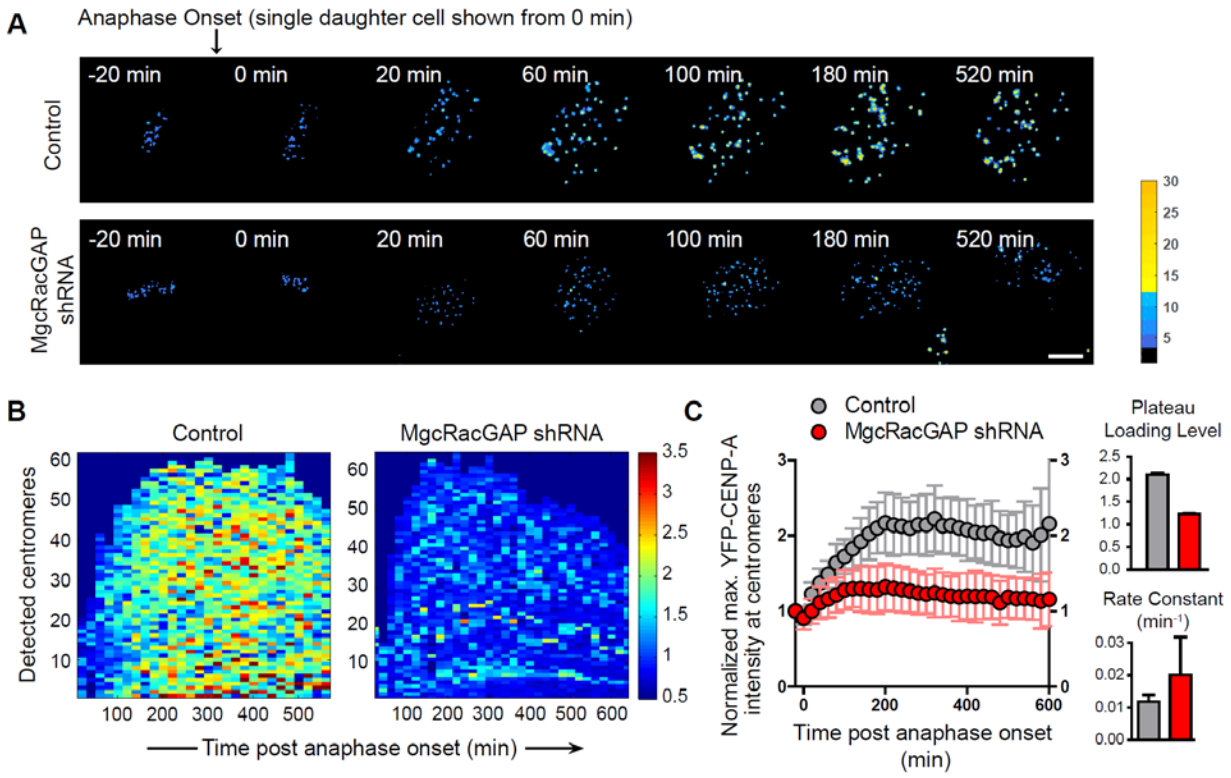

Figure 3.2. MgcRacGAP depletion causes defective CENP-A loading in early G1

(A) High-resolution ratiometric live-cell imaging showing unsuccessful YFP-CENP-A loading in early G1 upon MgcRacGAP depletion. The first frame after anaphase onset were aligned to be time point 0 min, and only one of two daughter cells was shown in each panel after anaphase onset. Identical lookup table was used over time for both control and MgcRacGAP knockdown. Warmer pseudo-color shows higher levels of centromeric YFP-CENP-A. Scale bar, 5 μm.

(B) Time-lapse heat map showing the intensity of YFP-CENP-A at each single centromere automatically detected over time in the control and MgcRacGAP depleted cells shown in (A). Each colored box represents one single centromere, the color of that box coded based on the normalized intensity of that centromere at that particular time point. Due to low sampling frequency, a horizontal trace in the plot may not necessarily indicate the track of the same centromere over time.

(C) (Left) Quantification of centromeric YFP-CENP-A levels during G1 phase. Thousands of centromeres from ten cells over the whole time course in either control of MgcRacGAP knockdown were clustered into each cell's average trace before being plotted as ensemble average ± 95% confidence intervals. (Right) Bar graphs (mean±SE) showing the plateau loading levels of YFP-CENP-A and the rate constants resultant from nonlinear regression of the raw data plotted on the left.

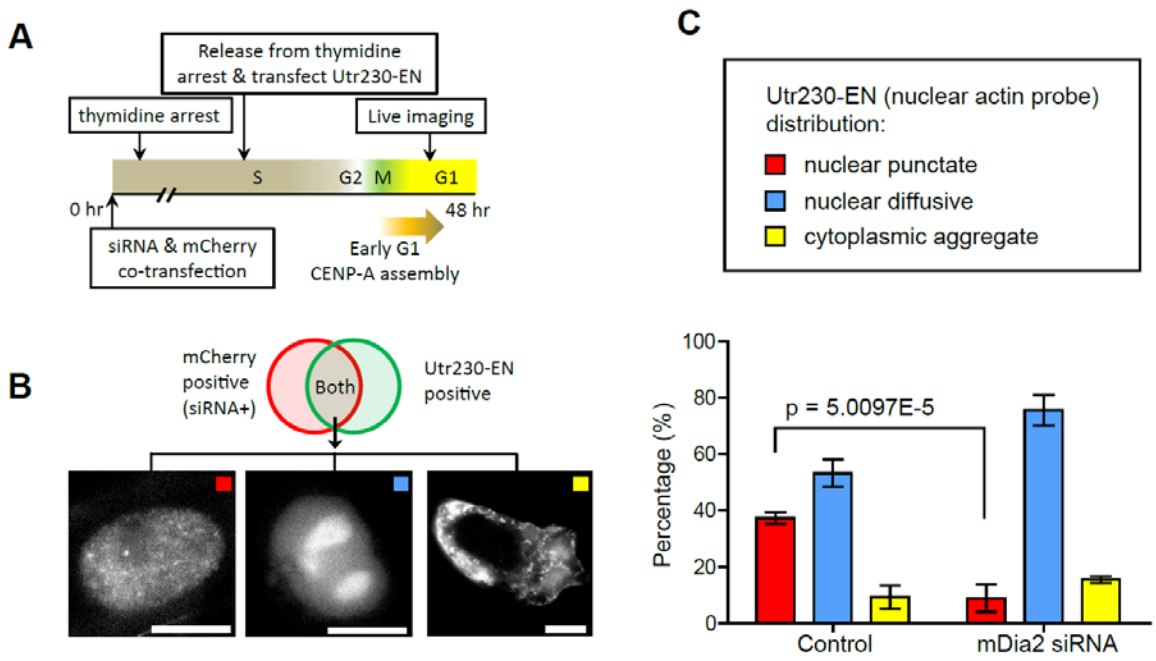

Figure 3.3. The formin mDia2 is necessary for the formation of short and dynamic nuclear actin in G1 cells

(A) Schematics for co-transfection of mDia2 siRNA with marker mCherry, as well as subsequent transfection of the nuclear actin probe Utr230-EN (Utr230-EGFP-NLS).

(B) Representative localization patterns of Utr230-EN in live G1 cells expressing the probe. Scale bar, 10 μm.

(C) The percentage of live cells showing the nuclear actin punctate structure upon expressing Utr230-EN analyzed in cells transfected with control (GAPDH) and mDia2 siRNA as indicated ($n > 50$ from three independent transfections). Error bars show standard deviations of three experiments. The p-value was computed using two tailed z-test comparing two-sample proportions.

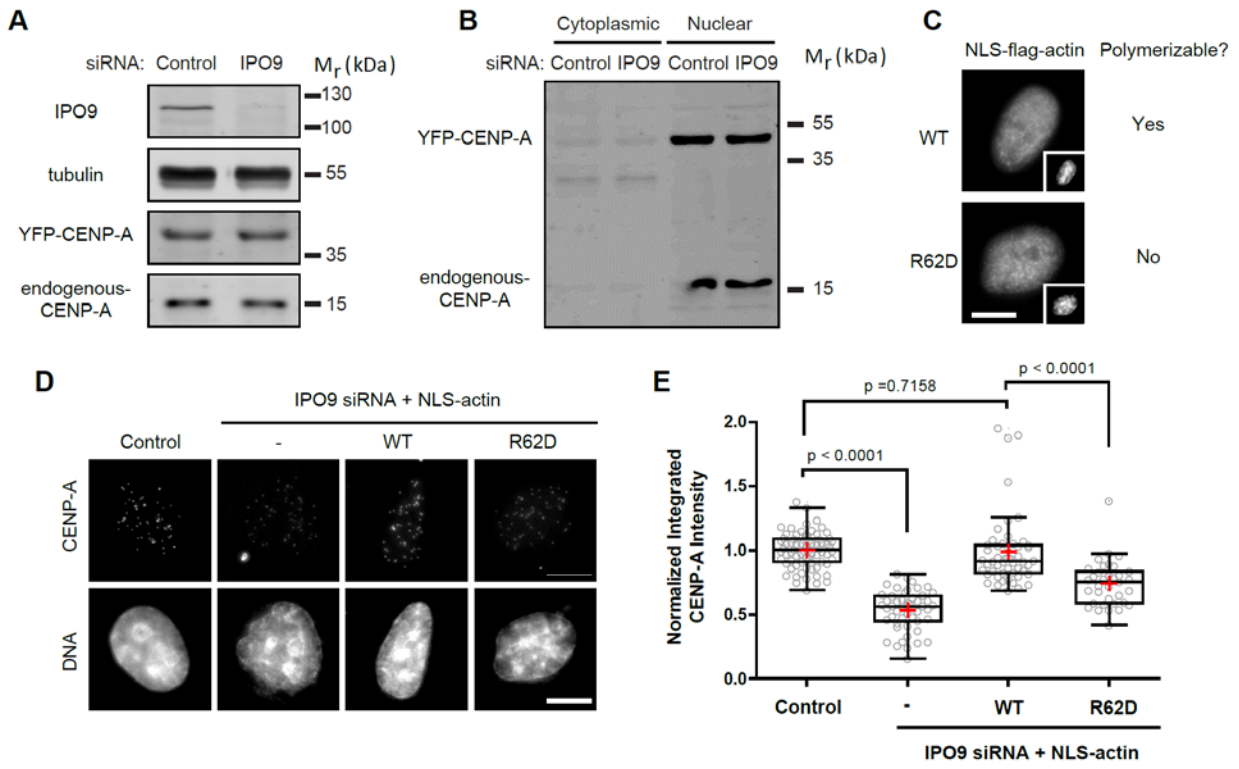

Figure 3.4. Polymerizable actin inside the nucleus is important for stable maintenance of CENP-A levels at the centromeres

(A and B) Depleting IPO9 does not change the levels of CENP-A inside the nucleus. Total YFP-CENP-A and endogenous CENP-A were immunoblotted for control and IPO9 knockdown (A). CENP-A levels were immunoblotted using cell lysates separated into cytoplasmic and nuclear fractions in both control and IPO9 knockdown (B). Control immunoblotting for fractionation assay is shown in **Figure S3.2A**.

(C) Nuclear localization signal (NLS) and flag-tagged actin localizes inside the nucleus. Flag staining showing both the wild type and the non-polymerizable R62D mutant accumulate inside the nucleus.

(D) Polymerizable actin inside the nucleus rescues reduced CENP-A levels caused by IPO9 knockdown. Representative immunofluorescence images showing CENP-A levels at centromeres. DNA are stained with DAPI. Scale bar, 10 µm.

(E) Quantification of the normalized CENP-A integrated intensity per nucleus using Whisker-Tukey boxplots overlaid with scatterplots. The boxes span the 25th to 75th percentile of the data, whereas the center bar denotes the median and the + marks the mean. n = 74 (Control), 50 (IPO9 siRNA), 52 (IPO9 siRNA + NLS-actin-WT), 35 (IPO9 siRNA + NLS-actin-R62D) cells. The p-values were computed using two-tailed *t* test.

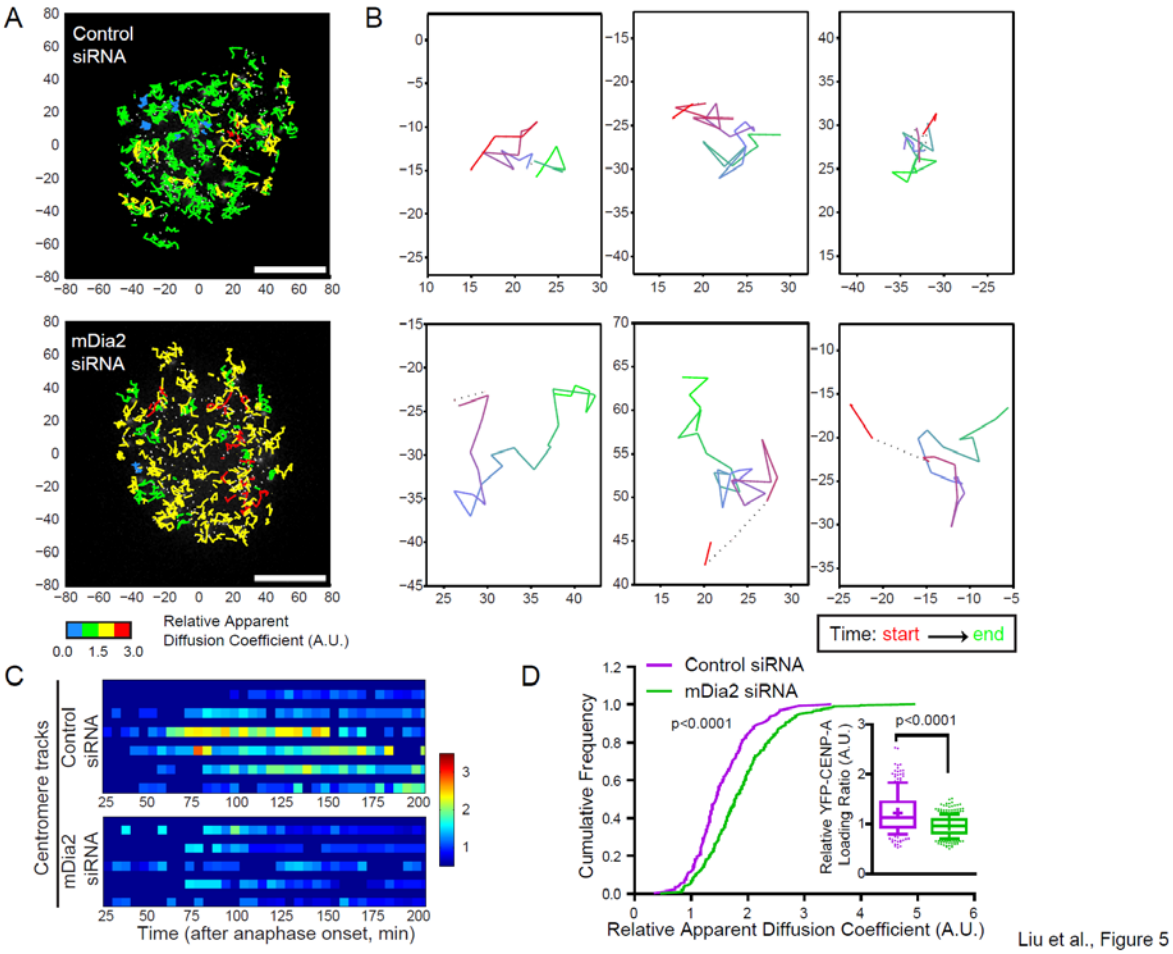

Figure 3.5. Tracking of centromere dynamics in live G1 cells

(A) A control cell (upper) and a cell depleted of mDia2 (lower) stably expressing YFP-CENP-A in early G1. Color-coded centromere-tracks were overlaid on the YFP-CENP-A image from the corresponding movie. Centromere tracks are color-coded based on their relative apparent diffusion coefficient (blue – low, red – high). Scale bar, 5 μm.

(B) Representative centromere-tracks during early G1 from respective cells in (A). Centromere tracks are color-coded based on time: each track starts in red and ends in green. Occasional dotted lines are due to tracking gaps. Units on both axes are pixels.

(C) Heat map showing representative centromere-tracks' intensity profiling in early G1. Control and mDia2 knockdown are scaled so that their intensity levels at the beginning of the profiling (~25 min after anaphase onset) are comparable. Each horizontal bar is one track spanning from 25 min to 200 min after anaphase onset. Intensity information of YFP-CENP-A tracks at each frame is color-coded (blue – low intensity, yellow/ red – high intensity).

(D) Quantification of the dynamics of centromere movement in early G1. Cumulative frequency was plotted for the relative apparent diffusion coefficients of cells transfected with control (GAPDH) or mDia2 siRNA. The p-value ($p < 0.0001$) was computed using Kolmogorov-

Smirnov test and two tailed t-test with the same conclusion. Insets are the boxplots showing the relative YFP-CENP-A loading ratio per track (see EXPERIMENTAL PROCEDURES for algorithm details). The boxes span 10-90 percentile of the data, while the center bar denotes median and the '+' marks mean. The p-value for insets was computed using two tailed t-test. Control (GAPDH) siRNA: n = 225 tracks and mDia2 siRNA: n = 344 tracks.

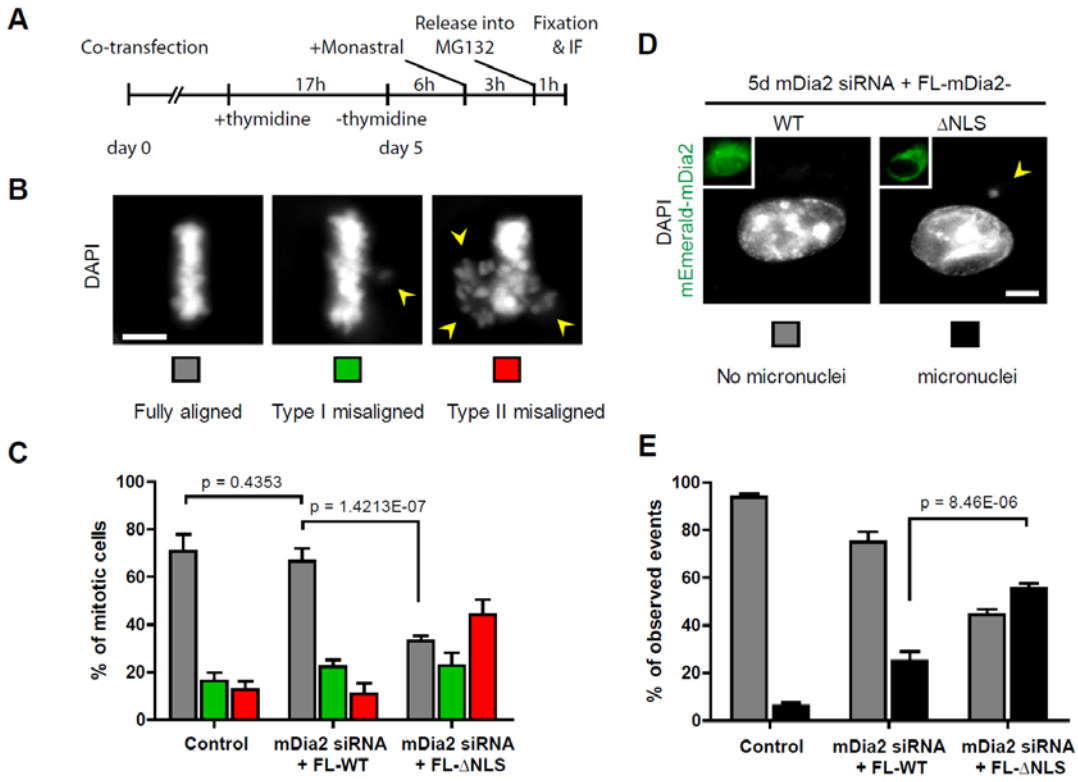

Figure 3.6. Chromosomal phenotypes after long term replacement of endogenous mDia2 with ΔNLS mutant

(A) Scheme for the transfection and synchronization strategies in analyzing metaphase chromosomal alignment 5 days after depleting endogenous mDia2 and replacing it with full length WT- or ΔNLS-mDia2.

(B) Representative immunofluorescence images showing three categories of metaphase chromosomal alignment patterns. Fully aligned with all chromosomal mass aligned into the metaphase plate; Type I misalignment characterized with only one or two chromosomal masses outside the metaphase plate; Type II misalignment characterized with more than two chromosomal masses outside the plate. Yellow arrow heads indicate misaligned chromosomes. Scale bar, 5 µm.

(C) Mean percentage of each alignment category with error bars showing SEM from three experiments (control: n = 135, mDia2 siRNA + FL-WT: n = 129, mDia2 siRNA + FL-NLS: n = 132 cells). The p-values were computed using two-tailed z-test. Control group is cells transfected with GAPDH siRNA.

(D) Representative immunofluorescence images showing a cell with normal interphase nucleus and a cell with micronucleus. Scale bar, 5 m. Insets (30% of the main images) are mEmerald channel showing the mDia2 proteins expressed.

(E) Mean percentage of cells containing micronuclei with error bars showing SD from three experiments (control: n = 180, mDia2 siRNA + FL-WT: n = 104, mDia2 siRNA + FL-NLS: n = 103 cells). The p-values were computed using two-tailed z-test. Control group is cells transfected with GAPDH siRNA.

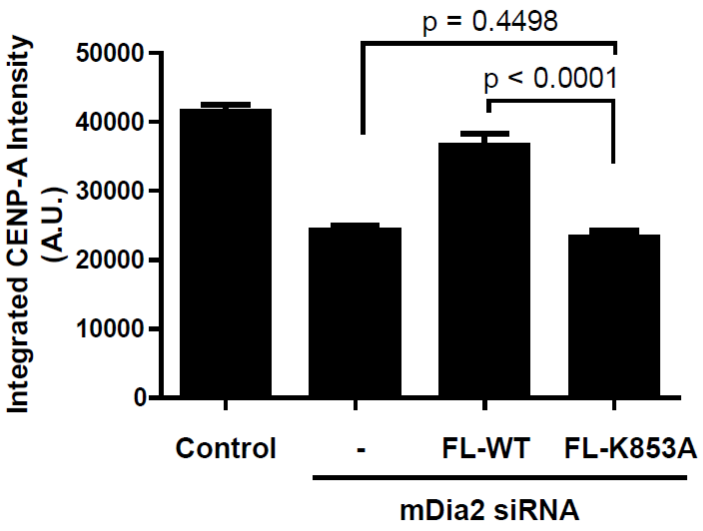

Figure S3.1. Full length mDia2 with an actin nucleation/polymerization mutation in the FH2 domain failed to rescue CENP-A levels upon depleting endogenous mDia2

Quantification of the CENP-A integrated intensity per nucleus. Bar graphs show mean±SEM of each group. The p-values were computed using two-tailed *t* test. Control group is cells transfected with GAPDH siRNA.

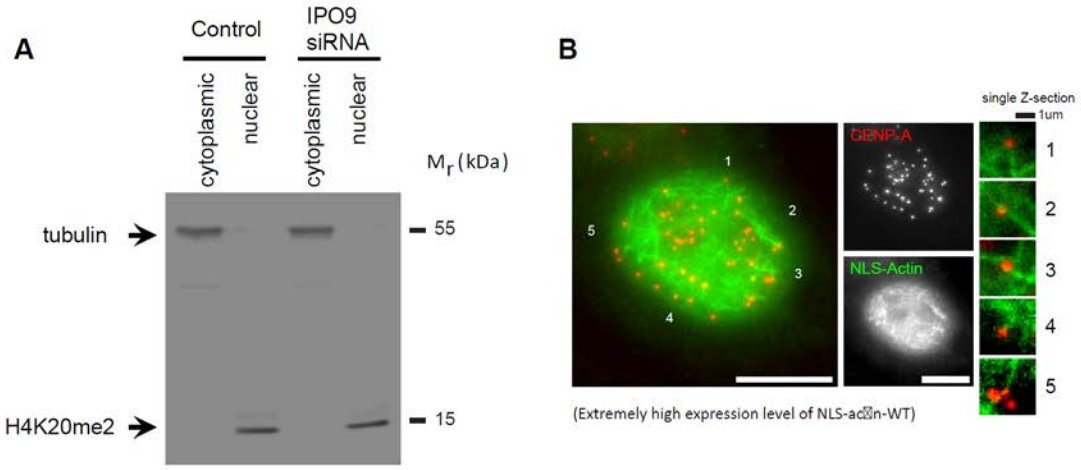

Figure S3.2. Polymerizable actin inside the G1 nucleus

(A) Immunoblot showing marker protein species in the cellular fractionation assay. Tubulin was used to mark the cytoplasmic fraction while H4K20me2 for the nuclear fraction.

(B) Putative non-diffusive nuclear actin filaments in close proximity to G1 centromeres was observed in fixed cells over expressing WT- but not R62D-NLS-actin (data for R62D-NLS-actin not shown). Scale bar, 10 μm.

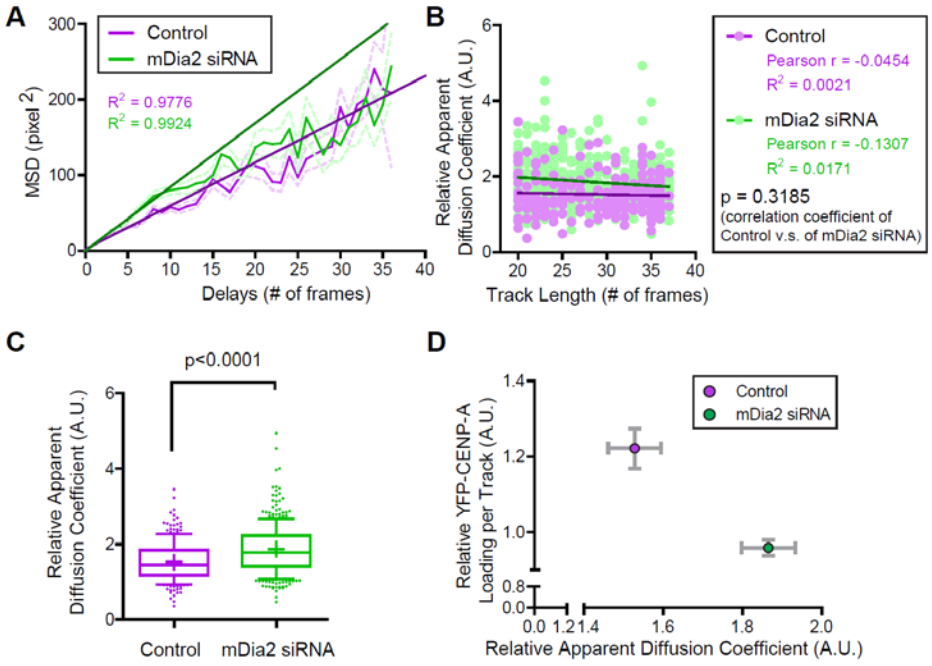

Figure S3.3. Relatively confined centromere motion depends on mDia2-mediated nuclear actin

(A) Ensemble average of MSD curves (plotted as mean ± SEM) from single particle tracking of centromere movement in early G1 control (GAPDH) and mDia2 knockdowns. Solid lines overlaid indicate linear regression (least-square fit) performed on the first 25% of the curves. Ensemble MSD curves demonstrate that MSD appear to saturate with a slightly concave curvature, indicative of impeded movement (anomalous diffusion) rather than free diffusion or directed transportation.

(B) Scatter plot of relative apparent diffusion coefficient (A.U.) as a function of track length (number of frames in each track). Correlation analysis and linear regression (least-square fit) were performed, and regression lines were overlaid with scatter plots. The p-value comparing the Pearson coefficient of control and that of mDia2 knockdown was computed using two tailed z-test.

(C) Whisker-Tukey boxplots show the normalized apparent diffusion coefficient of G1 centromeres in control and mDia2 nockdown cells. The boxes span 10-90 percentile of the data, while the center bar denotes median and the '+' marks mean. The p-value was computed using two tailed t-test.

(D) Relative YFP-CENP-A loading ratio was plotted as a function of the relative apparent diffusion coefficient. Mean ± 95% confidence intervals were plotted on both axes.

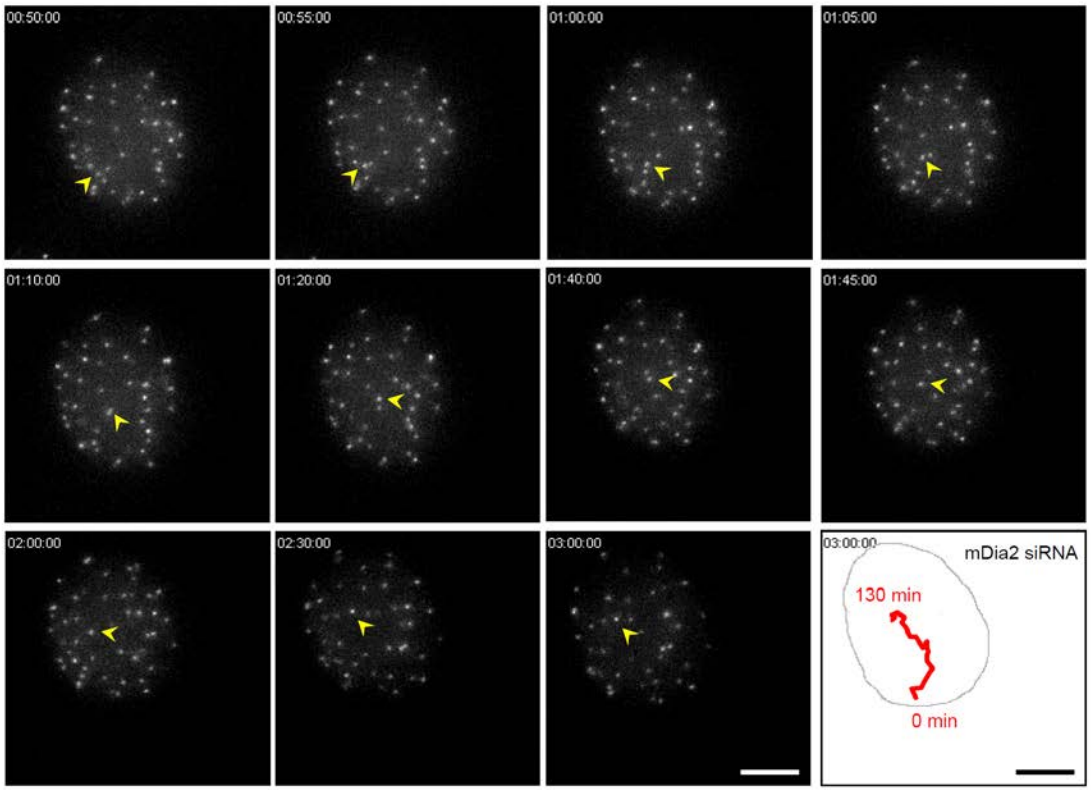

Figure S3.4. A representative example of long range centromere movement in early G1 cells depleted of mDia2

A time-lapse sequence showing the positions of centromeres in an mDia2 depleted cell during early G1. The centromere of interest is marked with a yellow arrow head across all the frames. Centromeres are marked with YFP-CENP-A and scaled on the identical look up table over time. The full trajectory (red) is depicted in the last panel, where the nuclear contour is depicted in gray. Scale bar, 5 μm.

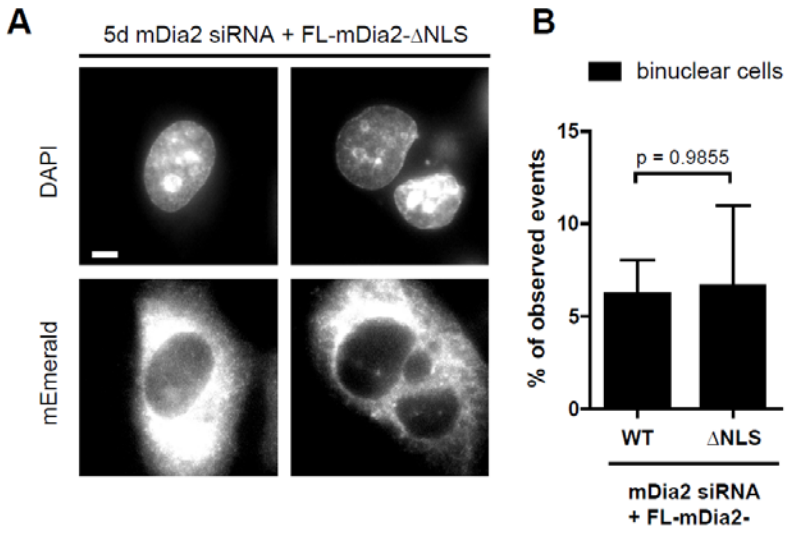

Figure S3.5. Long-term replacement of endogenous mDia2 with ΔNLS mutant does not cause higher indices of binuclear cells compared to WT

(A) Representative immunofluorescence images showing a cell with normal interphase nucleus and a binuclear cell. Scale bar, 5 m. mEmerald channels show the mDia2 proteins expressed.

(B) Mean percentage of binuclear cells with error bars showing SEM from three experiments (control: n = 181, mDia2 siRNA + FL-WT: n = 98, mDia2 siRNA + FL-NLS: n = 99 cells). The p-values were computed using two-tailed z-test.

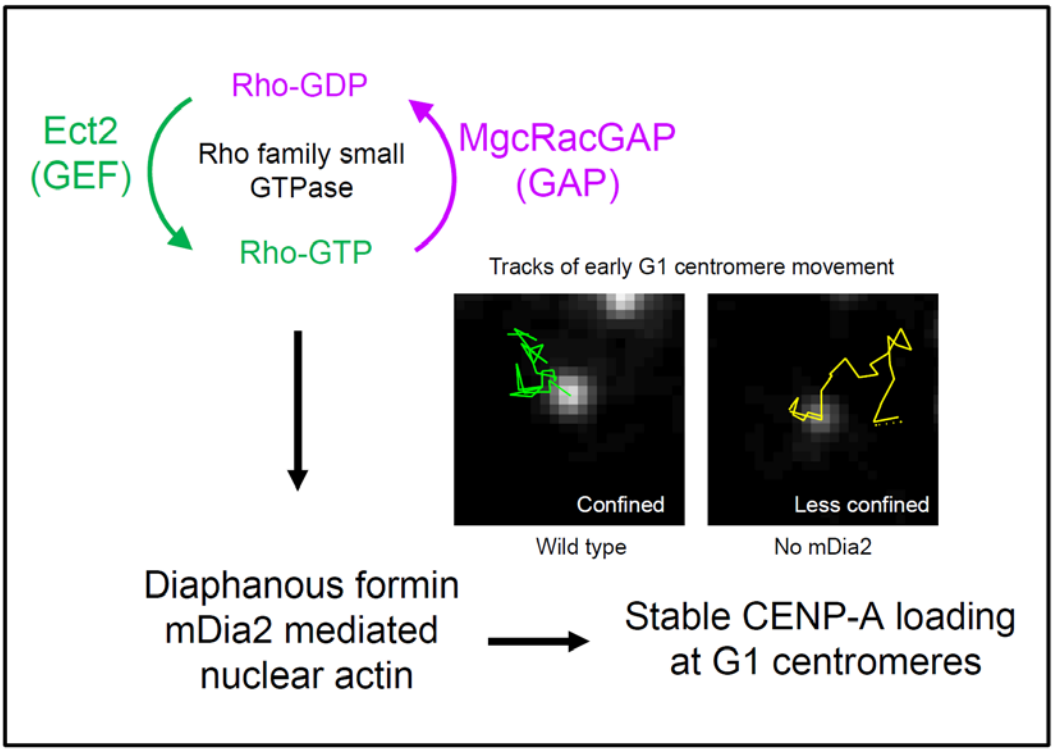

Figure S3.6. Graphical summary

Graphical summary of the role of mDia2 in bridging upstream small GTPase signaling and downstream nuclear environment during stable CENP-A loading at the moving centromeres in early G1 phase.

Chapter Four *: A dynein independent role of Tctex-1 at the kinetochore

*This chapter is reproduced from:

A dynein independent role of Tctex-1 at the kinetochore
Liu, C., Chuang, J.-Z., Sung, C.-H., and Mao, Y.
Cell Cycle, 14:9, 1379-1388 (2015)

Where the author of this thesis is the first author.

Abstract

Dynein light chains are accessory subunits of the cytoplasmic dynein complex, a minus-end directed microtubule motor. Here, we demonstrate that the dynein light chain Tctex-1 associates with unattached kinetochores and is essential for accurate chromosome segregation. Tctex-1 knockdown in cells does not affect the localization and function of dynein at the kinetochore, but produces a prolonged mitotic arrest with a few misaligned chromosomes, which are subsequently missegregated during anaphase. This function is independent of Tctex-1's association with dynein. The kinetochore localization of Tctex-1 is independent of the ZW10-dynein pathway, but requires the Ndc80 complex. Thus, our findings reveal a dynein independent role of Tctex-1 at the kinetochore to enhance the stability of kinetochore-microtubule attachment.

Introduction

Accurate chromosome segregation during mitosis requires proper interactions between chromosomes and plus ends of microtubules of the mitotic spindle [198,199]. The kinetochore, the proteinaceous complex assembled at the centromere region, serves as the microtubule attachment site at each mitotic chromosome [140,200]. Although there is much support for the KMN network (KNL1, Mis12, and Ndc80 complexes) serving as the core microtubule binding apparatus at the kinetochore [108,109], it is quite clear that many other kinetochore- and microtubule-associated proteins play important roles in maintaining the stable connection between kinetochores and dynamic microtubule plus ends. Depletion of the Ska1/RAMA complex [110-113] or a formin mDia3 [114,115] results in chromosome misalignment phenotypes in mammalian cultured cells, reminiscent of depletion of the Ndc80 complex. Two force-producing kinetochore-associated motors, the plus end-directed microtubule motor CENP-E and the minus end-directed microtubule motor cytoplasmic dynein, are associated with the outermost region of the kinetochore and have been implicated in the initial stages of microtubule interactions [201]. A group of microtubule plus-end-tracking proteins are delivered to the kinetochore by microtubule plus ends and possibly act as tethers, as well as modulators of microtubule dynamics, at attachment sites [202,203].

The dynein light chains are accessory subunits of the cytoplasmic dynein motor complexes and form a complex with the dynein intermediate chains at the base of the dynein heavy chains [204]. While the light chains directly link dynein to its cargo as an adaptor protein [205], recent studies suggest that these noncatalytic subunits may play a dynein-independent role in diverse cellular functions. For example, the LC8 family members of dynein light chains have been shown to interact, besides dynein, with a large number of proteins [206]. Similarly, the Tctex family member

of Tctex-1 (or DYNLT1) has dynein-independent roles in actin remodeling during neurite outgrowth [207] and in ciliary resorption [208,209]. We now show that Tctex-1 associates with unattached kinetochores and participates in stable microtubule attachment independent of cytoplasmic dynein.

Results

Both Tctex-1 and CLIP-170 associate with dyneinless kinetochores

We have shown that the formin mDia3 and its interaction with EB1, a microtubule plus-end-tracking protein, are essential for accurate chromosome segregation [114]. Knockdown the mDia3 protein in cells results in a loss of EB1, but an increase of CLIP-170, another microtubule plus-end-tracking protein, at kinetochores aligned at the metaphase plate (**Figures 4.1A, B and D**), judging by their relative signals against anti-centromere antibody (ACA) as the kinetochore marker. The compositional change of microtubule plus ends attached to kinetochores does not affect the release of cytoplasmic dynein from aligned kinetochores, judging by the loss of kinetochore staining of dynein intermediate chain (DIC) (**Figures 4.1C and 4.1D**). In contrast, the level of Tctex-1, a dynein light chain, is significantly increased on aligned kinetochores in mDia3 knockdown cells (**Figures 4.1C and 4.1D**). These results show that at least a population of Tctex-1 and CLIP-170 can be recruited onto kinetochores without dynein.

Tctex-1 is an outer kinetochore component

To confirm that Tctex-1 is a kinetochore component, we examined the kinetochore localization of Tctex-1 in fixed cells (**Figure 4.2A**). Indirect immunofluorescence showed strong Tctex-1 kinetochore staining, which colocalized with ACA, during mitosis but not interphase. Tctex-1 associated with kinetochores in prophase and remained at the kinetochore until metaphase. Furthermore, in late prometaphase cells, we detected Tctex-1 kinetochore signals on unaligned, but not aligned, chromosomes. Using N-SIM super-resolution microscopy system, we examined the localization of Tctex-1 within the kinetochore and found that Tctex-1 localized peripherally to

Hec1, a component of the outer kinetochore protein complex Ndc80 (**Figure 4.2B**). In addition, in cells treated with monastrol to produce monopolar spindles with monotelic chromosomes (with only one sister kinetochore attached to microtubule and the other unattached), Tctex-1 localized to only one of two sister kinetochores on many chromosomes (**Figure S4.1A**). The strong Tctex-1 staining was observed on the kinetochore further from the pole while the kinetochore closer to the pole had much less Tctex-1 staining. This asymmetric staining of sister kinetochores on monotelic chromosomes in monastrol-treated cells are similar to previously documented kinetochore localization of Mad2, a mitotic checkpoint protein which localizes only to unattached kinetochores [210]. These results collectively suggest that Tctex-1 is an outer kinetochore component and associates only with unattached kinetochores.

Cytoplasmic dynein is also recruited onto unattached kinetochores and departs from attached kinetochores along with mitotic checkpoint proteins through a dynein self-removal mechanism [211]. Despite the similar kinetochore localization pattern, we identified some differences in the timing in which Tctex-1 appeared at kinetochores in comparison with dynein. Judging by immunofluorescence staining compared to late prometaphase kinetochores, the prophase and early prometaphase kinetochores were able to recruit a significant amount of Tctext-1 with no or little dynein (**Figure S4.1B**). This result is consistent with the possibility that the recruitment of Tctex-1 onto unattached kinetochores can occur independently of dynein.

Tctex-1 plays a role in metaphase chromosome alignment and accurate chromosome segregation, and this function is independent of its ability to bind to dynein.

To test for the functions of Tctex-1 at the kinetochore, we transfected cells with a plasmid encoding Tctex-1 short hairpin RNA (shRNA) and far red fluorescent protein (HcRed). The expression of Tctex-1 shRNA had resulted in a clear reduction of Tctex-1 protein level after either 48 hr (**Figure 4.3A**), as well as 72 hr (data not shown), and a loss of Tctex-1 at unattached kinetochores by immunofluorescence microscopy (**Figure 4.3B**). The loss of Tctex-1 at kinetochores could be rescued by expressing a shRNA-resistant Flag-tagged Tctex-1 construct (**Figure 4.3B**), further supporting that Tctex-1 is a kinetochore component.

Chromosome movement and mitotic progression upon Tctex-1 depletion were assessed by live cell imaging in unperturbed mitoses using cells stably expressing the Histone H2B-EYFP fusion protein. Depletion of Tctex-1 (72 hr post-transfection of the Tctex-1 shRNA construct) extended the average duration of mitosis (to 171 min) compared to control cells (51 min) (**Figures 4.3C and 4.4D, Movies S1 and S2**). More importantly, this mitotic delay is caused by a few chromosomes chronically misaligned near the spindle poles, which were subsequently missegregated at anaphase onset (**Figures 4.3D, 4.4E and 4.4F**). The existence of only a few unaligned chromosomes is consistent with the observation that Tctex-1 depletion did not affect the overall cold-stable microtubules in metaphase cells (**Figure S4.2**). Besides polar chromosomes, many Tctex-1-depleted cells also exhibited chromosome bridges upon anaphase onset. The importance of Tctex-1 in mitotic progression is confirmed by the rescue with the expression of the shRNA resistant wild-type Flag-Tctex-1 protein in Tctex-1-depleted cells (**Figures 4.3B-4.3D**).

These results demonstrate that Tctex-1 is important for metaphase chromosome alignment and accurate chromosome segregation.

Tctex-1 directly binds to dynein intermediate chain and has a predicted threonine 94 (T94) phosphorylation site [207]. Only the nonphosphorylatable Tctex-1-T94A protein, but not the phosphomimetic Tctex-1-T94E protein, is able to associate with the dynein complex [207]. In agreement, we confirmed that both Flag-wild type Tctex-1 and Flag-Tctex-1-T94A, but not Flag-Tctex-1-T94E, were co-immunoprecipitated with endogenous dynein (DIC) in mitotic extracts (**Figure 4.4A**). We examined whether the expression of these two Tctex-1 proteins can rescue mitotic defects caused by the depletion of endogenous Tctex-1. Judging by live cell imaging, both Tctex-1-T94A and Tctex-1-T94E substantially reduced the duration of mitosis to a similar degree (**Figures 4.4B, 4.4C and 4.4D, Movies S3 and S4**). Furthermore, the incidents of misaligned and missegregated chromosomes were similarly reduced in cell expressing T94A and T94E for the rescue (**Figures 4.4B, 4.4C and 4.4F**). These results confirm an important role of Tetex1 for accurate chromosome segregation and suggest that this function of Tctex-1 at the kinetochore does not depend on its interaction with dynein.

Tectx-1 knockdown does not affect dynein-Tctex-1L at kinetochores

It has been shown that another dynein light chain DYNLT3/Tctex-1L associates with kinetochores and binds to Bub3, a mitotic checkpoint protein [212]. These results have been interpreted as the Tctex-1L to contribute to dynein cargo binding specificity. We examined whether the chromosome misalignment and missegregation phenotype caused by Tctex-1

depletion could attribute to the change of the population of dynein-Tectx-1L at kinetochores. Indirect immunofluorescence analysis revealed that Tctex-1L indeed associated with unattached kinetochores along with dynein (DIC) (**Figures, S4.3A and S4.3B**) as reported previously [212]. Depletion of ZW10 from unattached kinetochores resulted in a significant loss of both dynein (DIC) and Tctex-1L to a similar extent (**Figures, S4.3A and S4.3B**), suggesting that the kinetochore association of Tctex-1L is dependent of dynein. In contrast, depletion of Tctex-1 did not change the amount of Tctex-1L associated with unattached kinetochores (**Figures, S4.3C and S4.3D**). These results clearly suggest that depletion of Tctex-1 does not affect the pool of dynein-Tctex-1L at kinetochores.

The kinetochore localization of Tctex-1 is independent of cytoplasmic dynein

An important role for dynein during mitosis is to transport of mitotic checkpoint proteins off kinetochores toward spindle poles upon microtubule capture [211]. BubR1 and Mad1 are two mitotic checkpoint proteins whose kinetochore localization depends on microtubule attachment [213,214]. Immunofluorescence staining revealed the presence of BubR1 and Mad1 at unattached kinetochores of polar chromosomes, but not on attached kinetochores of chromosomes aligned at the metaphase plate in both control and Tctex-1 depleted cells (**Figure 4.5**). This suggests that depletion of the dynein light chain Tctex-1 does not have an effect on dynein-dependent removal of mitotic checkpoint proteins from attached kinetochores. Furthermore, this result supports the idea that Tetex1 has a direct role on microtubule capture at unattached kinetochores independent of dynein.

To further support a possible dynein-independent role of Tctex-1 at the kinetochore, we examined the inter-dependency of kinetochore recruitment between Tctex-1 and cytoplasmic dynein. Depletion of Tctex-1 from unattached kinetochores did not affect kinetochore association of cytoplasmic dynein (**Figures 4.6A and 4.6B**). Furthermore, knocking down of ZW10, a component of the RZZ (Rod/ZW10/Zwilch) complex that recruits dynein to kinetochores [215,216], significantly reduced the level of dynein at unattached kinetochores (**Figures 4.6A and 4.6C**). By contrast, ZW10 suppression only modestly diminished kinetochore recruitment of Tctex-1 (**Figures 4.6A and 4.6C**). In combination with the observation of Tctex-1 localization at kinetochores without dynein in mDia3 knockdown cells (**Figures 4.1C and 4.1D**) and prophase cells (**Figure S4.1B**), these results demonstrate that at least a portion of Tctex-1 can be recruited onto unattached kinetochores independent of dynein.

Tctex-1 kinetochore localization depends on the Ndc80 complex

The position of Tctex-1 in the hierarchical structure of the kinetochore will clearly provide us with crucial indications of Tctex-1's role at the kinetochore. To understand how Tctex-1 is targeted to the kinetochore, we searched for kinetochore components that are required for kinetochore recruitment of Tctex-1. We found that the level of Tctex-1 on unattached kinetochores was substantially reduced in Hec1 (a component of the Ndc80 complex) knockdown cells (**Figure 4.6D,** middle panel), suggesting an Ndc80-depedent kinetochore localization of the Tctex-1 protein. Conversely, knockdown of Tctex-1 did not affect kinetochore recruitment of the Ndc80 complex (Hec1) (**Figure 4.6D,** bottom panel). Furthermore, depletion of CENP-E, the microtubule plus end-directed motor, did not affect the recruitment of Tctex-1 onto unattached kinetochores (**Figure 4.6E**). Depletion of Ndc80 components does not significantly affect the

level of dynein at kinetochores [217]. Thus, this result is consistent with a dynein-independent recruitment of Tctex-1 onto kinetochores.

Discussion

It has been suggested that both Dynein-dynactin complex and CLIP-170 are present only at the unattached kinetochores and are released upon microtubule attachment [218]. The kinetochore localization of CLIP-170 might depend on the dynein/dynactin pathway [219-222]. We now show that CLIP-170 and Tctex-1, but not cytoplasmic dynein, remains at attached kinetochores which lack EB1 upon depletion of the formin mDia3. Our work argues that the dissociation of CLIP-170 from attached kinetochores is neither a direct response from microtubule attachment nor through a dynein-dependent removal pathway. Instead, the removal of CLIP-170 might involve changes of microtubule plus-end dynamics regulated by the accumulation of EB1 through its interaction with the kinetochore-associated mDia3 protein. Furthermore, this result also indicates that the kinetochore localization of Tctex-1, a dynein light chain, does not depend on the dynein complex.

Increasing evidence suggests that dynein light chains can bind to proteins other than cytoplasmic dynein in diverse cellular functions [206]. Our study unravels an important function for the dynein light chain Tctex-1 at the kinetochore in a dynein independent manner. Evidence for this model includes the following. First, Tctex-1 can be recruited onto kinetochores through dynein-independent mechanisms. Tctex-1 associates with dynein-free kinetochores in prophase cells and in ZW10 knockdown cells, suggesting that at least part of Tctex-1 enriched at unattached kinetochores is free from the dynein complex. Second, depletion of Tctex-1 does not affect dynein self-removal and the removal of the mitotic checkpoint proteins from attached kinetochores, implying that Tctex-1 is not functionally important for kinetochore-associated dynein. Third, a phosphomimetic Tctex-1T94E protein, which has been shown to be unable to incorporate into the dynein complex in transfected cells [207] and now by coimmunoprecipitation analysis using mitotic

cell extracts, can rescue mitotic defects caused by the depletion of endogenous Tctex-1 proteins just like its nonphosphorylatable counterpart Tctex-1T94A that can associate with the dynein complex. And fourth, depletion of the Ndc80 complex, but not ZW10-dynein, at unattached kinetochores results in a significant loss of Tctex-1. These results coherently suggest that the functional role in metaphase chromosome alignment and accurate chromosome segregation by kinetochore-associated Tctex-1 is largely independent from its association with the dynein complex.

Induction of a dimeric Tctex-1 "trap" results in rapidly disruption of early endosomal and lysosomal organization, but has no obvious effect on mitosis [223]. On one hand, these results support that Tctex-1 is not functionally important for dynein in mitotic progression. On the other hand, these results, along with other observations, indicate that kinetochore-associated Tctex-1 proteins may be not in rapid exchange with the free cytosolic pool, as is observed with dynein for endosomes and lysosomes. Structural studies support a role for dynein light chains to promote protein dimerization and structural stabilization [206]. These light chains can allosterically bind to and regulate, besides dynein, diverse proteins and protein complexes. Future work will require the identification of the binding partner for the dynein-independent population at kinetochores.

Materials and Methods

Cell culture, transfection, and drug treatment

T98G cells were maintained in DME medium supplemented with 10% FBS at 37°C in 5% CO_2. The Tctex-1 shRNA construct and rescue plasmids are as described previously [207,208]. Transfection was performed using HiPerfect (QIAGEN) based on the manufacturer's instructions (48hr or 72hr, as indicated in figures/figure legends), and cells transfected with shRNA were identified by the co-expressed HcRed. The mDia3 siRNA was purchased from QIAGEN. ZW10 and CLIP-170 siRNAs were purchased from Dharmacon (Thermo Scientific) and used as instructed by the manufactures. Nocodazole, monastrol and MG132 were purchased from Sigma-Aldrich and used at final concentrations of 100 ng/ml, 100 μM and 10 μM, respectively. All drug treatments were performed for particular length of time, as described in figure legends.

Immunofluorescence microscopy and live cell imaging

A commercial Tctex-1 antibody (H-60, Santa Cruz) was used in this study for all the data obtained. ACA (purified human anti-centromere protein IgG) was from Antibodies Incorporated. Other commercial antibodies used in this study included anti-EB1 (1A11/4 & H-70, Santa Cruz), anti-CLIP-170 (F3 & H300, Santa Cruz), anti-Flag-M2 (F3165, Sigma-Aldrich), anti-DIC (74.1, Ab23905, Abcam), anti-Hec1 (9G3, Abcam), anti-αTubulin(DM1α, T6199, Sigma-Aldrich), anti-BubR1(8G1, Abcam), anti-Mad1 (9B10, Santa Cruz), anti-CENP-E (C-5, Santa Cruz), and anti-Tctex-1L (E15, Santa Cruz).

For indirect immunofluorescence, cells grown on poly-D-lysine coated coverslips were washed in pre-warmed PBS, extracted with 0.1% Triton-X-100 in PBS for 1 min, fixed in cold methanol at -20 °C for 10 min, and blocked in 5% BSA in PBS at 4 °C overnight. Coverslips were subjected to primary antibodies diluted in PBS and DyLight488, Rhodamine or Cy5 conjugated secondary antibodies (Jackson Immuno-Research Laboratories, Inc.), both at room temperature for 1 hr. DAPI (final concentration 16.67 ng/mL) was used to stain nuclei/chromosomes. Coverslips were mounted using antifade reagent (ProLong Gold; Molecular Probes). Images were acquired at room temperature using an inverted microscope (IX81; Olympus) with a 60×, NA 1.42 Plan Apochromat oil immersion objective (Olympus), a monochrome charge-coupled device camera (Sensicam QE; Cooke Corporation), which are controlled by the SlideBook software (3i and Olympus). 10 z-sections 0.5 μm apart spanning 5 μm were taken for each cell. All images in each experiment along with appropriate controls were collected on the same day with identical exposure time. No-neighbor deconvolution and/or maximum z-projection was performed on selected stacks of representative images, which were subsequently scaled in ImageJ (NIH) or MATLAB (Mathworks, Inc.) for visual comparison. Quantitative image analysis was performed with ImageJ (NIH). To measure fluorescent intensities at each individual kinetochore, unassigned unit 16-bit tiff images of whole stacks or of maximum z-projections were exported from the SlideBook with all bit depth information being preserved. ROIs (regions of interest) were generated covering each kinetochore based on channel-merged image and the integrated pixel intensities were then measured for each channel within the ROI. In each cell, five cytosolic ROIs near the kinetochore ROIs were also quantitated as above and averaged for background subtraction. Intensity data were then subjected to ratio calculation and normalization before plotting.

For live cell imaging, cells stably expressing H2B-EYFP were plated onto Poly-D-Lysine coated 35 mm glass-bottom dishes (MatTek Corporation) and maintained in CO_2 independent medium (Gibco #18045) supplemented with 4 mM L-glutamine and 10% FBS, with an environmentally controlled chamber at 37°C during imaging. Images were acquired every 3 min using an inverted microscope (IX81; Olympus) with a 40×, NA 0.6 LUCPLFLN air objective (Olympus) and a interline transfer cooled CCD camera (ORCA-R2 C10600-10B; HAMAMATSU Photonics), which were controlled by the MetaMorph software (Molecular Devices, LLC).

Structured Illumination Microscopy (N-SIM)

Cells grown on No. 1.5 (0.17 mm thick) cover glasses coated with poly-D-lysine were washed, extracted and fixed as in common immunofluorescence. Endogenous Ndc80 and Tctex-1 proteins were recognized by mouse anti-hec1 antibody (9G3, Abcam) and rabbit anti-Tctex-1 (H-60, Santa Cruz), which were subsequently labeled by secondary antibodies conjugated with DyLight488 (Jackson Immuno-Research Laboratories, Inc.) and Alexa Fluor 568 (Life Technologies), respectively. ProLong Gold without DAPI (Life Technologies) was used as mounting medium to achieve a refractive index as close to 1.515 as possible. Mounted samples were completely cured and sealed before imaging. To rule out any potential shift between different channels due to the optics of the microscope, a custom-built reference slide was used for channel alignment and post-hoc pixel registration. Manufacturer's imaging procedure (N-SIM, Nikon) was followed. In particular, a 100x oil objective (Apo TIRF 100x Oil DIC N2, NA 1.49) was used in conjunction with Andor DU-897 X-6050 EMCCD camera. 3D-SIM mode imaging was performed with laser lines 488 and 561 nm at constant temperature under control. 41 z-sections 0.125 μm apart spanning 5 μm were taken with MCL NanoDrive PiezoZ Drive. For each z-section,

15 different moiré fringes resulted from illuminations with known, high spatial frequency patterns were captured. Reconstruction was performed with N-SIM module inside NIS-Elements using optimal parameters, to create super-resolution images by processing multiple moiré patterns.

Immunoprecipitation and immunoblotting analysis

Immunoprecipitation were performed using Dynabeads® following standard protocol provided by the manufacturer (Life technologies) with minor modifications. Confluent mitotic cells (arrested in nocodazole for 9 hrs) growing on 10 cm dish were trypsinized and collected into 50 ml vials. Centrifugations were performed (with second time in PBS supplemented with protease inhibitor cocktail, Roche 04-693-159-001) at 4°C, 1500 rpm for 5 min each to harvest cells. Dynabeads with Protein G (Life technologies) were washed in PBS for three times, and incubated with primary antibodies (anti-dynein intermediate chain 74.1) at a ratio of 10 µg antibodies per 1 mg beads, for 2 hrs on 4°C rocker. IP lysis buffer [1% NP-40, 25 mM Tis-HCl (pH 7.5), 150 mM NaCl, 5 mM EDTA (pH 8.0)] supplemented with protease inhibitor cocktail was added into the harvested cells (400 µl per sample), mixed well and incubated on 4°C rocker for 30 min, after which DNA were destroyed with syringe needle (BD-25G5/8) followed by additional 15 min incubation. The lysate mixture was then centrifuged at 12000 rpm for 10 min to remove insoluble materials, after which 20 µl input was retrieved, boiled with SDS sample buffer and stored. After incubation with primary antibodies, beads were washed three times. 380 µL of the supernatant of cell lysate were then added into the beads and gently homogenized by pipetting. Beads-lysate mixture were incubated on 4°C rocker for 1 hr, after which the beads were washed three times and boiled in SDS sample buffer [30% glycerol, 350 mM 1M Tris (pH 6.8), 10% SDS, 0.05% bromophenol blue and 5% 2-mercaptoethanol].

For immunoblotting, cells were lysed in RIPA buffer [50 mM Tris-HCl (pH 7.5), 150 mM NaCl, 1% NP-40, 0.1% SDS, 0.5% Na-Deoxycholate Acid] and denatured in SDS sample buffer. Cell lysates were then subjected to 10% SDS-PAGE followed by membrane transfer (Immobilon-P, Millipore; Towbin transfer buffer, pH 8.3). Immunoblots on the membrane were blocked with Tris-buffered saline with tween (TBST) [20 mM Tris−HCl (pH 7.4), 150 mM NaCl, 0.05% Tween] containing nonfat dry milk and then probed with affinity-purified primary antibodies in TBST. Primary antibodies were visualized using horseradish peroxidase (HRP)-labeled goat secondary antibodies and enhanced chemiluminescence (ECL), or using AF680 anti mouse (Life technologies) and IRDye800 anti rabbit antibodies (LI-COR Biosciences) together with the LI-COR imaging system (LI-COR Biosciences).

Statistical analysis and graphing

All statistical analyses were done in Prism 5 (Graphpad) or Stata 12 (StataCorp, LP). Unpaired two-tailed student's t-test was performed at the 5% level of significance unless otherwise noted. Statistical decisions are made after computing p-values: $p > 0.05$, not significant; p is between 0.01 and 0.05, significant; p is between 0.001 and 0.01, very significant; $p < 0.001$, extremely significant. Two-way ANOVA test was performed in particular experiments to test if the interaction between two variables [e.g. treatment (control/siZW10) *v.s.* protein (DIC/Tctex-1) in **Figures 4.6C** and **S4.3B**] is significant at the 5% level of significance. After calculation, a significant outcome suggests that the effects of treatment (siZW10) vary by different proteins (i.e.

DIC and Tctex-1 behave significantly differently upon the same treatments). All graphs were prepared in either Prism 5 (Graphpad) or Origin 8.6 (OriginLab).

Acknowledgements

We thank all members of the Mao laboratory for stimulating discussion. We also thank Ruijun Zhu (Columbia University), Lynne Chang (Nikon) and the Marine Biological Laboratory for technical helps with the Structured Illumination Microscopy. This work has been supported by grants from the National Institute of Health (GM89768 to Y.M. and EY11307 to C.-H.S.) and research awards from the Irma T. Hirschl/Monique Weill-Caulier Trusts (Y.M.) and Research to Prevent Blindness (C.-H.S.).

Figures

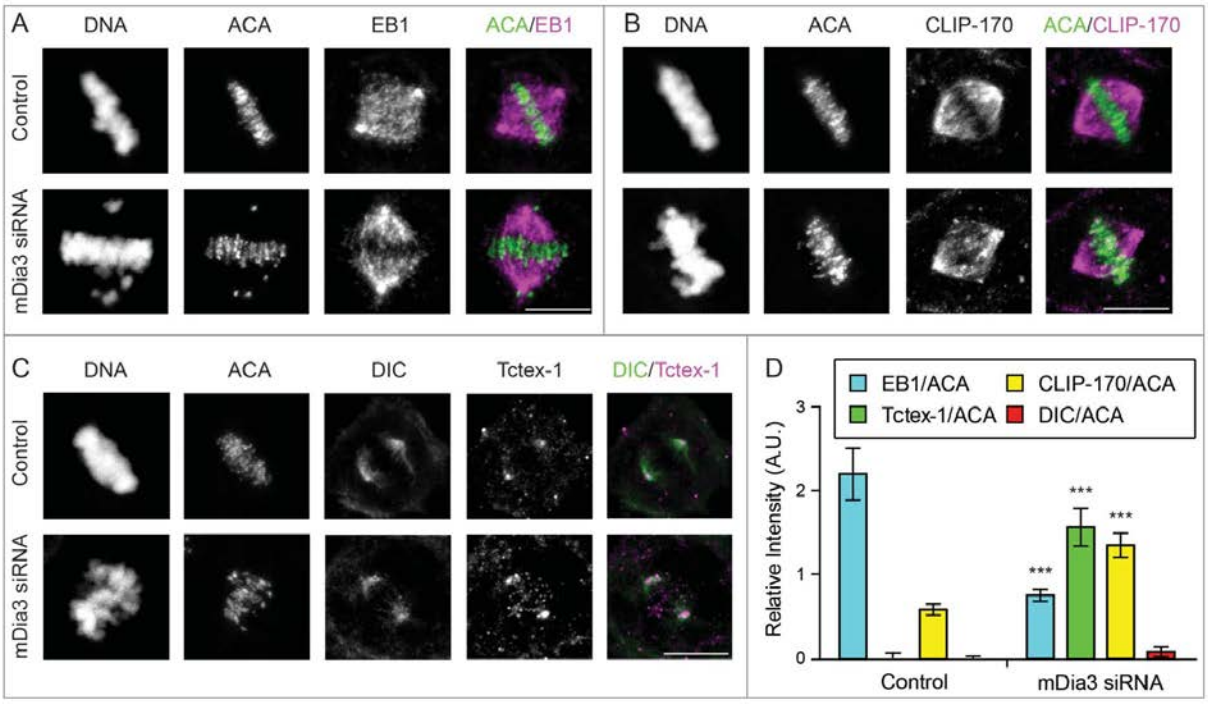

Figure 4.1. CLIP-170 and Tctex-1, but no dynein, remain at attached kinetochores without mDia3 and EB1.

(A - C) Indirect immunofluorescence staining of DNA (DAPI staining) and ACA, along with EB1 (A), CLIP-170 (B), Dynein (DIC in C), and Tctex-1 (C) in control and mDia3 knockdown metaphase cells as indicated (72 hr post-transfection). Cells were treated with nocodazole for 4 hrs and then released into MG132 for 1 hr prior to fixation. Bar, 5 μm.

(D) Quantification of the relative intensities (per kinetochore) at aligned kinetochores of EB1/ACA, CLIP-170/ACA, DIC/ACA, and Tctex-1/ACA in metaphase cells (mean with 95% confidence interval, $p < 0.0001$ as indicated by *** based on more than 30 kinetochores from at least 5 cells).

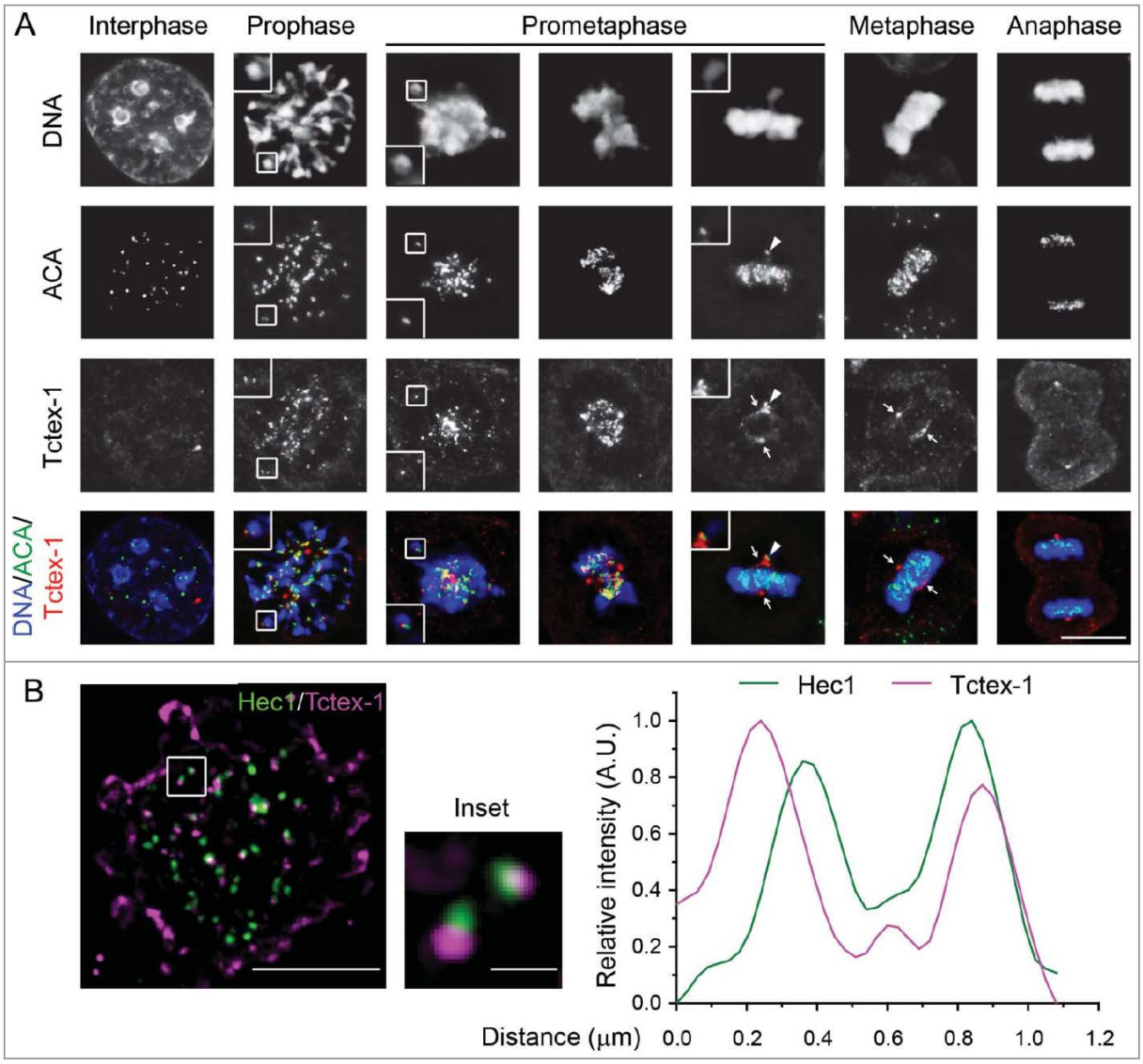

Figure 4.2. The dynein light chain Tctex-1 associates with unattached kinetochores.

(A) Immunofluorescence detection of ACA, Tctex-1, and DNA (DAPI staining) in mitotic cells. In merged panels: ACA – green, Tctex-1 – red, and DNA – blue. Insets: colocalization of Tctex-1 and ACA at a pair of sister kinetochores. Arrows point to spindle poles and arrow heads point to unattached kinetochore on a polar chromosome. Bar, 5 μm.

(B) Left panel: N-SIM Super-resolution images showing Hec1 (green) and Tctex1 (magenta). Right panel: graph showing a representative linescan of the fluorescent intensity of a pair of sister kinetochores that is highlighted in left panel (inset).

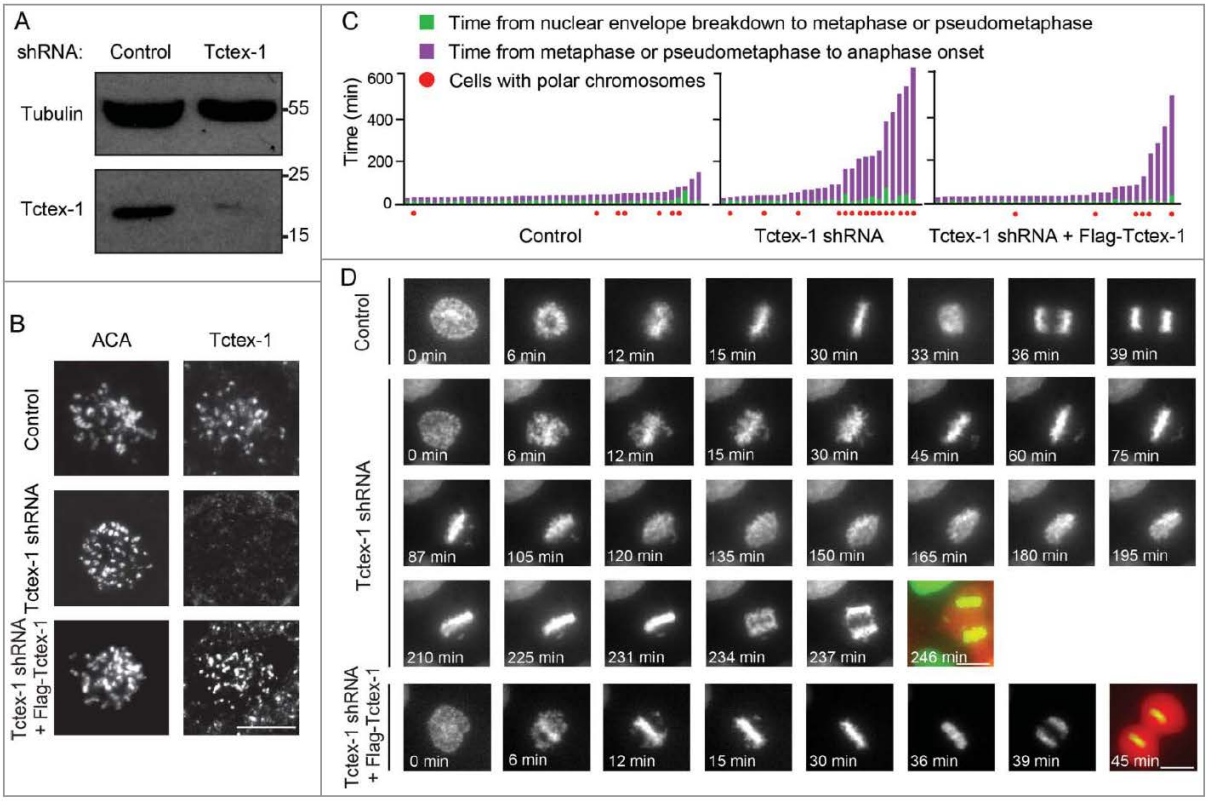

Figure 4.3. Tctex-1 is essential for accurate chromosome segregation.

(A) Immunoblotting of cell lysates 48 hr posttransfection with control or Tctex-1 shRNA plasmids as indicated.

(B) Immunofluorescence staining of ACA and Tctex-1 in mitotic cells 48 hr posttransfected with control or Tctex-1 shRNA plasmids, as well as the wild-type Flag-Tctex-1 expression vector, as indicated. For Tctex-1 shRNA + Flag-Tctex-1 cells, Tctex-1 was stained with anti-Flag antibody. Bar, 5 μm.

(C) Time spent from nuclear envelope breakdown to metaphase (or pseudometaphase) (green) and from metaphase (or pseudometaphase) to anaphase onset (magenta) of cells (expressing H2B-EYFP) transiently transfected with control or Tctex-1 shRNA plasmids, as well as the wild-type Flag-Tctex-1 vector (72 hr post-transfection). Each vertical bar represents a single cell. The transfected cells were identified by HcRed, which are coexpressed by the shRNA plasmid, before live cell imaging. Pseudometaphase is designated as when the majority of chromosomes are aligned with an obvious metaphase plate and a few polar chromosomes.

(D) Stills of live-cell imaging showing cells transfected with control or Tctex-1 shRNA plasmids, as well as the wild-type Flag-Tctex-1 expression vector, as indicated, during unperturbed mitoses. The transfected cell was identified by cytosolic red signals from the co-expression of HcRed as showed in the last still image. Bar, 5 μm.

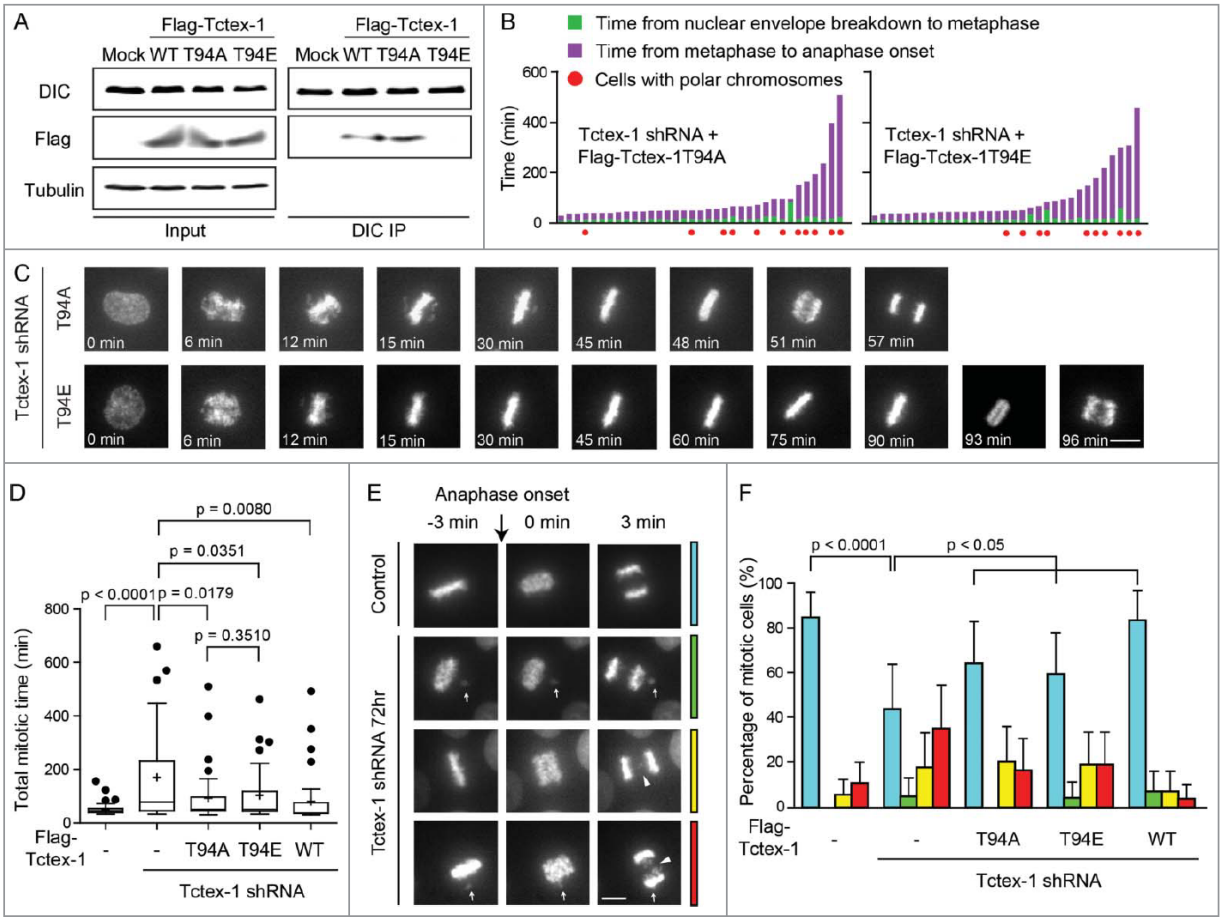

Figure 4.4. The mitotic role of Tctex-1 does not depend on its interaction with dynein.

(A) Immunoprecipitates from mitotic cell extracts with DIC antibody and then probed with DIC and Flag antibodies as indicated. Cells were transfected with Flag tagged wild-type Tctex-1, Tctex-1-T94A or Tctex-1-94E.

(B) Time spent from nuclear envelope breakdown to metaphase (or pseudometaphase) (green) and from metaphase (or pseudometaphase) to anaphase onset (magenta) of cells (expressing H2B-EYFP) transiently transfected with Tctex-1 shRNA plasmids and expression vectors for the nonphosphorylatable Tctex-1T94A or the phosphomimetic Tctex-1T94E variants (72 hr post-transfection). Each vertical bar represents a single cell.

(C) Stills of live-cell imaging showing cells transfected with Tctex-1 shRNA plasmids and expression vectors for the nonphosphorylatable Tctex-1T94A or the phosphomimetic Tctex-1T94E variants, as indicated, during unperturbed mitoses. Bar, 5 µm.

(D) Distribution of total time spent in mitosis (from nuclear envelope breakdown to anaphase onset) in cells transfected with shRNAs and expression vectors as indicated. Whisker-Tukey boxes span 25-75 percentile, while center bar denotes median and "+" marks mean.

(E) Stills of live-cell imaging showing a control cell and cells transfected with Tctex-1 shRNA plasmids at the anaphase onset. Arrows indicate missegregated polar chromosomes and arrow heads indicate chromosome bridges. Bar, 5 µm.

(F) The percentage of mitotic cells with normal segregation (blue), missegregated polar chromosomes (green), chromosome bridges (yellow), and both (red) at the anaphase onset were analyzed in cells transfected with shRNAs and expression vectors as indicated. Mean with 95% confidence interval were plotted with chi-square test being performed to compute the p-value.

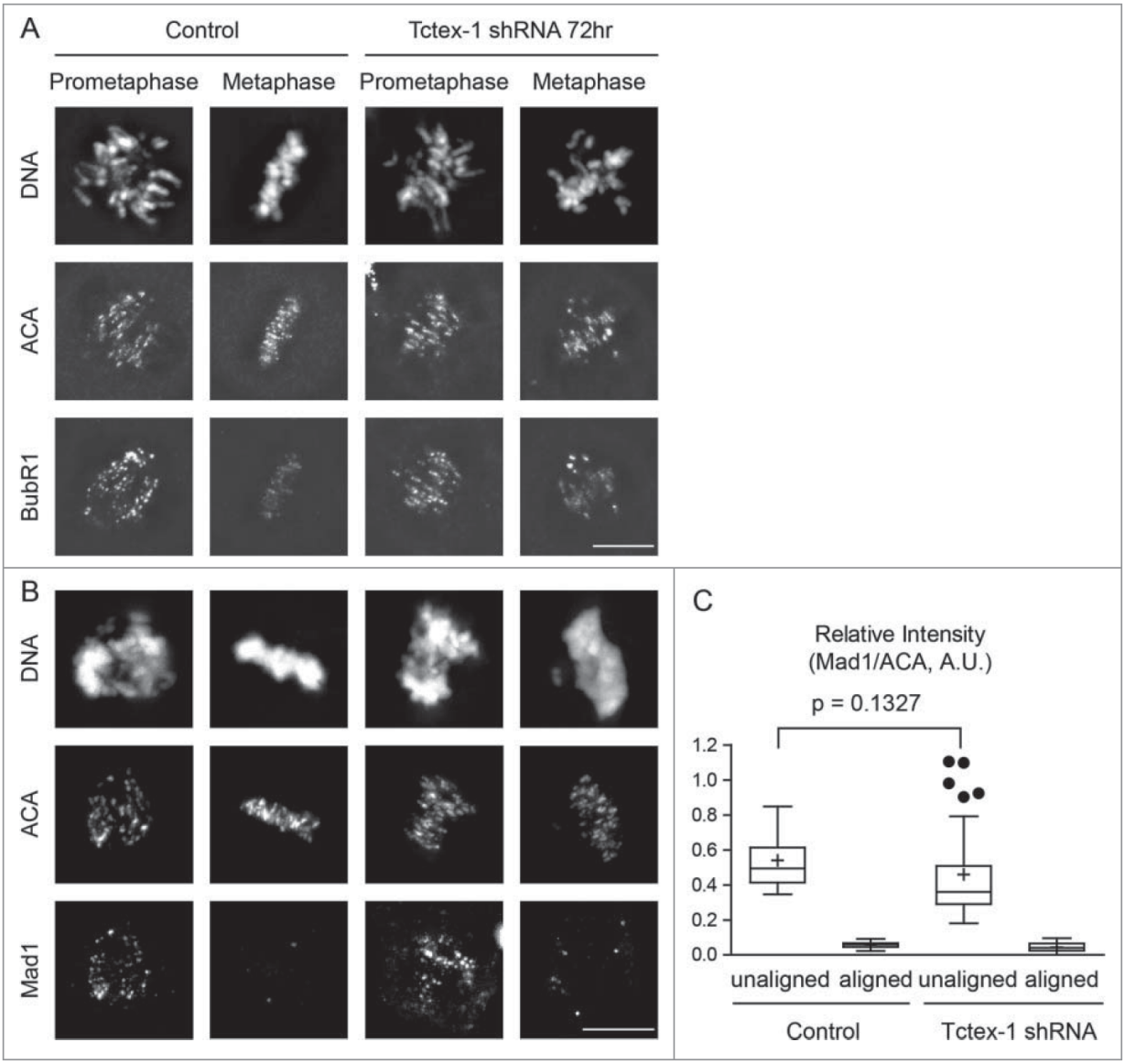

Figure 4.5. Tctex-1 depletion does not affect the association of the mitotic checkpoint proteins at unattached kinetochore and their release from attached kinetochores.

(A and B) Immunofluorescence detection of DNA, ACA, BubR1 (A) and Mad1 (B) in prometaphase and metaphase cells transfected with control or Tctex-1 shRNA plasmids as indicated. Bar, 5 μm.

(C) Quantification of the normalized relative kinetochore intensities (per kinetochore) of Mad1/ACA in mitotic cells. Whisker-Tukey boxplots span 25-75 percentile, while center bar denotes median and "+" marks mean. Quantifications were based on 30 kinetochores (control unaligned), 30 kinetochores (control aligned), 37 kinetochores (Tctex-1 shRNA unaligned) and 30 kinetochores (Tctex-1 shRNA aligned) from multiple cells.

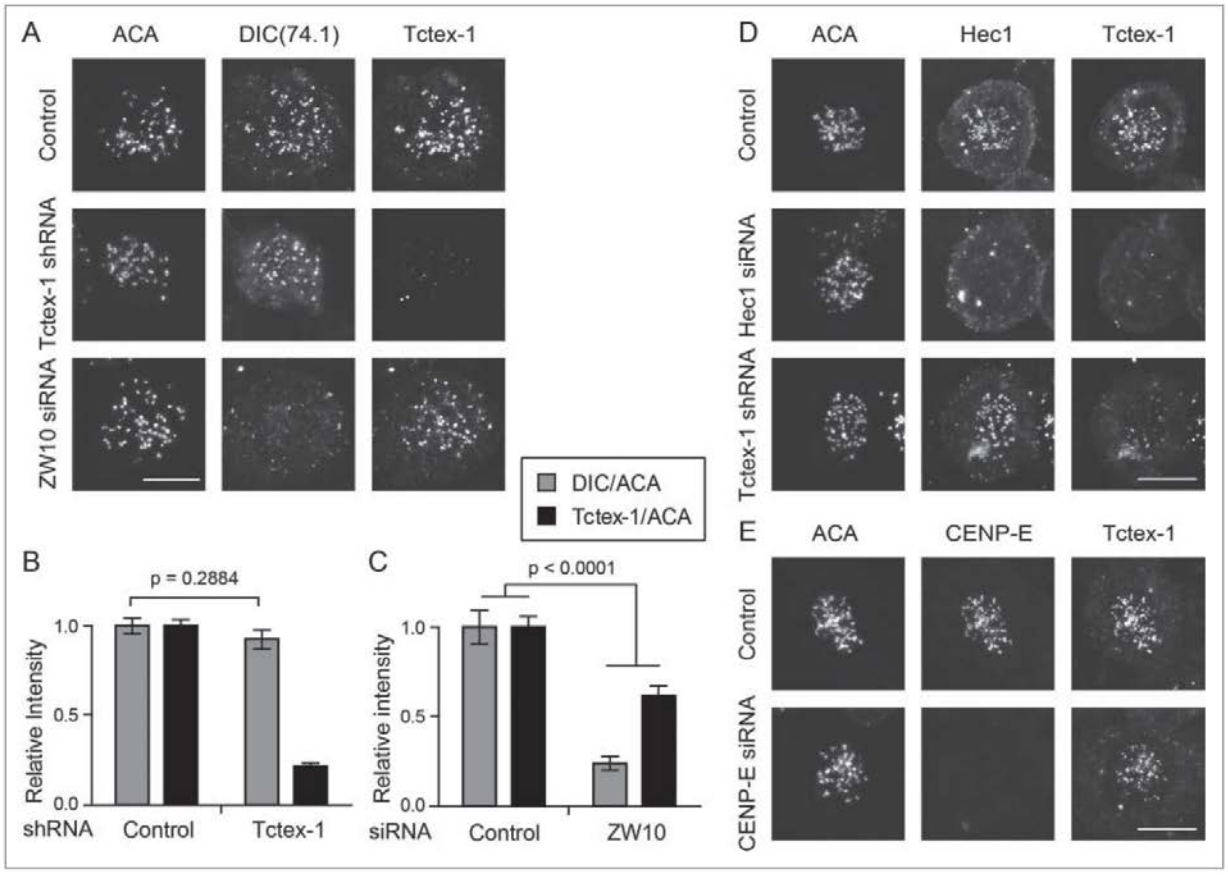

Figure 4.6. Tctex-1 kinetochore localization is dynein independent.

(A) Immunofluorescence detection of ACA, dynein (DIC), and Tctex-1 in nocodazole treated (3 hrs) mitotic cells transfected with Tctex-1 shRNA plasmids or ZW10 siRNA as indicated. Bar, 5 μm.

(B and C) Quantification of the normalized relative kinetochore intensities (per kinetochore) of DIC/ACA and Tctex-1/ACA (mean ± SEM) in mitotic cells. In (B), 63 (control) and 57 (Tctex-1 shRNA) kinetochores from multiple cells were measured. In (C), 83 (control) and 41 (ZW10 siRNA) kinetochores from multiple cells were measured.

(D and E) Immunofluorescence detection of ACA, Hec1 (A) or CENP-E (B), and Tctex-1 in mitotic cells transfected with Hec1 (A) or CENP-E (B) siRNA. Bar, 5 μm.

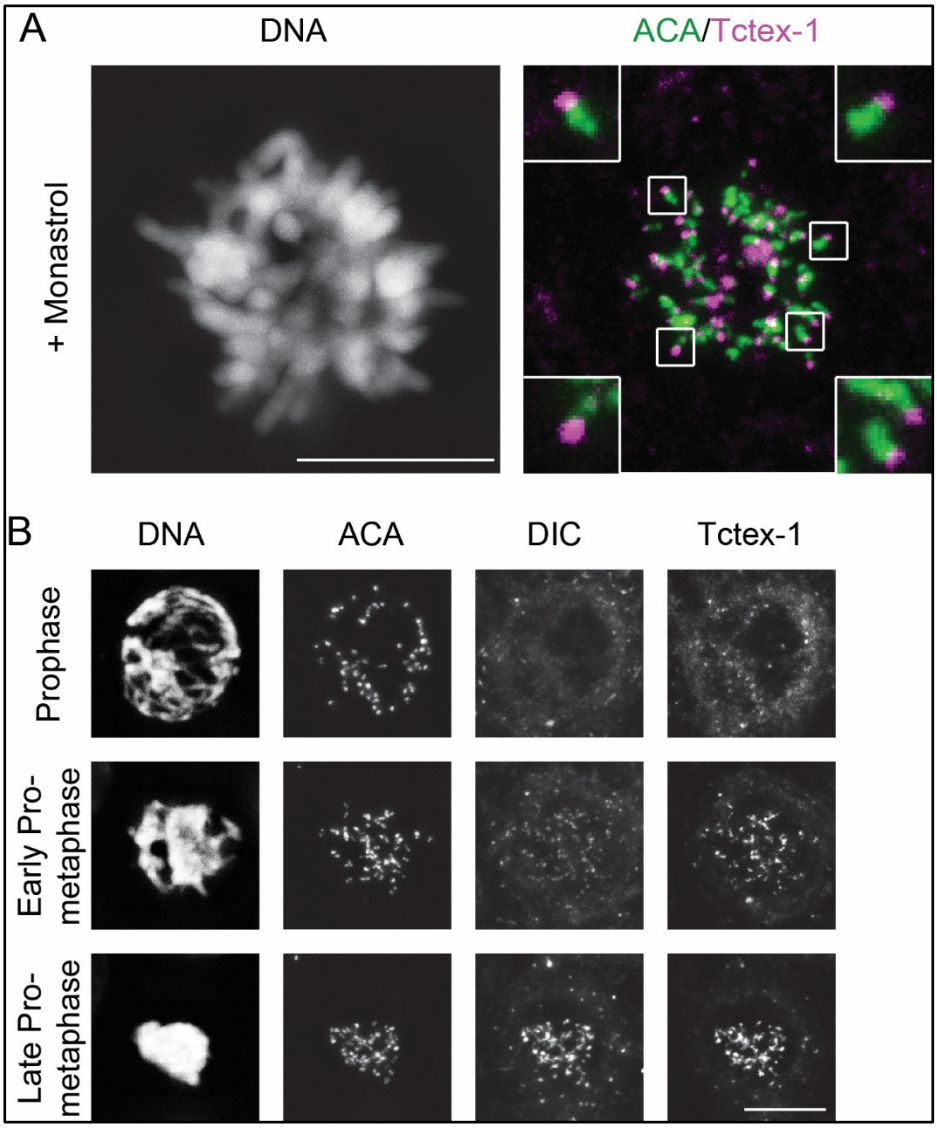

Figure S4.1. Tctex-1 is an outer kinetochore component.

(A) A T98G cell with a monopolar spindle upon monastrol treatment (100 μM for 30 min) stained with DNA (left panel) as well as ACA (green) and Tctex-1 (magenta) (right panel) showing Tctex-1 strong localized to the unattached outward-facing kinetochores (see inserts). Bar, 5 μm.

(B) Indirect immunofluorescence staining of ACA, dynein (DIC), Tctex-1, and DNA in prophase and prometaphase cells as indicated. Bar, 5 μm.

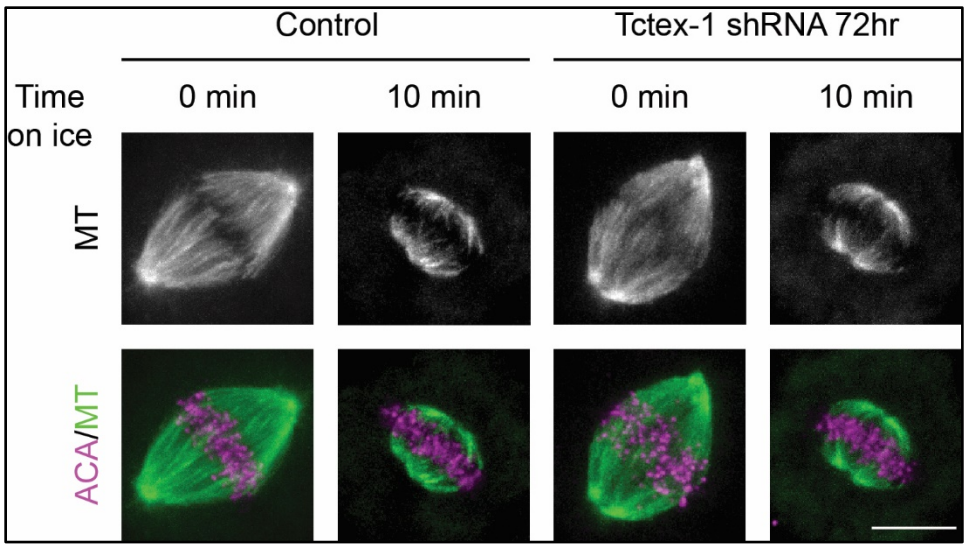

Figure S4.2. Tctex-1 depletion does not affect the global stability of kinetochore bound microtubule fibers.

T98G cells were transfected with control or Tctex-1 shRNA plasmids. After 72 hr, cells were incubated on ice for 10 min before they were fixed and processed for immunofluorescence staining for tubulin (green) and ACA (magenta). Bar, 5 μm.

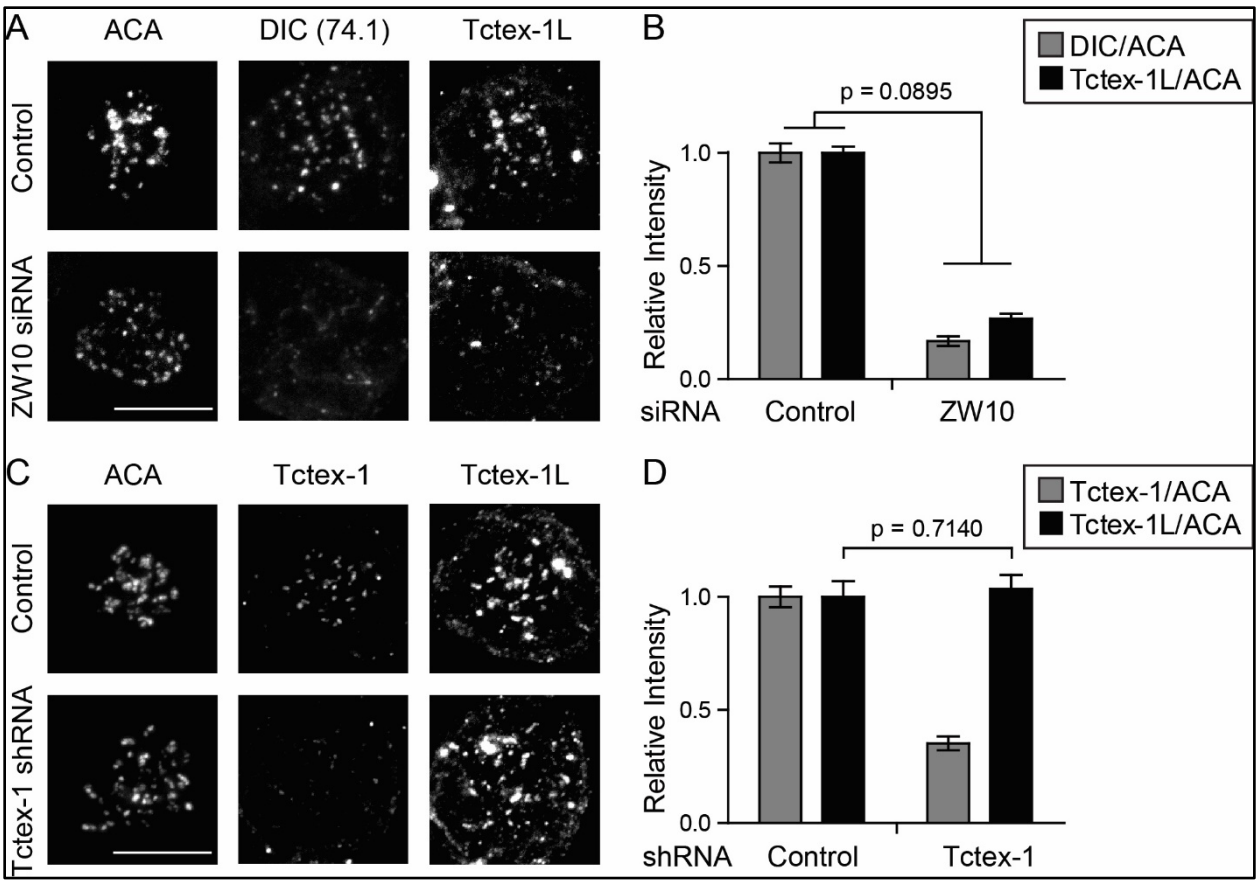

Figure S4.3. Knockdown of Tctex-1 does not affect kinetochore recruitment of dynein-Tctex-1L

(A and C) Immunofluorescence detection of ACA, dynein (DIC), and Tctex-1L in nocodazole treated mitotic cells transfected with ZW10 siRNA or Tctex-1 shRNA plasmids as indicated. Bar, 5 μm.

(B and D) Quantification of the normalized relative kinetochore intensities (per kinetochore) of DIC/ACA and Tctex-1/ACA (mean ± SEM) in mitotic cells. In (B), 184 kinetochores from 14 control cells and 186 kinetochores from 13 ZW10 siRNA cells were measured. In (C), 98 kinetochores from 13 control cells and 68 kinetochores from 10 ZW10 siRNA cells were measured.

Chapter Five: Discussion and future directions

FORMIN centromere's epigenetic identity

(1) Diaphanous formin mediated nuclear actin regulates CENP-A maintenance at the centromere

In mammalian cells, accurate chromosome segregation is guided by the centromere, a specialized chromosomal region epigenetically defined by nucleosomes containing the histone H3 variant CENP-A. In order to keep centromere identity with ongoing CENP-A dilution caused by S phase genome replication, new CENP-A proteins are deposited at preexisting centromeres in G1 phase of the cell cycle. Multiple molecular pathways have so far been identified underlying CENP-A replenishment, however, little is known in terms of how new CENP-A proteins become stably incorporated into centromeric nucleosomes. In Chapter 2 and 3 of this thesis, I identified the cytoskeletal protein diaphanous formin mDia2 is essential for newly synthesized CENP-A to be stably deposited at G1 centromeres, using quantitative imaging and pulse chase analysis. Using high resolution quantitative ratiometric live cell imaging, we further provided temporal evidence that the MgcRacGAP-based small GTPase small molecular switch is required from early G1 phase. Formin mDia2 functions downstream of the MgcRacGAP-dependent small GTPase pathway, as ectopic activation of endogenous mDia2 in the absence of MgcRacGAP is sufficient to maintain stable CENP-A loading. This novel function of mDia2 depends on its nuclear localization and its ability to polymerize actin. Dynamic and short actin filaments were observed in early G1 nuclei in an mDia2 dependent manner. Indeed, centromeric CENP-A level was reduced in cells depleted of IPO9 and expressing a nonpolymerizable actin mutant. To further examine the physical role of mDia2 mediated nuclear actin during CENP-A replenishment, single particle tracking of centromere movement was performed in early G1

nuclei over the time scale of initial CENP-A loading. Quantitative analysis uncovered subdiffusive behaviors where normal G1 centromeres movements are relatively confined. The confinement of centromere motion, however, is significantly impaired upon mDia2 knockdown. Finally, depletion of mDia2 results in a prolonged association of HJURP, the dedicated CENP-A loading chaperone, at the centromere. Thus, our findings suggest the diaphanous formin mDia2 forms a link between the upstream small GTPase signaling and the downstream confined nuclear environment, and therefore regulates the stable assembly of new CENP-A containing nucleosomes at least in part through the timely turnover of centromeric HJURP to mark centromere's epigenetic identity (**Figure 5.1**). Our findings have solved a key problem in the CENP-A field: what are the substrates or effectors that link small GTPase signaling to the loading/maintenance of CENP-A molecules at the centromere. Furthermore, with the identification of actin nucleation activity of mDia2 and polymerizable nuclear actin per se being essential for the stable maintenance of centromeric CENP-A levels, we have discovered a new nuclearskeletal mechanism that participates in the epigenetic regulation of CENP-A maintenance coupled to centromere chromatin movement. Lastly, with the finding that mDia2 depletion influences HJURP dwelling, but not its recruitment at G1 centromeres, we have identified a new route of crosstalk where mDia2-mediated nuclear actin has a potential role in the timely removal/turnover of CENP-A's loading machineries.

It didn't escape our notice that diaphanous formin mDia2 could also participate in the regulation of nuclear events indirectly through the megakaryocytic acute leukemia protein (MAL) – serum response factor (SRF) pathway. It has been shown that mDia1/2 can nucleate actin polymerization inside somatic cell nuclei, and the polymerization of nuclear actin plays an

important role in abolishing the inhibitory effect of monomeric actin toward MAL, thus enable MAL to be a cofactor for SRF's transcriptional activity[94]. SRF is a transcriptional factor required for the expression of many immediate early genes, cytoskeletal genes as well as muscle-specific genes[224,225]. By immunoblot against the total protein levels of CENP-A inside the cells, we did not find any difference in the expression level of CENP-A itself, upon mDia2 depletion. Together with the fact that YFP-CENP-A (which is controlled from 5' sequences distinct from the endogenous locus of CENP-A) also has reduced levels at the centromere, this makes it unlikely that CENP-A is a downstream target gene of SRF pathway and the phenotype we observed was due to transcriptional level regulation[177]. Interestingly, among the many target genes of SRF is CENP-B, which is expressed in heart and differentially regulated in *Srf*-/- embryonic stem cells[226]. Although CENP-B has been implicated in centromere function as mentioned earlier in the introduction part of the thesis[74], it is unlikely to be the reason underlying the CENP-A phenotype we had. On one hand, we didn't observe any changes in centromeric CENP-B foci in cells depleted of mDia2[177]; on the other hand, even if CENP-B is reduced upon mDia2 depletion (and the SRF transcriptional activity based on mDia2) by more than 90%, centromeric CENP-A levels have been shown to remain unchanged at least within the time frame of our assay[74]. Currently we have not tested any other downstream factors of SRF is involved in CENP-A maintenance, nor have we tested whether any of the other molecular components in the CENP-A loading pathway have changed expression levels upon mDia2 depletion. Future work will include systems scale screen using microarray or RNA-seq against known CENP-A loading factors upon mDia2 depletion to rule out possible indirect effects.

Apart from possible differences in target gene expression downstream of the mDia-nuclear actin-SRF pathway, another alternative explanation lies in the relationship between transcription and centromere chromatin. It has been shown that the definition of centromeres at the holocentric chromosomes of *C.elegans* inversed correlated with germline transcription, shown by the complementary occupancy of CeCENP-A and RNA Polymerase II across the *C.elegans* genome[227]. Interestingly, it has also been shown that filamentous nuclear actin polymers inversely correlates with the transcriptional activity of RNA Polymerase II[181,228]. These lines of evidence suggest a positive correlation between polymerized nuclear actin filaments and centromere identity, and implicates that there might be a connection between nuclear actin filaments and centromere determination, indirectly through the regulation of transcription activity of the chromatin. Nevertheless, recent findings in *Xenopus* and human cells also suggest that regional transcription permissive marks and the RNA polymerase II based transcripts at centromere are important for CENP-A inheritance, possibly through H3.3 exchange[69-72]. The exact relationship of RNA transcription and centromere determination therefore remains an important problem, especially with regard to the range of transcription permissive marks versus nonpermissive marks relative to centromere chromatin's position at the chromosome[229]. At this point we are unable to rule out possible influences on transcription due to mDia2 depletion. Nevertheless future work using ChIP-seq will enable the measurement of transcription activation/silencing upon mDia2 depletion, at the whole genome scale.

Based on our data, the current model we proposed at the beginning of this section (**Figure 5.1**) explains the correlated behaviors of mDia2's function downstream of MgcRacGAP-based small GTPase signaling, G1 CENP-A loading, nuclear actin dynamics, centromere motion

as well as the turnover of HJURP. However, caveats remain especially in terms of the localization of mDia2. We have not been able to document any enriched centromere localization of mDia2, either with antibody staining or overexpressed fluorescently tagged mDia2 protein. It remains to be tested with genome editing techniques that allows fluorescent tagging of endogenous mDia2 proteins. Additionally, it didn't escape our notice that an obvious temporal discrepancy exists between the role of mDia2 in early G1 and the apparent centromere localization of MgcRacGAP in late G1 judging from overexpression of fluorescently tagged MgcRacGAP proteins. One possibility is that MgcRacGAP starts to function at early G1 centromere even before their maximal centromere levels are reached. This is consistent with the finding that depleting MgcRacGAP results in similar phenotype in real time YFP-CENP-A loading (Chapter 3), and that MgcRacGAP binds to KNL2, a component of the licensing factors for CENP-A loading that already localizes at centromere in early G1[50]. Finally, it remains possible that the observed changes upon mDia2 depletion are concurrent yet not directly due to causal relationships, thus future work will be focused on evaluating the effect of IPO9 depletion on centromere movement in early G1 over the time window of CENP-A loading, as well as the impact of MgcRacGAP and/or IPO9 depletion on the turnover of HJURP at G1 centromeres.

(2) Systems-scale examination of formin's roles in epigenetic regulation of chromatin and chromosomes

Given our discoveries that diaphanous formin mDia2 functions downstream of the small GTPase molecular switch MgcRacGAP in stable centromeric CENP-A loading, one obvious question is: where does mDia2 localize inside the nucleus? Despite extensive efforts we haven't been able to detect any centromere specific localization of mDia2 in G1-phase. This could be due

to technical challenges in antibody or exogenous protein overexpression, which could be potentially addressed with new technologies such as tagging endogenous mDia2 with genome editing; on the other hand, endogenous mDia2 could actually have association beyond the centromere to be readily activated with differed inputs at difference locations at different times, with centromeric local activation by MgcRacGAP or small GTPase being only one of many inputs. Biochemical proteomic analysis will thus provide more insights regarding mDia2's potential binding partners in complexes where it is involved during centromere maintenance and beyond. Among many chromatin related complexes, certain chromatin remodeling complex use polymerized actin filaments in their functions[180,230]. Therefore, one possibility is mDia2 mediated nuclear actin filaments participates in chromatin remodeling complex, where interactions between mDia2/ nuclear actin and chromatin proteins could be important. Indeed, it has been reported that the FH2 domain of diaphanous formin can interact with CENP-A in a yeast-two hybrid assay[231]. Interestingly, our preliminary immunoprecipitation didn't detect CENP-A binding with EGFP-mDia2-FH1FH2, but instead has found histone H3 binding specifically with EGFP-mDia2-FH1FH2 (**Figure 5.2**). This result is quite surprising to us, one possibility is the technically low abundance of CENP-A in the lysate, while the other possibility consistent with non-specific binding to the chromatin while being specifically and locally activated by upstream signaling. The biochemical association of histone H3 with EGFP-mDia2-FH1FH2 is very interesting, not only because it confirms recent proteomic results, but also because it has been proposed that H3 (likely in particular H3.3) has to be "evicted" from centromeric nucleosomes to allow CENP-A incorporation[51]. Future work will further examine the biochemical association of mDia2, with a focus on chromatin proteins, using hypothesis driven approaches or unbiased screens based on mass spectrometry analysis.

On the other hand, from the chromosomal point of view, it is interesting to know whether centromeric chromatin the only chromosomal target of formin-based regulation? Although we have shown that another nonconventional histone variant H2A.Z remains the same levels globally, closer examination is required to test for other nonconventional histone variants under conditions like DNA damage. Finally, our results on the constrained centromere movement inside G1 nuclei during CENP-A loading is consistent with earlier observations of the motion of interphase chromosome foci in yeast and flies[232], as well as the fractal globule model of interphase chromosome territory[192]. Because we have observed several long range centromere movements in mDia2 depleted cells, whether this reflects global rearrangement of chromosome territories upon mDia2 depletion remains to be investigated in the future.

(3) An ever-expanding repertoire of nuclear actin-based epigenetic processes

After over 40 years of controversies, it is now clear that both actin and actin motors exist inside the nucleus[88,89,91]. In particular, the existence of polymerized actin filaments are not confirmed until recently with multiple meticulously designed probes[94,96]. We now know that polymerized actin filaments do exist inside the nucleus, although it has been debated whether actin polymerization inside the nucleus functions by simply depleting the monomer pool, or by contrast, actually does mechanical work using the polymerized filaments. On the one hand, it has been shown that actin polymerization inside the nucleus release the inhibitory effect of monomeric actin on MAL (megakaryocytic acute leukemia protein), a cofactor for the transcriptional factor SRF (serum response factor)[94,95]. On the other hand, our results together with other groups' results strongly suggest it is the filament specific functions that participate in regulating certain epigenetic processes[97]. In the meantime, emerging evidence suggest that multiple forms of morphology of filamentous actin as well as multiple paths to nucleation co-

exist inside somatic cell nuclei (e.g. FMN2 mediated DNA damage response v.s. mDia2 mediated CENP-A loading), underlying the diversified mechanisms a cell can use to specifically address highly-regulated processes. Future work include close examination of the indices and morphology of filamentous nuclear actin as a function of cell cycle time, as well as on any potential crosstalk between the diversified nucleation pathways. Finally, our findings about the role of mDia2 mediated nuclear actin in centromere maintenance suggest a unappreciated mechanism to ensure genome integrity, where actin comes in first to help maintain centromere identity long before microtubules actually get in touch with the kinetochores assembled on centromeres. Such mechanism could be part of a growing list of biological functions participated by polymerizable nuclear actin (e.g. anti-gravity buffering[233], DNA damage response etc.) that demonstrate novel organizational capability. Future work combining *in vivo* perturbation and *in vitro* reconstitution[234] would provide new perspective in understanding the dynamic epigenetic events inside the nucleus across nanometer to micron scale in space, over cellular to organismal scale in time.

(4) Quantitative measurements of centromere identity

Faithful transmission of the chromosomal information over continuous rounds of cell division in all higher eukaryotes depends on centromeres. It is crucial for each replicated chromosome to have one and only one centromere, as it has been shown that acentric fragments or dicentric chromosomes are often times missegregated during cell division[235-237]. In mammals, to allow each chromosome to “remember” where the centromere is, the centromere protein A (CENP-A) was used to specifically label active centromeric chromatin upon which kinetochore assembly will occur[238]. For the last two decades, great progress has been made toward

understanding how CENP-A maintains its own levels at the centromere in order to stably make the epigenetic mark. It became apparent that accurate measurement of CENP-A levels is the key to the systematic dissection of essential molecular requirements underlying stable CENP-A maintenance. While important discoveries on those molecular requirements being made by various groups, different quantitative methods were formulated and applied (**Table 5.1**). Each of those established methods in making quantitative measurements of CENP-A levels has its merits and limitations. In order to achieve high throughput, automated and non-subjective measurement that can take into account pixel intensities from all centromeres for a given cell, we developed the integrated nuclear CENP-A (INCA) measurement using custom code in MATLAB. First, at the core of the INCA algorithm heterogeneous local backgrounds for each image or cell were acknowledged and addressed by kernel filtering (**Figure 5.3**) on the original raw images, prior to quantitative measurement of the integrated CENP-A pixel intensities from all centromeres from one cell within its nuclear mask (**Figure 5.4**). Importantly, by applying the INCA measurement, integrated intensity measurement is not prone to the risk of thresholding-based masks generated upon single centromeres which can result in tremendous artifacts, and can quickly generate clustered measurement that reflects 'loading' capacity for each cell. Of course the INCA method has its own limitation: e.g. SNR of the images need to be within certain range such that no visible nucleoplasmic, non-centromeric pixel intensities will remain after kernel filtering. It is a criteria met with our current studies and fixation protocols, but nonetheless necessitates future improvement based on our quantitative measurement algorithm, potentially through combining Gaussian mixed-model fitting for local centroid amplitude detection and measurement, rather than Otsu-thresholding based centromere detection and measurement[239].

During the course of our study, another method called 'Centromere Recognition and Quantification (CRaQ)' was developed by the Jansen lab, using automated macros in ImageJ and multivariate parameters for thresholding-based measurement[42,240]. While being a great way to automatically measure intensity values on each individual centromeres, almost 50% percent of centromeres per cell are excluded, and the resultant measurements may not necessarily reflect the integrated 'loading' capacity of one cell (especially if potential spatial reorganization of G1 centromeres were to be considered, e.g. should loaded centromeres move less and thus tend to cluster). Future improvement based on either CRaQ or INCA will thus be focused on more precise detection and measurement using thresholding-free and fitting-based method.

A Tctex-1 based molecular "Velcro" at the kinetochore beyond cytoplasmic dynein complex

In Chapter 4 of this thesis, we have identified the dynein light chain T-complex testis-specific protein 1 (Tctex-1 or DYNLT1) as a novel factor important for the regulation of kinetochore-microtubule attachment during mitotic chromosome alignment. Using quantitative imaging and live cell analysis, we found that Tctex-1 associates with unattached kinetochores and localizes at the outer layer of kinetochores. Depleting Tctex-1 does not affect the recruitment or removal of dynein at the kinetochore, but results in prolonged mitotic arrest due to misaligned chromosomes. Tctex-1 does not rely on dynein for its function at the kinetochore, as both the dynein-bound and the dynein-free mutants of Tctex-1 can rescue the phenotype of mitotic chromosome misalignment/missegregation to a similar level, and the kinetochore localization of Tctex-1 is independent of the ZW10-based dynein pathway. Therefore, we have uncovered a

dynein-independent function of Tctex-1at the kinetochore. All three types of light chain (LC) proteins of the dynein complex (LC8, LC7/roadblock, and Tctex-1) dimerize and assemble on the intermediate chain (IC) and together bind to the tail domain of dynein heavy chain homodimers[104]. Apart from mediating interactions between dynein complex and dynein accessory proteins[101], light chain proteins also can interact with a broad range of proteins outside of the dynein complex. For instance, Tctex-1 can interact with Fyn, DOC2, FIP1, CD155, rhodopsin and the poliovirus receptor[241]; LC8 has been shown to be a tail-binding light chain for dynein and myosin 5a, and to have more than 40 binding partners in various cellular contexts such as transport, mitosis and transcription[242]. Importantly, the LC8 binding motifs found in LC8's binding partners are often located near the coiled-coil or other dimerization domains[242]. Therefore, an attractive model has been proposed that LC8 could function as a general 'molecular velcro' that facilitates dimerization. Structural analysis revealed tertiary fold similarity between LC8 and Tctex-1 despite no sequence identity based on structural alignment[241], and suggested that Tctex-1 binds to its targets in a way similar to LC8[241,243]. Therefore 'molecular velcro' could have a more general role in dimerization and/or protein complex formation, with the use of either LC8 or Tctex-1 to achieve specificity among diversified cellular processes. Adding to the dynein-independent roles of Tctex-1 in actin remodeling underlying neurite outgrowth[244], our findings revealed a fundamental function of Tctex-1 underlying accurate chromosome segregation in mitosis.

Currently there is no evidence for the known Tctex-1 binding partners outside of the dynein complex to be involved in regulating kinetochore function and mitotic chromosome segregation[241], and our current data have not addressed the fundamental question – what is the binding partner of the dynein-free Tctex-1 that contributes to kinetochore/microtubule

attachment? Nevertheless, with clues from structural studies (regarding the 'Tctex-1 binding motif') and lessons learned from LC8[242,243], bioinformatics prediction in conjunction with mass spectrometry profiling can be conducted in the future to screen for potential mitotic proteins that associate with Tctex-1 at the kinetochore.

(1) A phosphorylation suppressed self-removal mechanism regulates the localization of kinetochore dynein, but not Tctex-1

While studying the dynein-independent role of Tctex-1 at the kinetochore, we noticed that the regulated kinetochore localization of Tctex-1 differs from the dynein motor, regarding their response towards Aurora kinase inhibition. Marked by the dynein intermediate chain (DIC), the dynein motor's kinetochore localization in monopolar spindle, but not in prophase, requires Aurora kinase activity. As the small molecule ZM447439, a potent inhibitor towards Aurora B kinase, abolishes DIC's kinetochore localization in monastrol treated cells. However, neither Tctex-1's kinetochore localization in monopolar spindle or prophase requires Aurora kinase activity (**Figure 5.5**). This results indicate yet another differed properties of Tctex-1 and dynein motor at the kinetochore, thus providing further supports to a dynein-independent function of Tctex-1 at the kinetochore.

Since the main difference between monastrol generated monopolar spindle and prophase cell is microtubule-kinetochore attachment present in the former but not the latter, we decided to test if the differential response of dynein upon Aurora inhibition is dependent on microtubule-kinetochore attachment. Dynein's kinetochore localization is assessed using immunofluorescence imaging in the presence or absence of Aurora kinase activity, when microtubule attachment to kinetochores are abolished. Interestingly, Aurora kinase activity is

dispensable for kinetochore dynein (DIC) recruitment upon nocodazole treatment. By contrary, Aurora kinase activity is required for kinetochore dynein (DIC) localization upon MT attachment, in a monopolar spindle's kinetochores where microtubule attachment have been established. This results suggest a model where the role of Aurora phosphorylation, instead of being required for dynein's recruitment to kinetochores, is required for suppressing the microtubule-based self-removal of dynein motors so that they can maintain their kinetochore localization (**Figure 5.6**). Our result differs from previous reports that Aurora B is required for the recruitment of dynein to kinetochores[245]. Future work will include in vitro examination of dynein's motor activity in the presence or absence of Aurora B kinase.

(2) A novel asymmetric "antagonistic" module at kinetochore microtubule plus ends

After identifying a dynein-independent pool of Tctex-1 at the kinetochore, the next logical question is how does Tctex-1localize at the kinetochore and what does it do at the kinetochore? Similar to the chromosome alignment phenotype caused by Tctex-1 depletion, knocking down the microtubule plus end tracking protein CLIP-170 has been reported to result in misaligned chromosome and prolonged mitosis[246]. Importantly, CLIP-170 has the same asymmetric localization biased toward distal sister kinetochore in prometaphase cells[247]. Therefore, we decided to look into the relationship between Tctex-1 and CLIP-170. Immunofluorescence confirmed that CLIP-170 has asymmetric localization at sister kinetochores in monopolar spindle, similar to Tctex-1. Interestingly, knocking down CLIP-170 CLIP-170 or Tctex-1 negatively affect the kinetochore localization of one another (**Figure 5.7**). These data suggest that Tctex-1 associates with CLIP-170 and they are required for each other's robust residence at the kinetochore. Indeed, bioinformatics predictions uncovered possible regions on CLIP-170 and DIC that could bind to Tctex-1 (**Figure 5.8**). Interestingly, potential Tctex-1 binding motifs

coincide with low-probability coiled-coil regions (for DIC and CLIP-170) or regions near the end of the proteins (CLIP-170), consistent with a role in providing additional 'molecular velcro' for robust localization and function.

Given that both Tctex-1 and its possible interactor CLIP-170 are enriched at distal sister kinetochore, while the master microtubule plus end tracking protein EB1 is enriched near proximal sister kinetochore (**Figure 5.9**), it is possible that the apparently opposite localization is actively regulated. Indeed, upon mDia3 depletion, the level of kinetochore EB1 decreases while that of Tctex-1 and CLIP-170 increases[136], suggesting an "antagonistic" network at the kinetochore-microtubule plus ends. Importantly, in order to test if EB1 and microtubule plus end dynamics itself is required for this antagonistic regulation, we performed a "chemical epistatic analysis" where all microtubules were depolymerized using nocodazole, followed by measurement of Tctex-1 and CLIP-170 at the kinetochore in the absence of mDia3. No increase in kinetochore Tctex-1 or CLIP-170 were observed in mDia3 knockdowns when treated with nocodazole (**Figure 5.10**), suggesting that microtubule plus-end dynamics is required for the asymmetric "antagonistic" protein network at outer kinetochore, composed of mDia3 and Tctex-1/CLIP-170. By dissecting the inter-dependence between various kinetochore modules, we have identified a novel asymmetric "antagonistic" module at kinetochore microtubule plus ends (**Figure 5.10** and **Figure 5.11**): A compositional change is initiated by mDia3 depletion, mediated by EB1 and microtubule plus-end dynamics, and executed by Tctex-1 and CLIP-170. The exact role of this module in the mechanochemical biology of kinetochore remains to be examined.

Toward a quantitative understanding of kinetochore-microtubule interactions at the microtubule plus ends

As a key modulator in the aforementioned asymmetric "antagonistic" module, mDia3 itself is an outer kinetochore protein (**Figure 5.12**) that can bind to and stabilize microtubules[1]. Point-mutation (4E) in mDia3 abolishes its microtubule stabilization activity, and interestingly dampens the ordinary oscillatory movement of aligned kinetochores (Figure 5.11). Since kinetochore oscillation is a complex function of k-fiber coordination and microtubule turnover[248], we set out to test if 4E-mDia3 changes the turnover of microtubule itself. Interestingly, immunofluorescence revealed an elevated level of acetylated tubulin in cells expressing 4E-mDia3 (**Figure 5.13, A and B**). Tubulin acetylation depends on time and happens preferentially on stable microtubules. The elevated acetylated tubulin signals accumulate inside the spindle or near the poles, consistent with the situation where upon losing the microtubule stabilization activity of mDia3, dynamic instability at the plus ends occurs at higher frequencies thus the turnover (i.e. treadmilling) of tubulin subunit into the bulk of spindle occurs at a lower rate. Further *in vitro* reconstitution using TIRF microscopy is needed to better understand the mechanisms by which both WT- and 4E-mDia3 influence microtubule dynamic instability. In addition, with Monte Carlo simulation based on a stochastic state model (**Figure 5.13, C and D**), fitting *in vitro* measurement to theoretical growth/shortening rates could provide mechanistic insights of the energetic landscape of the kinetochore-microtubule interactions.

Figures

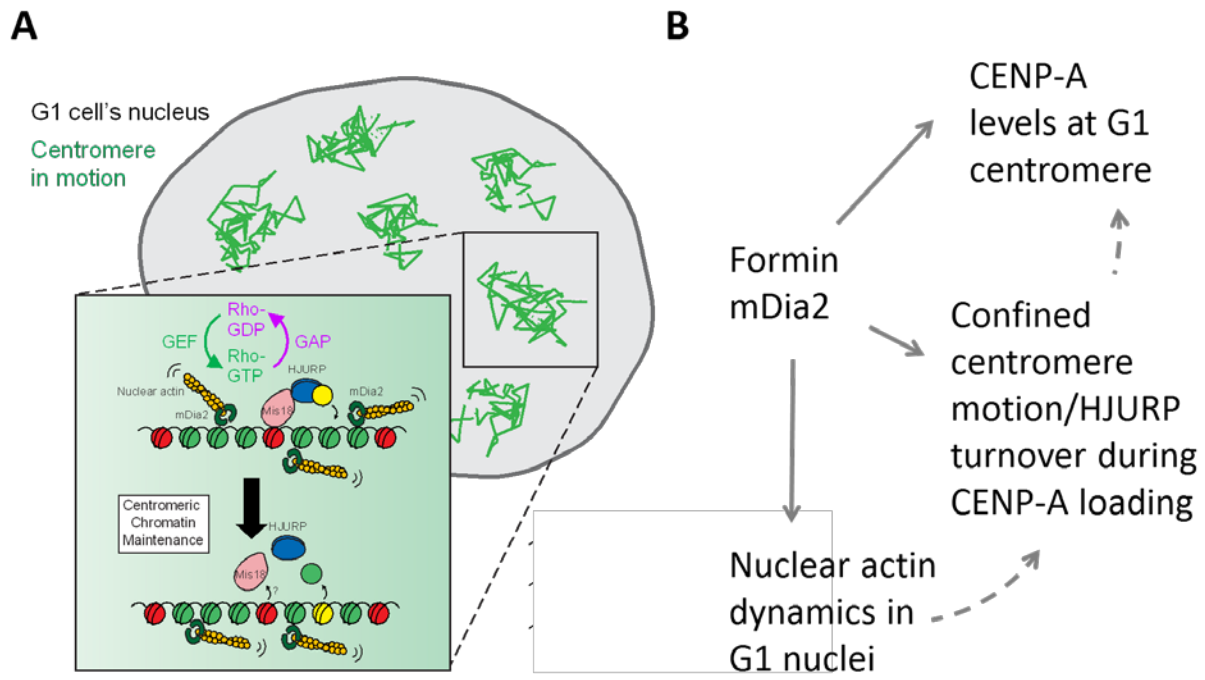

Figure 5.1. Working model for the diaphanous formin mDia2 mediated nuclear actin regulating CENP-A maintenance at the centromere

(A) Cartoon showing the functions of mDia2 downstream of the MgcRagGAP-based small GTPase pathway in regulating CENP-A loading at the moving centromeres. Green: H3 nucleosomes; Red: old CENP-A nucleosomes; Yellow: new CENP-A nucleosomes. (B) Schematics showing the correlative relationships between mDia2, G1 CENP-A loading, nuclear actin dynamics, centromere motion as well as the turnover of HJURP. Solid arrows indicate direct evidence for the requirement of mDia2 in each of the aspects; dashed arrows indicating putative causal relationships that require further test.

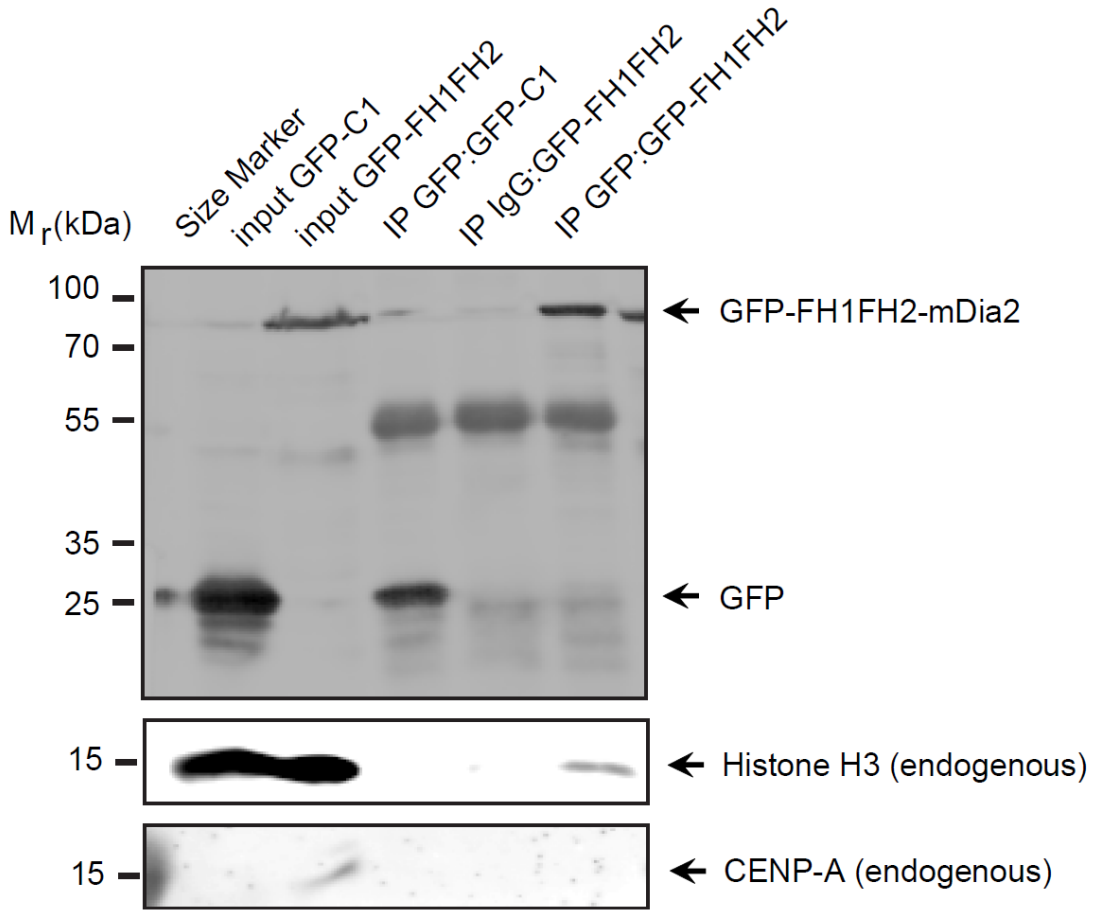

Figure 5.2. Immunoprecipitation using wild type mDia2-FH1FH2-EGFP confirmed it co-complex with histone H3

Input and IP lanes are all shown. EGFP protein (GFP-C1) was used as a control with anti GFP antibody to rule out tag-effect. Anti-IgG antibody was also used as a control with mDia2-FH1FH2-EGFP protein to rule out antibody non-specific binding (unpublished data).

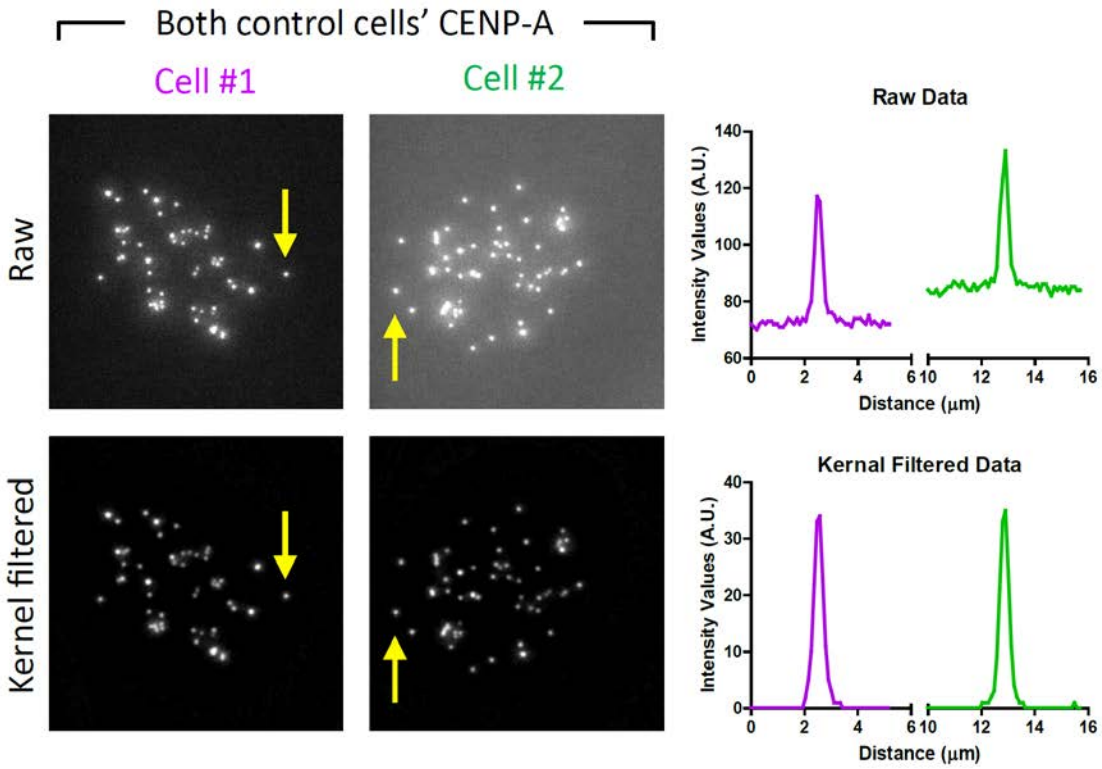

Figure 5.3. Kernel filtering and local background removal are critical to accurate quantitative measurement

Maximum Z-projected images from two control cells stained with CENP-A were shown on the identical scale for raw data (67-110), and for Kernel filtered data (0 – 40). Two different acquisitions of both control cells, even using the same batch of preparation and identical optical and software set up, could have different background levels. Therefore band-pass filtering and local background removal become key to accurate measurement against variations.

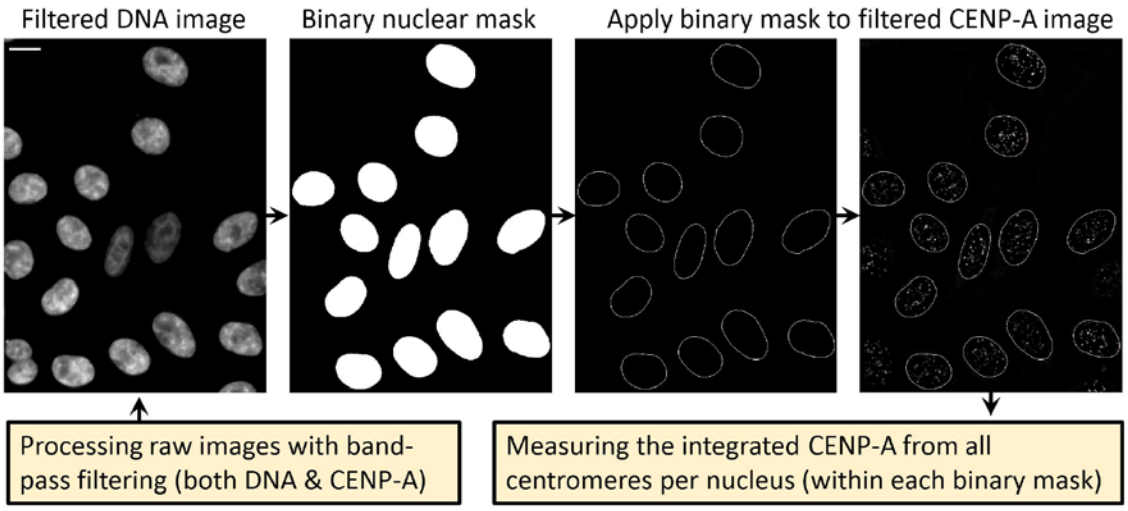

Figure 5.4. Integrated nuclear CENP-A measurement is a form of data clustering

Flowchart of the MATLAB program used in our study. Note that cells touching images' boarders were excluded to avoid edge effect. Each nuclear mask generated from DNA image (DAPI staining) provided a clustered measurement of the integrated centromeric CENP-A levels in that mask, representing the 'loading capacity' of CENP-A onto centromeres for that cell at the time being fixed. Combined with Figure 5.1, non-centromeric space inside the nuclear masks generally take zero intensity values.

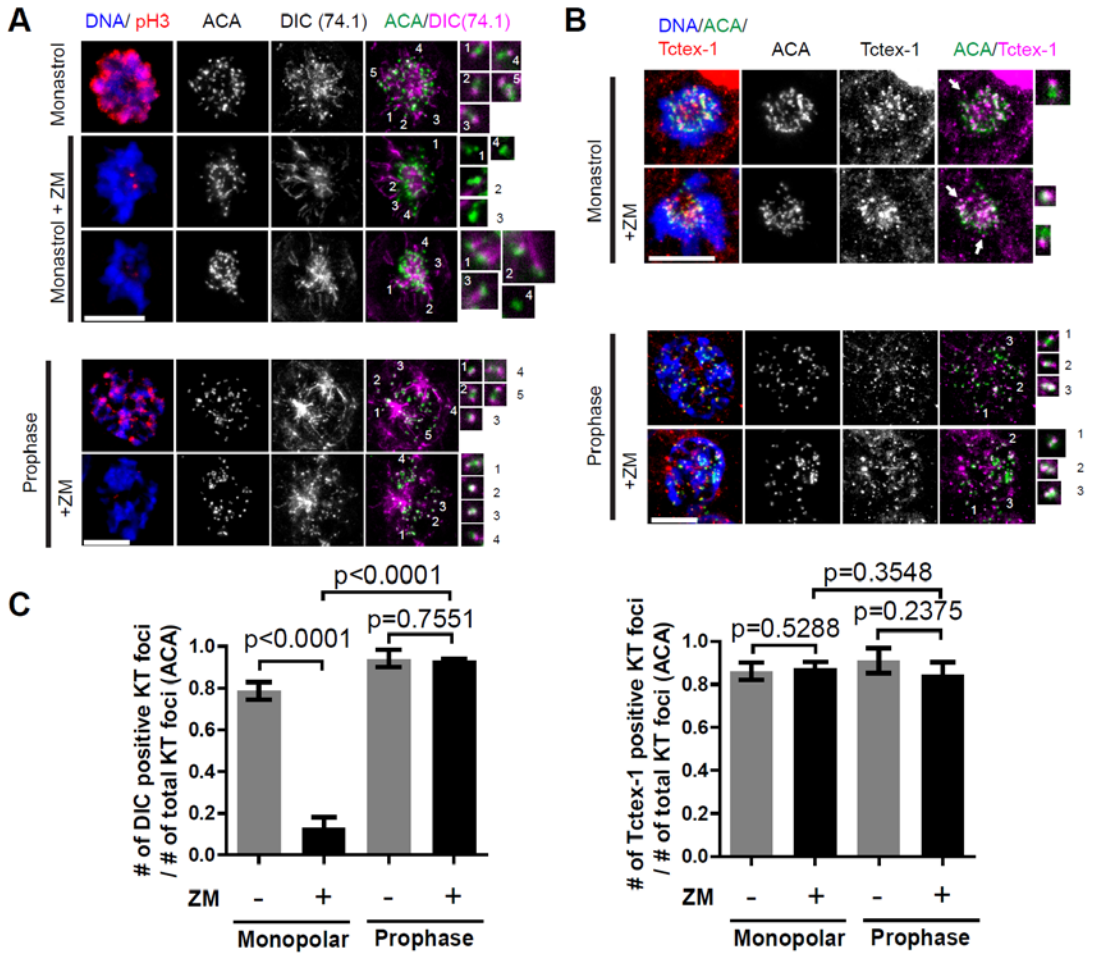

Figure 5.5. Tctex-1 and dynein have differed kinetochore localization response upon Aurora kinase inhibition

(A) Dynein intermediate chain (DIC)'s kinetochore localization in monopolar spindle, but not in prophase, requires Aurora kinase activity. Phosphorylated histone H3 (pH3) staining was used as a marker for Aurora kinase activity. (B) Neither Tctex-1's kinetochore localization in monopolar spindle or prophase requires Aurora kinase activity. (C) Quantifying the percentage of DIC or Tctex-1 localized kinetochore in all kinetochores (unpublished data).

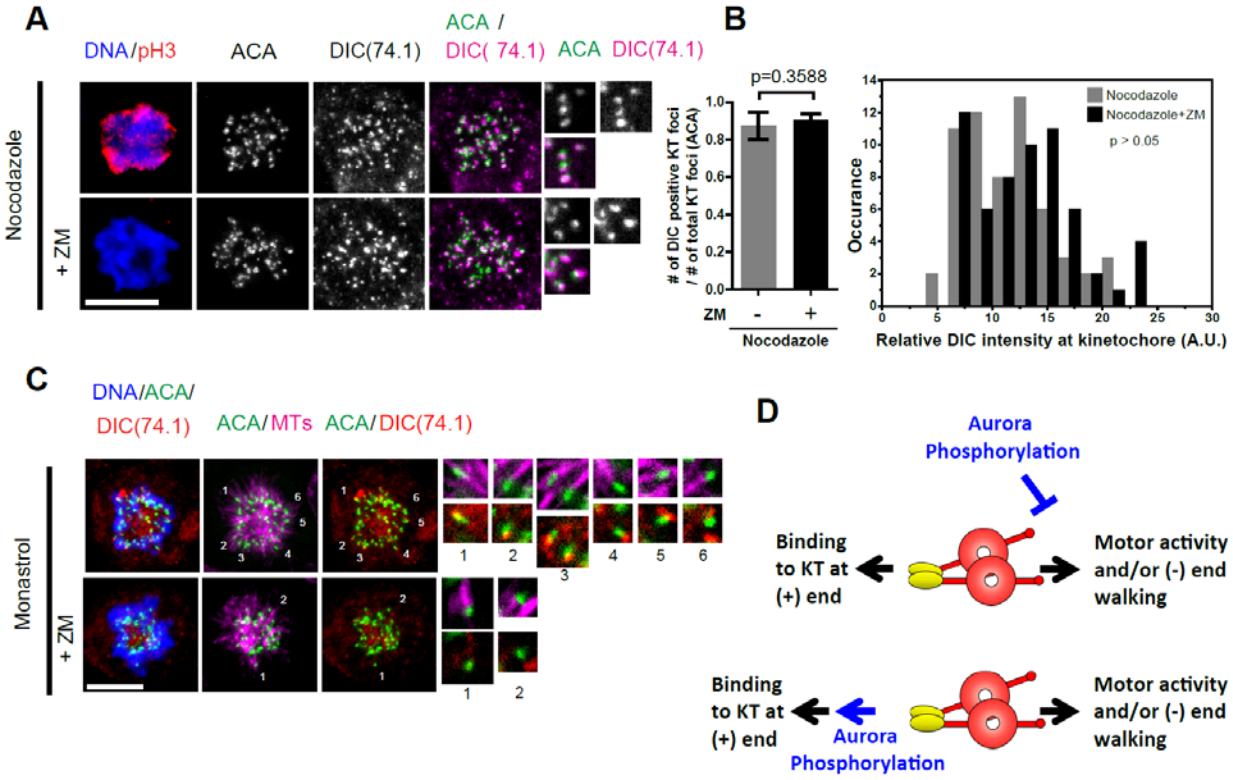

Figure 5.6. A phosphorylation suppressed self-removal mechanism regulates the localization of kinetochore dynein

(A) Aurora kinase activity is dispensable for kinetochore dynein (DIC) recruitment upon nocodazole treatment. (B) Quantifying the percentage of DIC localized kinetochore in all kinetochores, as well the the levels of DIC on kinetochores, upon nocodazole treatment, with or without Aurora activity. (C) Aurora kinase activity is required for kinetochore dynein (DIC) localization upon MT attachment. (D) Model for a role of Aurora phosphorylation, instead of being required for recruitment, is required for suppressing microtubule-based self-removal in dynein's kinetochore localization (unpublished data).

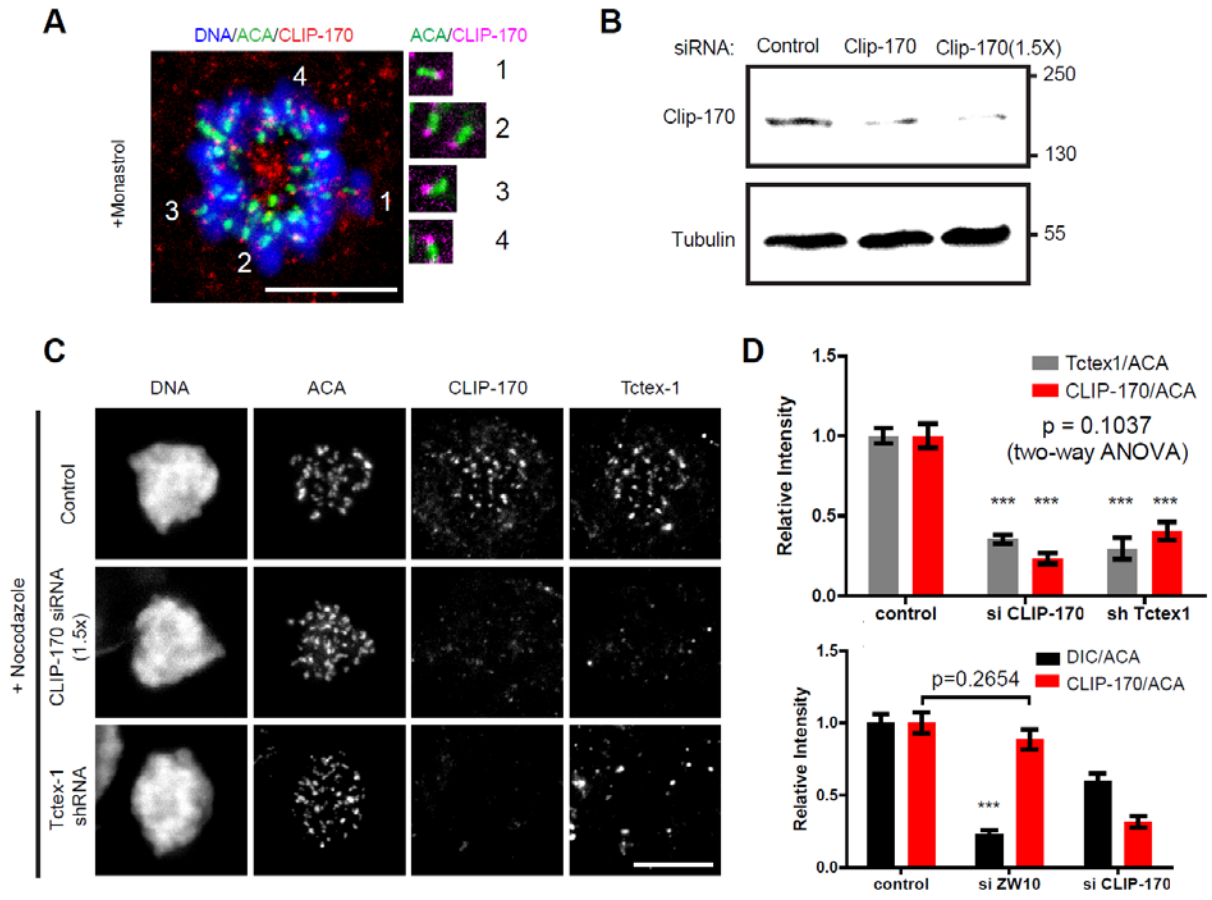

Figure 5.7. Tctex-1 associates with CLIP-170 and they affect each other's localization at the kinetochore

(A) CLIP-170 has asymmetric localization at sister kinetochores in monopolar spindle, similar to Tctex-1. (B) Immunoblot showing the knockdown of CLIP-170. (C) Knockding down CLIP-170 or Tctex-1 negatively affect the kinetochore localization of one another. (D) Quantification of the relative kinetochore levels of Tctex-1, CLIP-170 and DIC under various conditions (unpublished data).

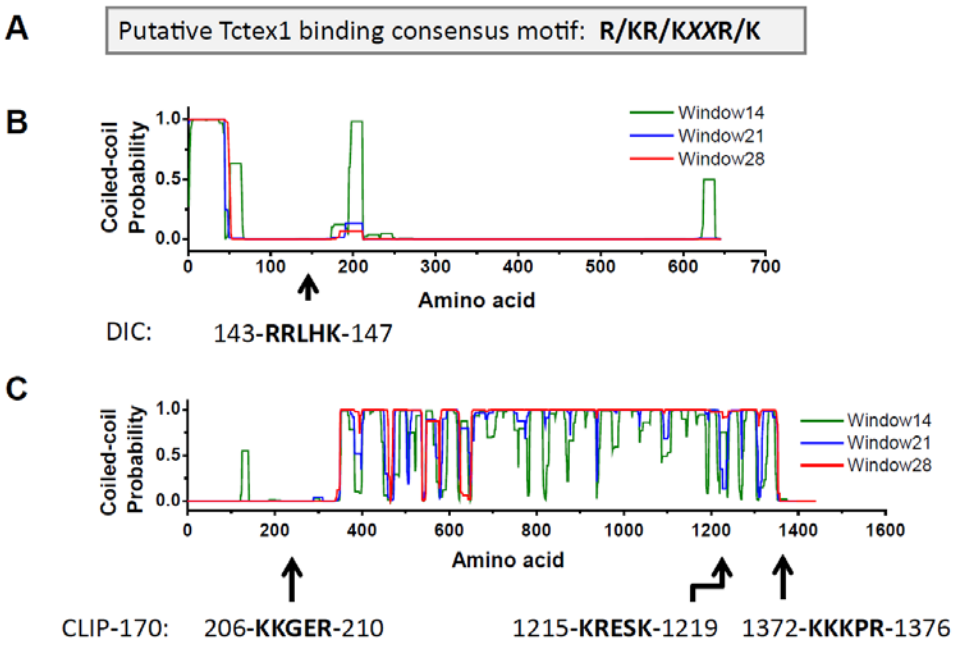

http://embnet.vital-it.ch/software/COILS_form.html

Figure 5.8. Bioinformatics prediction of possible regions on CLIP-170 and DIC that could bind to Tctex-1

Probability of coiled-coil structure along the proteins (CLIP-170 and DIC) are also shown. Note that potential Tctex-1 binding motifs coincide with low-probability coiled-coil region or regions near the end of the proteins to potential provide additional 'molecular velcro' for robust localization and function (unpublished data).

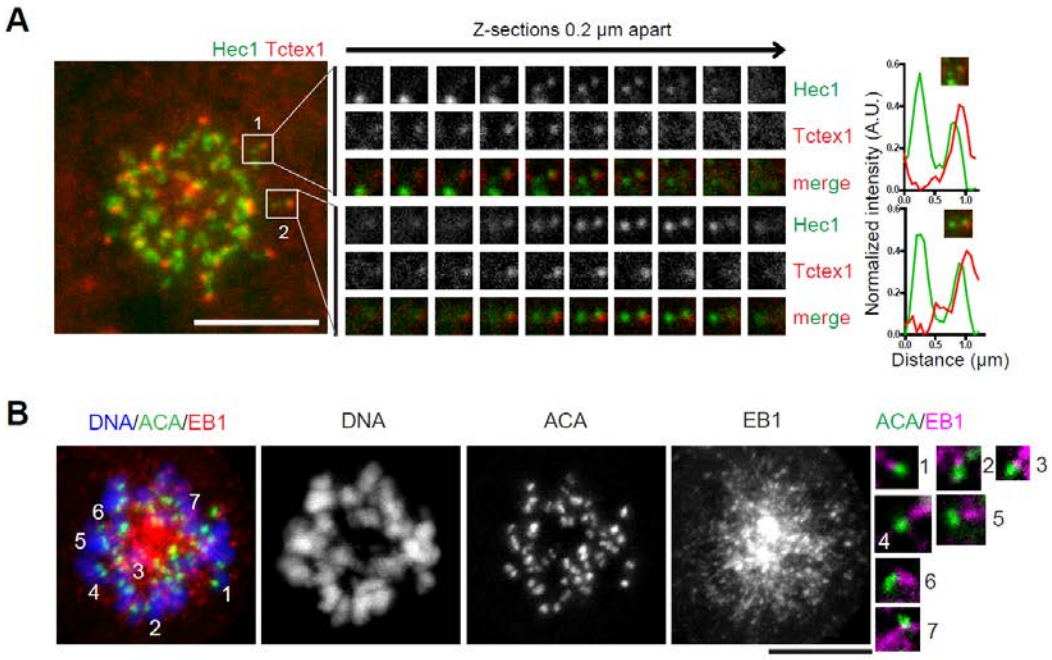

Figure 5.9. Tctex-1 and EB1 have opposite asymmetric kinetochore localizations

(A) Dual color immunofluorescence images of Tctex-1 (red) and the outer kinetochore protein Hec1 (green) in a monopolar spindle. Line-scans are from the center to the periphery of the spindle. Note that Tctex-1 accumulates near the distal sister kinetochore. (B) Representative immunofluorescence images of a monopolar spindle with EB1 accumulating near the proximal sister kinetochore (unpublished data).

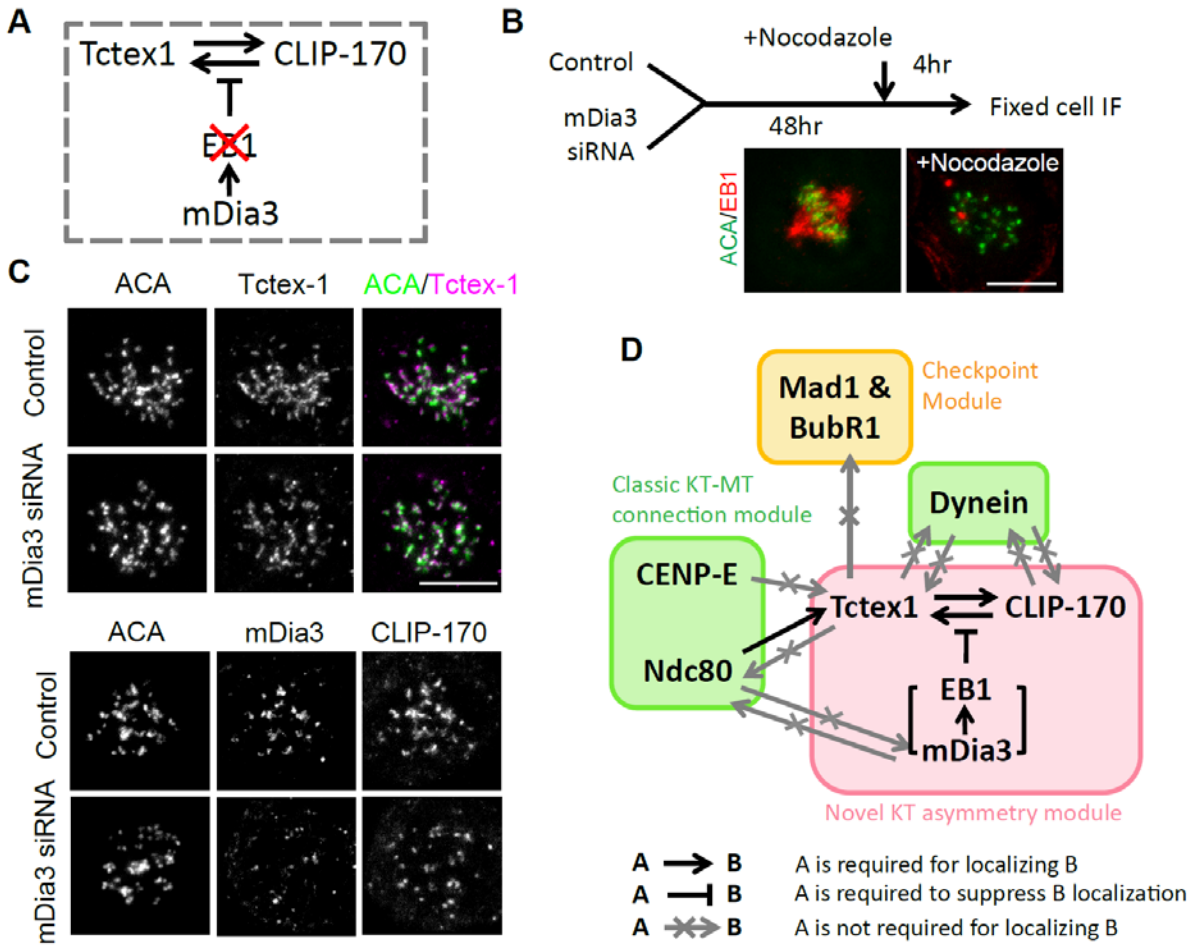

Figure 5.10. Microtubule plus-end dynamics is required for the asymmetric "antagonistic" protein network at outer kinetochore

(A and B) Schematics for the "chemical epistasis" analysis to test if EB1 is required for the compositional change following mDia3 depletion. (C) No increase in kinetochore Tctex-1 or CLIP-170 were observed in mDia3 knockdowns when treated with nocodazole. (D) Graphical summary of the relationships of different modules in fine-tuning kinetochore-microtubule attachment (unpublished data).

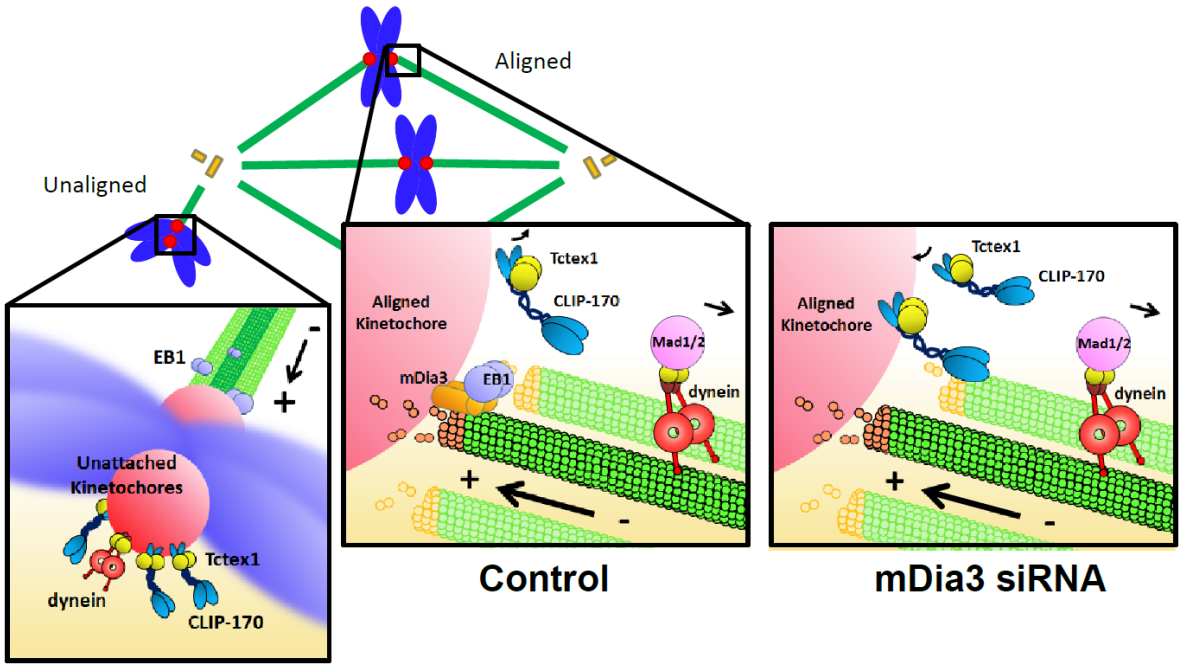

Figure 5.11. A novel asymmetric "antagonistic" module at kinetochore microtubule plus ends

Graphical model depicting the compositional change initiated by mDia3 depletion, mediated by EB1 and microtubule plus end dynamics, and executed by Tctex-1 and CLIP-170. The exact role of this module in the mechanochemical biology of kinetochore remains to be examined (unpublished data).

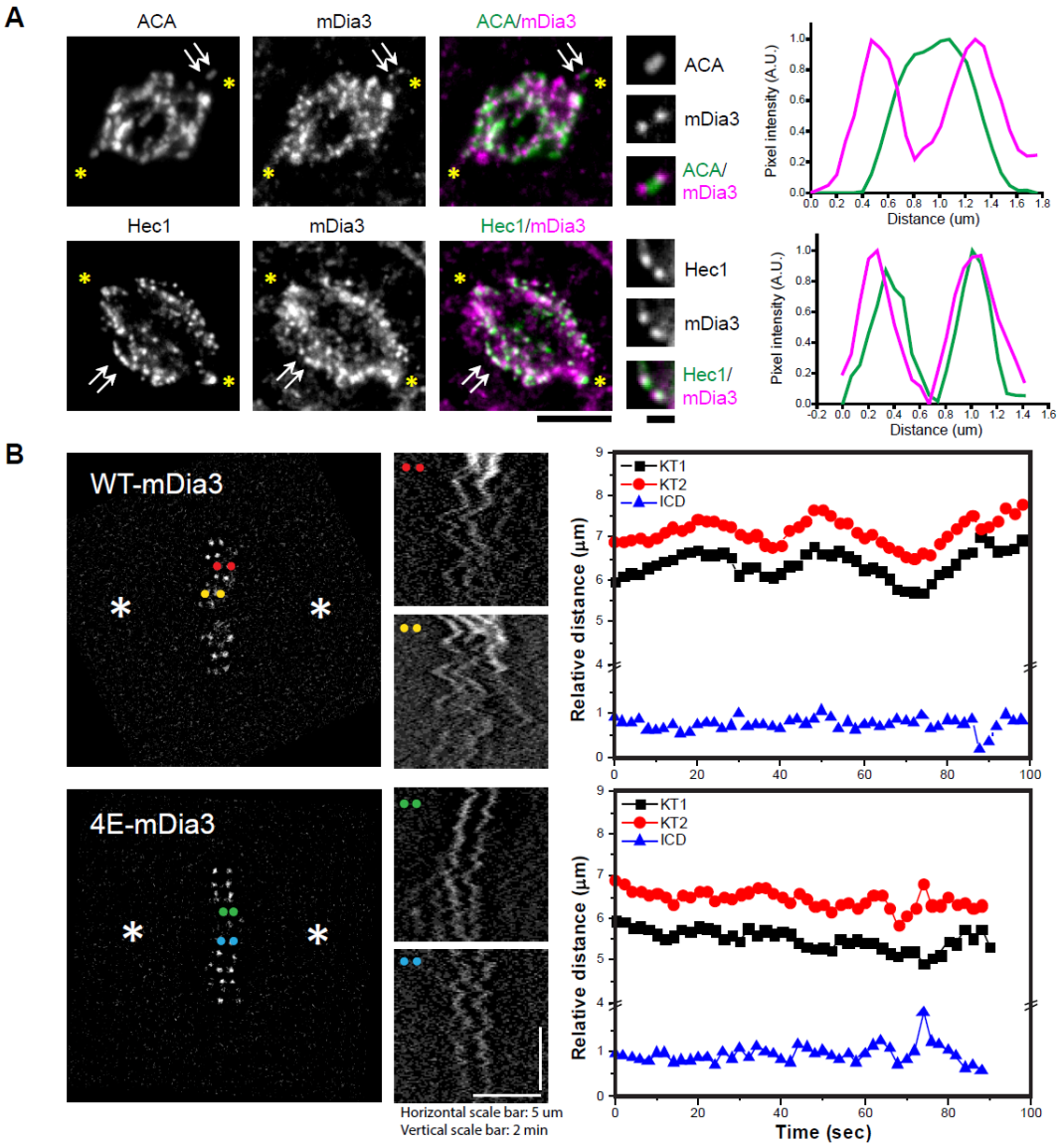

Figure 5.12. mDia3 is an outer kinetochore protein required for ordinary metaphase kinetochore oscillations

(A) Dual-color immunofluorescence images show mDia3's relative kinetochore localization. ACA was used as the positional marker for inner kinetochore and centromere. Hec1 was the positional marker for outer kinetochore. Asterisks mark spindle poles, arrows mark representative kinetochore pairs. (B) Kymographs (left) showing altered oscillatory behaviors of kinetochore movement (visualized with YFP-CENP-A) in cells expressing an mDia3 mutant (4E-mDia3) with defective microtubule stabilization activity. Quantification (right) show the relative distances from spindle poles to the respective kinetochores, ICD stands for inter-centromere distance (unpublished data).

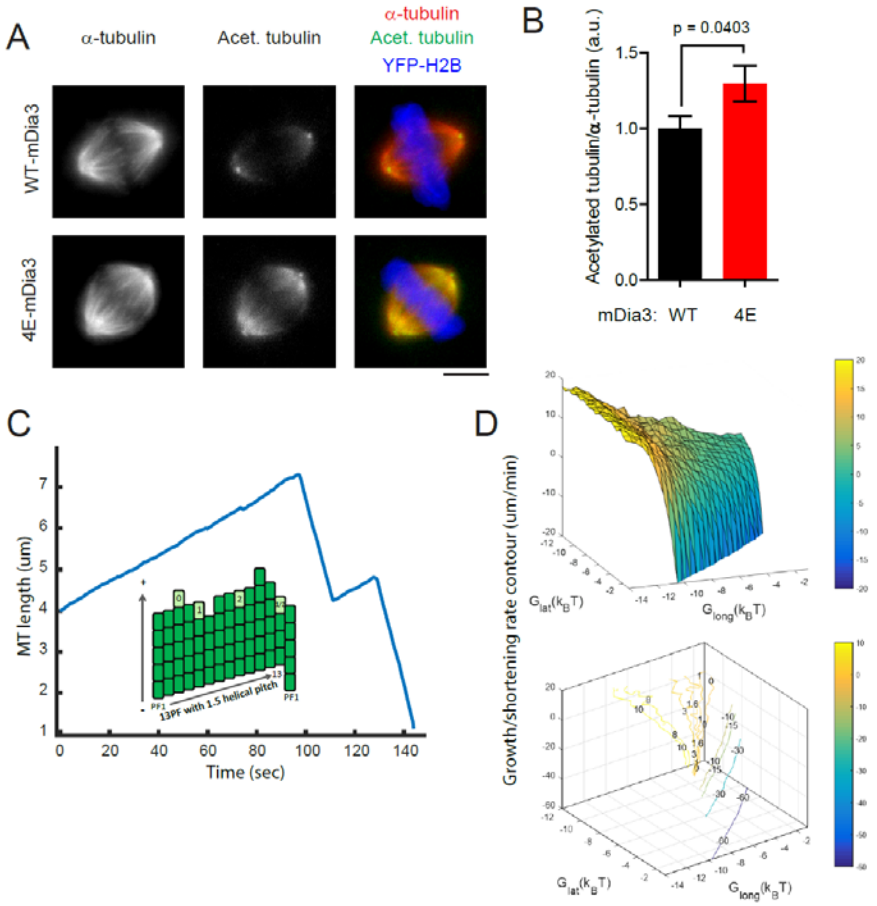

Figure 5.13. Toward a quantitative understanding of kinetochore-microtubule interactions

(A and B) Immunofluorescence images and quantifications demonstrate that defects in mDia3's microtubule stabilization activity correlate with higher levels of acetylated tubulin in metaphase spindles. (C)*in silico* modeling of microtubule plus end dynamics with Monte Carlo simulation. 2-dimentional rendering of the 13-3 lattice is shown as inset in a representative trace of simulated kymograph. (D) Contours of the simulated growth and shortening rate of microtubule plus ends as a function of different possible bond energies. Lateral bond energies (G_{lat}) and longitudinal bond energies (G_{long}) are both in the unit of k_BT (k_B, Boltzmann's constant; T, absolute temperature of the reaction). Future work fitting experimentally measured data using this model could provide mechanistic understandings of the energetic landscape of the kinetochore-microtubule interactions (unpublished data).

Tables

Table 1.1: Summary of current observations of nuclear actin filaments

Species	Methods	Features (morphology and regulation)	Function	Drug resistance	References
Rat2 cells and HeLa cells	Comformation specific antibody (2G2); IF and EM	dot-like 2G2 positive structures in the nucleus, particially overlap with phalloidin-positive actin species accumulated at discrete sites within the nucleus	NA	LatA resistant	Schoenenberger et al., 2005
Drosophila S2R+ cells	Exportin 6 depletion; IF	Prominent 'bars' or 'rods' inside the nucleus	Transcription regulation	NA	Dopie et al., 2012
NIH3T3 cells and HeLa cells	Serum stimulation and optogenetics control of mDia activation; Visualize by Lifeact-NLS	Transient, long filaments spanning several microns; mDia1/2 dependent; Arp2/3 independent	MAL nuclear accumulation and SRF transcriptional activity	LatB sensitive	Baarlink et al., 2013 Plessner et al., 2015
U2OS, UMUC3 and HeLa cells	DNA damage induced; Visualized by Utr230-EGFP-NLS	Relatively stable over time, short and dynamic filaments at submicron length	Scaffold in the nucleoplasm to help organize nuclear contents; DNA double-strand break repair	Resistant LatB or CytD (in certain range)	Belin et al., 2013 Belin et al., 2015

Table 2.1: Parameters used for numerical simulation of HJURP turnover

Parameter	Value	References
k_{on} of HJURP single molecule	6×10^{8} M^{-1} h^{-1}	Doherty et al., Mathematical Biosciences, 2014
[HJURP]	2.33×10^{-8} M	Doherty et al., Mathematical Biosciences, 2014
k_{off} of HJURP single molecule	~1 h^{-1}	Doherty et al., Mathematical Biosciences, 2014
Apparent duration of HJURP association on centromeres	3 h	Foltz et al., Cell, 2009
# of new CENP-A nucleosomes	100	Bodor et al., eLife, 2014
Timeline from thymidine release to fixation & observation of early G1 cell	11 hr	Foltz et al., Cell 2009; McKinley and Cheeseman, Cell, 2014

Table 5.1: Summary of representative current methods in quantitative CENP-A measurement

Method	Advantages	Disadvantages	References
Manual selection and quantification of single centromeres using ROIs of exactly the same size	Identical ROI size ensured comparable integrated intensity measurement; outliers could be excluded for single centromere measurement	Labor intensive and could be subjective	Jansen et al., 2007; Fachinetti et al., 2013
the maximum pixel intensity per nucleus	Fast	The maximum pixel per nucleus could be outlier and not relevant at all	Foltz et al., 2009
Averaged nuclear CENP-A measurement	High throughput, automated and non-subjective; all centromeric pixels included in each nuclear mask are measured	By calculating the average fluorescent intensity within the nuclear mask, the size of nuclear masks could have nonnegligible effect	Lagana et al., 2010
Individual centromere thresholding for integrated density measurement	Individual centromere measured; semi-automated	Thresholding parameters and ROI sizes from thresholding could significantly affect integrated density (intensity) within each centromere ROI	Bernad et al., 2011
Integrated nuclear CENP-A measrurement (INCA)	High throughput, automated and non-subjective; all centromeric pixels included in the measurement; clustered measurement that reflects 'loading' capacity for each cell	Relatively good SNR required to avoid false positive measurement of nucleoplasmic signals	Liu and Mao, 2016; This study

Bibliography

1 Cheng, L. *et al.* Aurora B Regulates Formin mDia3 in Achieving Metaphase Chromosome Alignment. *Developmental Cell* **20**, 342-352, doi:DOI: 10.1016/j.devcel.2011.01.008 (2011).
2 Hartwell, L. & Kastan, M. Cell cycle control and cancer. *Science* **266**, 1821-1828, doi:10.1126/science.7997877 (1994).
3 Cheeseman, I. M. & Desai, A. Molecular architecture of the kinetochore-microtubule interface. *Nat Rev Mol Cell Biol* **9**, 33-46, doi:http://www.nature.com/nrm/journal/v9/n1/suppinfo/nrm2310_S1.html (2008).
4 Jansen, L. E. T., Black, B. E., Foltz, D. R. & Cleveland, D. W. Propagation of centromeric chromatin requires exit from mitosis. *The Journal of Cell Biology* **176**, 795-805 (2007).
5 Darlington, C. D. The External Mechanics of the Chromosomes. I--The Scope of Enquiry. *Proceedings of the Royal Society of London. Series B - Biological Sciences* **121**, 264 (1936).
6 Morgan, D. O. *The Cell Cycle: Principles of Control*. (New Science Press, 2007).
7 Flemming, W. Z., Kern und Zelltheilung. (F. C. W. Vogel, Leipzig, 1882). (1882).
8 Tjio, J. H. & Levan, A. THE CHROMOSOME NUMBER OF MAN. *Hereditas* **42**, 1-6, doi:10.1111/j.1601-5223.1956.tb03010.x (1956).
9 Sturtevant, A. H. The linear arrangement of six sex-linked factors in Drosophila, as shown by their mode of association. *Journal of Experimental Zoology* **14**, 43-59, doi:10.1002/jez.1400140104 (1913).
10 Ris H & PL., W. Structure of the mammalian kinetochore. *Chromosoma* **82**, 153-170. (1981).
11 Brinkley, B. R. & Stubblefield, E. The fine structure of the kinetochore of a mammalian cell in vitro. *Chromosoma* **19**, 28-43, doi:10.1007/BF00332792 (1966).
12 CL, R. The formation, structure, and composition of the mammalian kinetochore and kinetochore fiber. *Int Rev Cytol* **79**, 1-58 (1982).
13 Cleveland, D. W., Mao, Y. & Sullivan, K. F. Centromeres and Kinetochores: From Epigenetics to Mitotic Checkpoint Signaling. *Cell* **112**, 407-421, doi:10.1016/s0092-8674(03)00115-6 (2003).
14 Wynne, D. J. & Funabiki, H. Kinetochore function is controlled by a phospho-dependent coexpansion of inner and outer components. *The Journal of Cell Biology* **210**, 899 (2015).
15 Mandrioli, M. & Manicardi, G. C. Unlocking Holocentric Chromosomes: New Perspectives from Comparative and Functional Genomics? *Current Genomics* **13**, 343-349, doi:10.2174/138920212801619250 (2012).
16 Henikoff, S. & Henikoff, J. G. "Point" Centromeres of Saccharomyces Harbor Single Centromere-Specific Nucleosomes. *Genetics* **190**, 1575-1577, doi:10.1534/genetics.111.137711 (2012).
17 Musacchio, A. & Salmon, E. D. The spindle-assembly checkpoint in space and time. *Nat Rev Mol Cell Biol* **8**, 379-393 (2007).
18 Kitagawa, K. & Hieter, P. Evolutionary conservation between budding yeast and human kinetochores. *Nat Rev Mol Cell Biol* **2**, 678-687 (2001).
19 Wan, X. *et al.* Protein Architecture of the Human Kinetochore Microtubule Attachment Site. *Cell* **137**, 672-684, doi:10.1016/j.cell.2009.03.035 (2009).
20 Clarke, L. & Carbon, J. Genomic substitutions of centromeres in Saccharomyces cerevisiae. *Nature* **305**, 23-28 (1983).
21 Carbon J & L, C. Structural and functional analysis of a yeast centromere (CEN3). *J Cell Sci Suppl.* **1**, 43-58 (1984).
22 McGrew, J., Diehl, B. & Fitzgerald-Hayes, M. Single base-pair mutations in centromere element III cause aberrant chromosome segregation in Saccharomyces cerevisiae. *Molecular and Cellular Biology* **6**, 530-538 (1986).

23 Henikoff, S., Ahmad, K. & Malik, H. S. The Centromere Paradox: Stable Inheritance with Rapidly Evolving DNA. *Science* **293**, 1098 (2001).
24 Saffery, R. *et al.* Human centromeres and neocentromeres show identical distribution patterns of >20 functionally important kinetochore-associated proteins. *Human Molecular Genetics* **9**, 175-185 (2000).
25 Sullivan, B. A. & Willard, H. F. Stable dicentric X chromosomes with two functional centromeres. *Nat Genet* **20**, 227-228 (1998).
26 Earnshaw, W., Bordwell, B., Marino, C. & Rothfield, N. Three human chromosomal autoantigens are recognized by sera from patients with anti-centromere antibodies. *Journal of Clinical Investigation* **77**, 426-430 (1986).
27 Earnshaw, W. C. Discovering centromere proteins: from cold white hands to the A, B, C of CENPs. *Nat Rev Mol Cell Biol* **16**, 443-449, doi:10.1038/nrm4001 (2015).
28 Palmer, D. K., O'Day, K., Trong, H. L., Charbonneau, H. & Margolis, R. L. Purification of the centromere-specific protein CENP-A and demonstration that it is a distinctive histone. *P Natl Acad Sci USA* **88**, 3734-3738 (1991).
29 DK Palmer, K O'Day, MH Wener, BS Andrews & Margolis, R. A 17-kD centromere protein (CENP-A) copurifies with nucleosome core particles and with histones. *The Journal of Cell Biology* **104**, 805-815 (1987).
30 Coffman, V. C., Wu, P., Parthun, M. R. & Wu, J.-Q. CENP-A exceeds microtubule attachment sites in centromere clusters of both budding and fission yeast. *The Journal of Cell Biology* **195**, 563 (2011).
31 Sullivan, B. A., Blower, M. D. & Karpen, G. H. Determining centromere identity: cyclical stories and forking paths. *Nat Rev Genet* **2**, 584-596 (2001).
32 Edwards, N. S. & Murray, A. W. Identification of Xenopus CENP-A and an Associated Centromeric DNA Repeat. *Molecular Biology of the Cell* **16**, 1800-1810 (2005).
33 Drinnenberg, I. A., deYoung, D., Henikoff, S. & Malik, H. S. Recurrent loss of CenH3 is associated with independent transitions to holocentricity in insects. *eLife* **3**, e03676, doi:10.7554/eLife.03676 (2014).
34 Oegema, K., Desai, A., Rybina, S., Kirkham, M. & Hyman, A. A. Functional Analysis of Kinetochore Assembly in Caenorhabditis elegans. *The Journal of Cell Biology* **153**, 1209 (2001).
35 Maddox, P. S., Hyndman, F., Monen, J., Oegema, K. & Desai, A. Functional genomics identifies a Myb domain–containing protein family required for assembly of CENP-A chromatin. *The Journal of Cell Biology* **176**, 757-763 (2007).
36 Barnhart, M. C. *et al.* HJURP is a CENP-A chromatin assembly factor sufficient to form a functional de novo kinetochore. *The Journal of Cell Biology* **194**, 229-243 (2011).
37 Mendiburo, M. J., Padeken, J., Fülöp, S., Schepers, A. & Heun, P. Drosophila CENH3 Is Sufficient for Centromere Formation. *Science* **334**, 686-690 (2011).
38 Heun, P. *et al.* Mislocalization of the Drosophila Centromere-Specific Histone CID Promotes Formation of Functional Ectopic Kinetochores. *Developmental cell* **10**, 303-315, doi:10.1016/j.devcel.2006.01.014 (2006).
39 Allshire, R. C. & Karpen, G. H. Epigenetic regulation of centromeric chromatin: old dogs, new tricks? *Nature reviews. Genetics* **9**, 923-937, doi:10.1038/nrg2466 (2008).
40 Blower, M. D., Sullivan, B. A. & Karpen, G. H. Conserved Organization of Centromeric Chromatin in Flies and Humans. *Developmental cell* **2**, 319-330 (2002).
41 Black, B. E., Jansen, L. E. T., Foltz, D. R. & Cleveland, D. W. Centromere Identity, Function, and Epigenetic Propagation Across Cell Divisions. *Cold Spring Harbor symposia on quantitative biology* **75**, 403-418, doi:10.1101/sqb.2010.75.038 (2010).
42 Bodor, D. L. *et al.* The quantitative architecture of centromeric chromatin. *eLife* **3** (2014).

43 Schuh, M., Lehner, C. F. & Heidmann, S. Incorporation of Drosophila CID/CENP-A and CENP-C into Centromeres during Early Embryonic Anaphase. *Current Biology* **17**, 237-243, doi:http://dx.doi.org/10.1016/j.cub.2006.11.051 (2007).
44 Hemmerich, P. *et al.* Dynamics of inner kinetochore assembly and maintenance in living cells. *The Journal of Cell Biology* **180**, 1101-1114 (2008).
45 Foltz, D. R. *et al.* The human CENP-A centromeric nucleosome-associated complex. *Nat Cell Biol* **8**, 458-469, doi:http://www.nature.com/ncb/journal/v8/n5/suppinfo/ncb1397_S1.html (2006).
46 Fujita, Y. *et al.* Priming of Centromere for CENP-A Recruitment by Human hMis18α, hMis18β, and M18BP1. *Developmental Cell* **12**, 17-30, doi:10.1016/j.devcel.2006.11.002 (2007).
47 Dunleavy, E. M. *et al.* HJURP Is a Cell-Cycle-Dependent Maintenance and Deposition Factor of CENP-A at Centromeres. *Cell* **137**, 485-497, doi:10.1016/j.cell.2009.02.040 (2009).
48 Foltz, D. R. *et al.* Centromere-Specific Assembly of CENP-A Nucleosomes Is Mediated by HJURP. *Cell* **137**, 472-484, doi:10.1016/j.cell.2009.02.039 (2009).
49 Perpelescu, M., Nozaki, N., Obuse, C., Yang, H. & Yoda, K. Active establishment of centromeric CENP-A chromatin by RSF complex. *The Journal of Cell Biology* **185**, 397-407 (2009).
50 Lagana, A. *et al.* A small GTPase molecular switch regulates epigenetic centromere maintenance by stabilizing newly incorporated CENP-A. *Nat Cell Biol* **12**, 1186-1193, doi:http://www.nature.com/ncb/journal/v12/n12/abs/ncb2129.html#supplementary-information (2010).
51 Dunleavy, E. M., Almouzni, G. & Karpen, G. H. H3.3 is deposited at centromeres in S phase as a placeholder for newly assembled CENP-A in G₁ phase. *Nucleus* **2**, 146-157 (2011).
52 Silva, Mariana C. C. *et al.* Cdk Activity Couples Epigenetic Centromere Inheritance to Cell Cycle Progression. *Developmental Cell* **22**, 52-63, doi:10.1016/j.devcel.2011.10.014 (2012).
53 McKinley, K. L. & Cheeseman, I. M. Polo-like kinase 1 licenses CENP-A deposition at centromeres. *Cell* **158**, 397-411, doi:10.1016/j.cell.2014.06.016 (2014).
54 Moree, B., Meyer, C. B., Fuller, C. J. & Straight, A. F. CENP-C recruits M18BP1 to centromeres to promote CENP-A chromatin assembly. *The Journal of Cell Biology* **194**, 855-871 (2011).
55 Kim, Ik S. *et al.* Roles of Mis18± in Epigenetic Regulation of Centromeric Chromatin and CENP-A Loading. *Molecular Cell* (2012).
56 Ridley, A. J. Rho GTPase signalling in cell migration. *Curr Opin Cell Biol* **36**, 103-112, doi:10.1016/j.ceb.2015.08.005 (2015).
57 Schaefer, A., Reinhard, N. R. & Hordijk, P. L. Toward understanding RhoGTPase specificity: structure, function and local activation. *Small GTPases* **5**, 6, doi:10.4161/21541248.2014.968004 (2014).
58 Dubash, A. D. *et al.* The small GTPase RhoA localizes to the nucleus and is activated by Net1 and DNA damage signals. *PloS one* **6**, e17380, doi:10.1371/journal.pone.0017380 (2011).
59 Srougi, M. C. & Burridge, K. The nuclear guanine nucleotide exchange factors Ect2 and Net1 regulate RhoB-mediated cell death after DNA damage. *PloS one* **6**, e17108, doi:10.1371/journal.pone.0017108 (2011).
60 Sandrock, K., Bielek, H., Schradi, K., Schmidt, G. & Klugbauer, N. The nuclear import of the small GTPase Rac1 is mediated by the direct interaction with karyopherin alpha2. *Traffic* **11**, 198-209, doi:10.1111/j.1600-0854.2009.01015.x (2010).
61 Guilluy, C. *et al.* Isolated nuclei adapt to force and reveal a mechanotransduction pathway within the nucleus. *Nature cell biology* **16**, 376-381, doi:10.1038/ncb2927 (2014).
62 Cha, K., Sen, P., Raghunayakula, S. & Zhang, X. D. The Cellular Distribution of RanGAP1 Is Regulated by CRM1-Mediated Nuclear Export in Mammalian Cells. *PloS one* **10**, e0141309, doi:10.1371/journal.pone.0141309 (2015).

63 Chalamalasetty, R. B., Hummer, S., Nigg, E. A. & Sillje, H. H. Influence of human Ect2 depletion and overexpression on cleavage furrow formation and abscission. *J Cell Sci* **119**, 3008-3019, doi:10.1242/jcs.03032 (2006).
64 Lagana, A. *et al.* A small GTPase molecular switch regulates epigenetic centromere maintenance by stabilizing newly incorporated CENP-A. *Nat Cell Biol* **12**, 1186-1193, doi:10.1038/ncb2129 (2010).
65 Glotzer, M. The 3Ms of central spindle assembly: microtubules, motors and MAPs. *Nat Rev Mol Cell Biol* **10**, 9-20 (2009).
66 Bergmann, J. H. *et al.* Epigenetic engineering shows H3K4me2 is required for HJURP targeting and CENP-A assembly on a synthetic human kinetochore. *The EMBO Journal* **30**, 328-340, doi:10.1038/emboj.2010.329 (2011).
67 Ohzeki, J.-i. *et al.* Breaking the HAC Barrier: Histone H3K9 acetyl/methyl balance regulates CENP-A assembly. *The EMBO Journal* **31**, 2391-2402, doi:10.1038/emboj.2012.82 (2012).
68 Nakano, M. *et al.* Inactivation of a Human Kinetochore by Specific Targeting of Chromatin Modifiers. *Developmental Cell* **14**, 507-522, doi:10.1016/j.devcel.2008.02.001 (2008).
69 Quénet, D. & Dalal, Y. A long non-coding RNA is required for targeting centromeric protein A to the human centromere. *eLife* **3**, e03254, doi:10.7554/eLife.03254 (2014).
70 Chan, F. L. *et al.* Active transcription and essential role of RNA polymerase II at the centromere during mitosis. *P Natl Acad Sci USA* **109**, 1979-1984, doi:10.1073/pnas.1108705109 (2012).
71 Grenfell, A. W., Heald, R. & Strzelecka, M. Mitotic noncoding RNA processing promotes kinetochore and spindle assembly in Xenopus. *The Journal of Cell Biology* **214**, 133 (2016).
72 McKinley, K. L. & Cheeseman, I. M. The molecular basis for centromere identity and function. *Nat Rev Mol Cell Biol* **advance online publication**, doi:10.1038/nrm.2015.5 (2015).
73 Falk, S. J. *et al.* CENP-C reshapes and stabilizes CENP-A nucleosomes at the centromere. *Science* **348**, 699-703 (2015).
74 Fachinetti, D. *et al.* DNA Sequence-Specific Binding of CENP-B Enhances the Fidelity of Human Centromere Function. *Developmental Cell* **33**, 314-327, doi:10.1016/j.devcel.2015.03.020 (2015).
75 Fachinetti, D. *et al.* A two-step mechanism for epigenetic specification of centromere identity and function. *Nat Cell Biol* **15**, 1056-1066, doi:10.1038/ncb2805

http://www.nature.com/ncb/journal/v15/n9/abs/ncb2805.html#supplementary-information (2013).
76 Herrmann, H., Bar, H., Kreplak, L., Strelkov, S. V. & Aebi, U. Intermediate filaments: from cell architecture to nanomechanics. *Nat Rev Mol Cell Biol* **8**, 562-573 (2007).
77 Pollard, T. D. & Borisy, G. G. Cellular Motility Driven by Assembly and Disassembly of Actin Filaments. *Cell* **112**, 453-465, doi:http://dx.doi.org/10.1016/S0092-8674(03)00120-X (2003).
78 Mostowy, S. & Cossart, P. Septins: the fourth component of the cytoskeleton. *Nat Rev Mol Cell Biol* **13**, 183-194, doi:http://www.nature.com/nrm/journal/v13/n3/suppinfo/nrm3284_S1.html (2012).
79 Desai, A. & Mitchison, T. J. MICROTUBULE POLYMERIZATION DYNAMICS. *Annual Review of Cell and Developmental Biology* **13**, 83-117, doi:10.1146/annurev.cellbio.13.1.83 (1997).
80 Pollard, T. D., Blanchoin, L. & Mullins, R. D. Molecular Mechanisms Controlling Actin Filament Dynamics in Nonmuscle Cells. *Annual Review of Biophysics and Biomolecular Structure* **29**, 545-576, doi:10.1146/annurev.biophys.29.1.545 (2000).
81 Akhmanova, A. & Steinmetz, M. O. Tracking the ends: a dynamic protein network controls the fate of microtubule tips. *Nat Rev Mol Cell Biol* **9**, 309-322, doi:http://www.nature.com/nrm/journal/v9/n4/suppinfo/nrm2369_S1.html (2008).

82 Novak, I. L., Slepchenko, B. M. & Mogilner, A. Quantitative Analysis of G-Actin Transport in Motile Cells. *Biophysical Journal* **95**, 1627-1638, doi:http://dx.doi.org/10.1529/biophysj.108.130096 (2008).
83 Mitchison, T. & Kirschner, M. Dynamic instability of microtubule growth. *Nature* **312**, 237-242 (1984).
84 Kueh, H. Y. & Mitchison, T. J. Structural Plasticity in Actin and Tubulin Polymer Dynamics. *Science (New York, N.Y.)* **325**, 960-963, doi:10.1126/science.1168823 (2009).
85 Luxton, G. W. G., Gomes, E. R., Folker, E. S., Vintinner, E. & Gundersen, G. G. Linear Arrays of Nuclear Envelope Proteins Harness Retrograde Actin Flow for Nuclear Movement. *Science* **329**, 956-959 (2010).
86 Pelham, R. J. & Chang, F. Actin dynamics in the contractile ring during cytokinesis in fission yeast. *Nature* **419**, 82-86, doi:http://www.nature.com/nature/journal/v419/n6902/suppinfo/nature00999_S1.html (2002).
87 Jordan, S. N. *et al.* Cortical PAR polarity proteins promote robust cytokinesis during asymmetric cell division. *The Journal of Cell Biology* **212**, 39-49 (2016).
88 Olave, I. A., Reck-Peterson, S. L. & Crabtree, G. R. NUCLEAR ACTIN AND ACTIN-RELATED PROTEINS IN CHROMATIN REMODELING. *Annual Review of Biochemistry* **71**, 755-781, doi:10.1146/annurev.biochem.71.110601.135507 (2002).
89 Dion, V., Shimada, K. & Gasser, S. M. Actin-related proteins in the nucleus: life beyond chromatin remodelers. *Current Opinion in Cell Biology* **22**, 383-391, doi:http://dx.doi.org/10.1016/j.ceb.2010.02.006 (2010).
90 de Lanerolle, P. Nuclear actin and myosins at a glance. *Journal of Cell Science* **125**, 4945-4949, doi:10.1242/jcs.099754 (2012).
91 Grosse, R. & Vartiainen, M. K. To be or not to be assembled: progressing into nuclear actin filaments. *Nat Rev Mol Cell Biol* **14**, 693-697, doi:10.1038/nrm3681 (2013).
92 Schoenenberger, C. A. *et al.* Conformation-specific antibodies reveal distinct actin structures in the nucleus and the cytoplasm. *Journal of Structural Biology* **152**, 157-168, doi:http://dx.doi.org/10.1016/j.jsb.2005.09.003 (2005).
93 Dopie, J., Skarp, K.-P., Kaisa Rajakylä, E., Tanhuanpää, K. & Vartiainen, M. K. Active maintenance of nuclear actin by importin 9 supports transcription. *Proceedings of the National Academy of Sciences* **109**, E544-E552 (2012).
94 Baarlink, C., Wang, H. & Grosse, R. Nuclear Actin Network Assembly by Formins Regulates the SRF Coactivator MAL. *Science* (2013).
95 Plessner, M., Melak, M., Chinchilla, P., Baarlink, C. & Grosse, R. Nuclear F-actin formation and reorganization upon cell spreading. *Journal of Biological Chemistry* (2015).
96 Belin, B. J., Cimini, B. A., Blackburn, E. H. & Mullins, R. D. Visualization of actin filaments and monomers in somatic cell nuclei. *Molecular Biology of the Cell* **24**, 982-994 (2013).
97 Belin, B. J., Lee, T. & Mullins, R. D. DNA damage induces nuclear actin filament assembly by Formin-2 and Spire-1/2 that promotes efficient DNA repair. *eLife* **4**, e07735, doi:10.7554/eLife.07735 (2015).
98 Paschal, B. M. & Vallee, R. B. Retrograde transport by the microtubule-associated protein MAP 1C. *Nature* **330**, 181-183 (1987).
99 Vallee, R. B., Wall, J. S., Paschal, B. M. & Shpetner, H. S. Microtubule-associated protein 1C from brain is a two-headed cytosolic dynein. *Nature* **332**, 561-563 (1988).
100 Varma, D., Monzo, P., Stehman, S. A. & Vallee, R. B. Direct role of dynein motor in stable kinetochore-microtubule attachment, orientation, and alignment. *The Journal of Cell Biology* **182**, 1045-1054 (2008).

101 Vallee, R. B., McKenney, R. J. & Ori-McKenney, K. M. Multiple modes of cytoplasmic dynein regulation. *Nat Cell Biol* **14**, 224-230 (2012).
102 Howell, B. J. *et al.* Cytoplasmic dynein/dynactin drives kinetochore protein transport to the spindle poles and has a role in mitotic spindle checkpoint inactivation. *The Journal of Cell Biology* **155**, 1159-1172 (2001).
103 Li, Y., Yu, W., Liang, Y. & Zhu, X. Kinetochore dynein generates a poleward pulling force to facilitate congression and full chromosome alignment. *Cell Res* **17**, 701-712, doi:http://www.nature.com/cr/journal/v17/n8/suppinfo/cr200765s1.html (2007).
104 Kardon, J. R. & Vale, R. D. Regulators of the cytoplasmic dynein motor. *Nat Rev Mol Cell Biol* **10**, 854-865 (2009).
105 Bader, J. R. & Vaughan, K. T. Dynein at the kinetochore: Timing, Interactions and Functions. *Seminars in Cell & Developmental Biology* **21**, 269-275, doi:10.1016/j.semcdb.2009.12.015 (2010).
106 Cheerambathur, D. K., Gassmann, R., Cook, B., Oegema, K. & Desai, A. Crosstalk Between Microtubule Attachment Complexes Ensures Accurate Chromosome Segregation. *Science* (2013).
107 Mao, Y., Varma, D. & Vallee, R. B. Emerging functions of force-producing kinetochore motors. *Cell Cycle* **9**, 715 - 719, doi: http://dx.doi.org/10.4161/cc.9.4.10763 (2010).
108 Rago, F. & Cheeseman, I. M. Review series: The functions and consequences of force at kinetochores. *J Cell Biol* **200**, 557-565, doi:10.1083/jcb.201211113 (2013).
109 Varma, D. & Salmon, E. D. The KMN protein network--chief conductors of the kinetochore orchestra. *J Cell Sci* **125**, 5927-5936, doi:10.1242/jcs.093724 (2012).
110 Daum, J. R. *et al.* Ska3 is required for spindle checkpoint silencing and the maintenance of chromosome cohesion in mitosis. *Curr Biol* **19**, 1467-1472, doi:S0960-9822(09)01399-2 [pii]

10.1016/j.cub.2009.07.017 (2009).
111 Gaitanos, T. N. *et al.* Stable kinetochore-microtubule interactions depend on the Ska complex and its new component Ska3/C13Orf3. *Embo Journal* **28**, 1442-1452, doi:DOI 10.1038/emboj.2009.96 (2009).
112 Raaijmakers, J. A., Tanenbaum, M. E., Maia, A. F. & Medema, R. H. RAMA1 is a novel kinetochore protein involved in kinetochore-microtubule attachment. *J Cell Sci* **122**, 2436-2445, doi:10.1242/jcs.051912 (2009).
113 Welburn, J. P. *et al.* The human kinetochore Ska1 complex facilitates microtubule depolymerization-coupled motility. *Dev Cell* **16**, 374-385 (2009).
114 Cheng, L. *et al.* Aurora B regulates formin mDia3 in achieving metaphase chromosome alignment. *Developmental Cell* **20**, 342-352, doi:10.1016/j.devcel.2011.01.008 (2011).
115 Yasuda, S. *et al.* Cdc42 and mDia3 regulate microtubule attachment to kinetochores. *Nature* **428**, 767-771 (2004).
116 Weaver, B. A. A. *et al.* Centromere-associated protein-E is essential for the mammalian mitotic checkpoint to prevent aneuploidy due to single chromosome loss. *The Journal of Cell Biology* **162**, 551-563 (2003).
117 Zhu, C. *et al.* Functional Analysis of Human Microtubule-based Motor Proteins, the Kinesins and Dyneins, in Mitosis/Cytokinesis Using RNA Interference. *Molecular Biology of the Cell* **16**, 3187-3199 (2005).
118 Kim, Y., Holland, A. J., Lan, W. & Cleveland, D. W. Aurora Kinases and Protein Phosphatase 1 Mediate Chromosome Congression through Regulation of CENP-E. *Cell* **142**, 444-455, doi:10.1016/j.cell.2010.06.039 (2010).

119 Guo, Y., Kim, C., Ahmad, S., Zhang, J. & Mao, Y. CENP-E–dependent BubR1 autophosphorylation enhances chromosome alignment and the mitotic checkpoint. *The Journal of Cell Biology* (2012).
120 Raaijmakers, J. A., Tanenbaum, M. E. & Medema, R. H. Systematic dissection of dynein regulators in mitosis. *The Journal of Cell Biology* **201**, 201-215 (2013).
121 Shrestha, Roshan L. & Draviam, Viji M. Lateral to End-on Conversion of Chromosome-Microtubule Attachment Requires Kinesins CENP-E and MCAK. *Current Biology* **23**, 1514-1526, doi:10.1016/j.cub.2013.06.040 (2013).
122 Xia, P. *et al.* EB1 acetylation by P300/CBP-associated factor (PCAF) ensures accurate kinetochore–microtubule interactions in mitosis. *Proceedings of the National Academy of Sciences* (2012).
123 Zhang, J., Neisa, R. & Mao, Y. Oncogenic Adenomatous Polyposis Coli Mutants Impair the Mitotic Checkpoint through Direct Interaction with Mad2. *Molecular Biology of the Cell* **20**, 2381-2388 (2009).
124 Chesarone, M. A., DuPage, A. G. & Goode, B. L. Unleashing formins to remodel the actin and microtubule cytoskeletons. *Nat Rev Mol Cell Biol* **11**, 62-74 (2010).
125 Goode, B. L. & Eck, M. J. Mechanism and Function of Formins in the Control of Actin Assembly. *Annual Review of Biochemistry* **76**, 593-627, doi:doi:10.1146/annurev.biochem.75.103004.142647 (2007).
126 Bartolini, F. *et al.* The formin mDia2 stabilizes microtubules independently of its actin nucleation activity. *The Journal of Cell Biology* **181**, 523-536, doi:10.1083/jcb.200709029 (2008).
127 Palazzo, A. F., Cook, T. A., Alberts, A. S. & Gundersen, G. G. mDia mediates Rho-regulated formation and orientation of stable microtubules. *Nat Cell Biol* **3**, 723-729, doi:10.1038/35087035 (2001).
128 Alberts, A. S., Bouquin, N., Johnston, L. H. & Treisman, R. Analysis of RhoA-binding proteins reveals an interaction domain conserved in heterotrimeric G protein beta subunits and the yeast response regulator protein Skn7. *J Biol Chem* **273**, 8616-8622 (1998).
129 Gasman, S., Kalaidzidis, Y. & Zerial, M. RhoD regulates endosome dynamics through Diaphanous-related Formin and Src tyrosine kinase. *Nat Cell Biol* **5**, 195-204, doi:10.1038/ncb935 (2003).
130 Ji, P., Jayapal, S. R. & Lodish, H. F. Enucleation of cultured mouse fetal erythroblasts requires Rac GTPases and mDia2. *Nat Cell Biol* **10**, 314-321, doi:10.1038/ncb1693 (2008).
131 Lammers, M., Meyer, S., Kuhlmann, D. & Wittinghofer, A. Specificity of interactions between mDia isoforms and Rho proteins. *J Biol Chem* **283**, 35236-35246, doi:10.1074/jbc.M805634200 (2008).
132 Peng, J., Wallar, B. J., Flanders, A., Swiatek, P. J. & Alberts, A. S. Disruption of the Diaphanous-related formin Drf1 gene encoding mDia1 reveals a role for Drf3 as an effector for Cdc42. *Curr Biol* **13**, 534-545 (2003).
133 Wallar, B. J., Deward, A. D., Resau, J. H. & Alberts, A. S. RhoB and the mammalian Diaphanous-related formin mDia2 in endosome trafficking. *Exp Cell Res* **313**, 560-571, doi:10.1016/j.yexcr.2006.10.033 (2007).
134 Watanabe, N., Kato, T., Fujita, A., Ishizaki, T. & Narumiya, S. Cooperation between mDia1 and ROCK in Rho-induced actin reorganization. *Nat Cell Biol* **1**, 136-143, doi:10.1038/11056 (1999).
135 Watanabe, N. *et al.* p140mDia, a mammalian homolog of Drosophila diaphanous, is a target protein for Rho small GTPase and is a ligand for profilin. *Embo J* **16**, 3044-3056 (1997).
136 Liu, C., Chuang, J.-Z., Sung, C.-H. & Mao, Y. A dynein independent role of Tctex-1 at the kinetochore. *Cell Cycle* **14**, 1379-1388, doi:10.1080/15384101.2014.1000217 (2015).
137 Miki, T. *et al.* mDia2 Shuttles between the Nucleus and the Cytoplasm through the Importin-α/β- and CRM1-mediated Nuclear Transport Mechanism. *Journal of Biological Chemistry* **284**, 5753-5762 (2009).

138 Daou, P. *et al.* Essential and nonredundant roles for Diaphanous formins in cortical microtubule capture and directed cell migration. *Molecular Biology of the Cell* **25**, 658-668 (2014).
139 Howard, J. Quantitative cell biology: the essential role of theory. *Molecular Biology of the Cell* **25**, 3438-3440 (2014).
140 Cleveland, D. W., Mao, Y. & Sullivan, K. F. Centromeres and kinetochores: from epigenetics to mitotic checkpoint signaling. *Cell* **112**, 407-421 (2003).
141 Fukagawa, T. & Earnshaw, W. C. The Centromere: Chromatin Foundation for the Kinetochore Machinery. *Dev Cell* **30**, 496-508, doi:10.1016/j.devcel.2014.08.016 (2014).
142 Nechemia-Arbely, Y., Fachinetti, D. & Cleveland, D. W. Replicating centromeric chromatin: spatial and temporal control of CENP-A assembly. *Exp Cell Res* **318**, 1353-1360, doi:10.1016/j.yexcr.2012.04.007 (2012).
143 Jansen, L. E., Black, B. E., Foltz, D. R. & Cleveland, D. W. Propagation of centromeric chromatin requires exit from mitosis. *J Cell Biol* **176**, 795-805, doi:10.1083/jcb.200701066 (2007).
144 Fujita, Y. *et al.* Priming of centromere for CENP-A recruitment by human hMis18alpha, hMis18beta, and M18BP1. *Dev Cell* **12**, 17-30, doi:10.1016/j.devcel.2006.11.002 (2007).
145 Hayashi, T. *et al.* Mis16 and Mis18 are required for CENP-A loading and histone deacetylation at centromeres. *Cell* **118**, 715-729, doi:10.1016/j.cell.2004.09.002 (2004).
146 Maddox, P. S., Hyndman, F., Monen, J., Oegema, K. & Desai, A. Functional genomics identifies a Myb domain-containing protein family required for assembly of CENP-A chromatin. *J Cell Biol* **176**, 757-763, doi:10.1083/jcb.200701065 (2007).
147 Dunleavy, E. M. *et al.* HJURP is a cell-cycle-dependent maintenance and deposition factor of CENP-A at centromeres. *Cell* **137**, 485-497, doi:10.1016/j.cell.2009.02.040 (2009).
148 Foltz, D. R. *et al.* Centromere-specific assembly of CENP-a nucleosomes is mediated by HJURP. *Cell* **137**, 472-484, doi:10.1016/j.cell.2009.02.039 (2009).
149 Xu, Y. *et al.* Crystal structures of a Formin Homology-2 domain reveal a tethered dimer architecture. *Cell* **116**, 711-723 (2004).
150 Baarlink, C., Wang, H. & Grosse, R. Nuclear actin network assembly by formins regulates the SRF coactivator MAL. *Science* **340**, 864-867, doi:10.1126/science.1235038 (2013).
151 Belin, B. J., Lee, T. & Mullins, R. D. DNA damage induces nuclear actin filament assembly by Formin-2 and Spire-(1/2) that promotes efficient DNA repair. *Elife* **4**, doi:10.7554/eLife.07735 (2015).
152 Miki, T. *et al.* mDia2 shuttles between the nucleus and the cytoplasm through the importin-{alpha}/{beta}- and CRM1-mediated nuclear transport mechanism. *J Biol Chem* **284**, 5753-5762, doi:10.1074/jbc.M806191200 (2009).
153 Daou, P. *et al.* Essential and nonredundant roles for Diaphanous formins in cortical microtubule capture and directed cell migration. *Mol Biol Cell* **25**, 658-668, doi:10.1091/mbc.E13-08-0482 (2014).
154 Masumoto, H., Masukata, H., Muro, Y., Nozaki, N. & Okazaki, T. A human centromere antigen (CENP-B) interacts with a short specific sequence in alphoid DNA, a human centromeric satellite. *J Cell Biol* **109**, 1963-1973 (1989).
155 Shao, X., Kawauchi, K., Shivashankar, G. V. & Bershadsky, A. D. Novel localization of formin mDia2: importin beta-mediated delivery to and retention at the cytoplasmic side of the nuclear envelope. *Biology open* **4**, 1569-1575, doi:10.1242/bio.013649 (2015).
156 Bartolini, F. *et al.* The formin mDia2 stabilizes microtubules independently of its actin nucleation activity. *J Cell Biol* **181**, 523-536 (2008).
157 Barnhart, M. C. *et al.* HJURP is a CENP-A chromatin assembly factor sufficient to form a functional de novo kinetochore. *J Cell Biol* **194**, 229-243, doi:10.1083/jcb.201012017 (2011).

158 Belin, B. J., Cimini, B. A., Blackburn, E. H. & Mullins, R. D. Visualization of actin filaments and monomers in somatic cell nuclei. *Mol Biol Cell* **24**, 982-994, doi:10.1091/mbc.E12-09-0685 (2013).
159 Gonsior, S. M. *et al.* Conformational difference between nuclear and cytoplasmic actin as detected by a monoclonal antibody. *J Cell Sci* **112 (Pt 6)**, 797-809 (1999).
160 McDonald, D., Carrero, G., Andrin, C., de Vries, G. & Hendzel, M. J. Nucleoplasmic beta-actin exists in a dynamic equilibrium between low-mobility polymeric species and rapidly diffusing populations. *J Cell Biol* **172**, 541-552, doi:10.1083/jcb.200507101 (2006).
161 Schoenenberger, C. A. *et al.* Conformation-specific antibodies reveal distinct actin structures in the nucleus and the cytoplasm. *Journal of structural biology* **152**, 157-168, doi:10.1016/j.jsb.2005.09.003 (2005).
162 Watanabe, S. *et al.* mDia2 Induces the Actin Scaffold for the Contractile Ring and Stabilizes Its Position during Cytokinesis in NIH 3T3 Cells. *Molecular Biology of the Cell* **19**, 2328-2338 (2008).
163 Otsu, N. Threshold selection method from gray-level histograms. *IEEE transactions on systems, man, and cybernetics* **9**, 62-66 (1979).
164 Lindeberg, T. Detecting salient blob-like image structures and their scales with a scale-space primal sketch: A method for focus-of-attention. *Int J Comput Vision* **11**, 283-318, doi:10.1007/bf01469346 (1993).
165 Shinya Inoué. in *Video Microscopy* Ch. 10, 327-392 (Plenum Press, 1986).
166 Bodor, D. L. *et al.* The quantitative architecture of centromeric chromatin. *Elife* **3**, e02137, doi:10.7554/eLife.02137 (2014).
167 Szentirmay, M. N. & Sawadogo, M. Spatial organization of RNA polymerase II transcription in the nucleus. *Nucleic Acids Res* **28**, 2019-2025 (2000).
168 Liu, C., Chuang, J. Z., Sung, C. H. & Mao, Y. A dynein independent role of Tctex-1 at the kinetochore. *Cell Cycle* **14**, 1379-1388, doi:10.1080/15384101.2014.1000217 (2015).
169 Watson JV, Chambers SH & Smith PJ. A pragmatic approach to the analysis of DNA histograms with a definable G1 peak. *Cytometry* **8**, 1-8 (1987).
170 Gillespie, D. T. Exact stochastic simulation of coupled chemical reactions. *The Journal of Physical Chemistry* **81**, 2340-2361, doi:10.1021/j100540a008 (1977).
171 Berger, S. L., Kouzarides, T., Shiekhattar, R. & Shilatifard, A. An operational definition of epigenetics. *Genes & Development* **23**, 781-783 (2009).
172 Bonasio, R., Tu, S. & Reinberg, D. Molecular Signals of Epigenetic States. *Science* **330**, 612 (2010).
173 Arzate-Mejía, R. G., Valle-García, D. & Recillas-Targa, F. Signaling epigenetics: Novel insights on cell signaling and epigenetic regulation. *IUBMB Life* **63**, 881-895, doi:10.1002/iub.557 (2011).
174 Fraser, P. & Bickmore, W. Nuclear organization of the genome and the potential for gene regulation. *Nature* **447**, 413-417 (2007).
175 Bickmore, W. A. & van Steensel, B. Genome Architecture: Domain Organization of Interphase Chromosomes. *Cell* **152**, 1270-1284 (2013).
176 Pueschel, R., Coraggio, F. & Meister, P. From single genes to entire genomes: the search for a function of nuclear organization. *Development* **143**, 910 (2016).
177 Liu, C. & Mao, Y. Diaphanous formin mDia2 regulates CENP-A levels at centromeres. *The Journal of Cell Biology* **213**, 415-424 (2016).
178 Liu, C. & Mao, Y. Formin-mediated epigenetic maintenance of centromere identity. *Small GTPases*, 1-6, doi:10.1080/21541248.2016.1215658 (2016).
179 Rando, O. J., Zhao, K., Janmey, P. & Crabtree, G. R. Phosphatidylinositol-dependent actin filament binding by the SWI/SNF-like BAF chromatin remodeling complex. *Proceedings of the National Academy of Sciences* **99**, 2824-2829 (2002).

180 Andrin, C. & Hendzel, M. J. F-actin-dependent Insolubility of Chromatin-modifying Components. *Journal of Biological Chemistry* **279**, 25017-25023 (2004).
181 Serebryannyy, L. A., Cruz, C. M. & de Lanerolle, P. A Role for Nuclear Actin in HDAC 1 and 2 Regulation. *Scientific Reports* **6**, 28460, doi:10.1038/srep28460

http://www.nature.com/articles/srep28460#supplementary-information (2016).
182 Palazzo, A. F., Cook, T. A., Alberts, A. S. & Gundersen, G. G. mDia mediates Rho-regulated formation and orientation of stable microtubules. *Nat Cell Biol* **3**, 723-729 (2001).
183 Kovar, D. R. Molecular details of formin-mediated actin assembly. *Current Opinion in Cell Biology* **18**, 11-17, doi:http://dx.doi.org/10.1016/j.ceb.2005.12.011 (2006).
184 Alberts, A. S. Identification of a Carboxyl-terminal Diaphanous-related Formin Homology Protein Autoregulatory Domain. *Journal of Biological Chemistry* **276**, 2824-2830 (2001).
185 Posern, G., Sotiropoulos, A. & Treisman, R. Mutant Actins Demonstrate a Role for Unpolymerized Actin in Control of Transcription by Serum Response Factor. *Molecular Biology of the Cell* **13**, 4167-4178, doi:10.1091/mbc.02-05-0068 (2002).
186 Chen, B. *et al.* Dynamic imaging of genomic loci in living human cells by an optimized CRISPR/Cas system. *Cell* **155**, 1479-1491, doi:10.1016/j.cell.2013.12.001 (2013).
187 Dimitrova, N., Chen, Y. C., Spector, D. L. & de Lange, T. 53BP1 promotes non-homologous end joining of telomeres by increasing chromatin mobility. *Nature* **456**, 524-528, doi:10.1038/nature07433 (2008).
188 Wang, X. *et al.* Rapid telomere motions in live human cells analyzed by highly time-resolved microscopy. *Epigenetics Chromatin* **1**, 4, doi:10.1186/1756-8935-1-4 (2008).
189 Zeitlin, S. G. *et al.* Double-strand DNA breaks recruit the centromeric histone CENP-A. *Proceedings of the National Academy of Sciences* **106**, 15762-15767 (2009).
190 Robson, A., Burrage, K. & Leake, M. C. Inferring diffusion in single live cells at the single-molecule level. *Philosophical Transactions of the Royal Society B: Biological Sciences* **368** (2012).
191 Gerlich, D. *et al.* Global chromosome positions are transmitted through mitosis in mammalian cells. *Cell* **112**, 751-764 (2003).
192 Mirny, L. A. The fractal globule as a model of chromatin architecture in the cell. *Chromosome Research* **19**, 37-51 (2011).
193 Jaqaman, K. *et al.* Robust single-particle tracking in live-cell time-lapse sequences. *Nat Meth* **5**, 695-702, doi:http://www.nature.com/nmeth/journal/v5/n8/suppinfo/nmeth.1237_S1.html (2008).
194 Spagnol, S. T. & Noel Dahl, K. Active cytoskeletal force and chromatin condensation independently modulate intranuclear network fluctuations. *Integrative Biology* **6**, 523-531, doi:10.1039/C3IB40226F (2014).
195 Ewers, H. *et al.* Single-particle tracking of murine polyoma virus-like particles on live cells and artificial membranes. *P Natl Acad Sci USA* **102**, 15110-15115 (2005).
196 Tarantino, N. *et al.* TNF and IL-1 exhibit distinct ubiquitin requirements for inducing NEMO–IKK supramolecular structures. *The Journal of Cell Biology* **204**, 231-245 (2014).
197 Saxton, M. J. in *Methods in Membrane Lipids* (ed Alex M. Dopico) 295-321 (Humana Press, 2007).
198 Cheerambathur, D. K. & Desai, A. Linked in: formation and regulation of microtubule attachments during chromosome segregation. *Curr Opin Cell Biol* **26**, 113-122, doi:10.1016/j.ceb.2013.12.005 (2014).
199 Guo, Y., Kim, C. & Mao, Y. New insights into the mechanism for chromosome alignment in metaphase. *International review of cell and molecular biology* **303**, 237-262, doi:10.1016/B978-0-12-407697-6.00006-4 (2013).

200 De Rop, V., Padeganeh, A. & Maddox, P. S. CENP-A: the key player behind centromere identity, propagation, and kinetochore assembly. *Chromosoma* **121**, 527-538, doi:10.1007/s00412-012-0386-5 (2012).
201 Mao, Y., Varma, D. & Vallee, R. Emerging functions of force-producing kinetochore motors. *Cell Cycle* **9**, 715-719 (2010).
202 Mao, Y. FORMIN a link between kinetochores and microtubule ends. *Trends in cell biology* **21**, 625-629, doi:10.1016/j.tcb.2011.08.005 (2011).
203 Tamura, N. & Draviam, V. M. Microtubule plus-ends within a mitotic cell are 'moving platforms' with anchoring, signalling and force-coupling roles. *Open biology* **2**, 120132, doi:10.1098/rsob.120132 (2012).
204 Tynan, S. H., Gee, M. A. & Vallee, R. B. Distinct but overlapping sites within the cytoplasmic dynein heavy chain for dimerization and for intermediate chain and light intermediate chain binding. *J Biol Chem* **275**, 32769-32774, doi:10.1074/jbc.M001537200 (2000).
205 Tai, A. W., Chuang, J. Z., Bode, C., Wolfrum, U. & Sung, C. H. Rhodopsin's carboxy-terminal cytoplasmic tail acts as a membrane receptor for cytoplasmic dynein by binding to the dynein light chain Tctex-1. *Cell* **97**, 877-887 (1999).
206 Rapali, P. *et al.* DYNLL/LC8: a light chain subunit of the dynein motor complex and beyond. *The FEBS journal* **278**, 2980-2996, doi:10.1111/j.1742-4658.2011.08254.x (2011).
207 Chuang, J. Z. *et al.* The dynein light chain Tctex-1 has a dynein-independent role in actin remodeling during neurite outgrowth. *Dev Cell* **9**, 75-86, doi:10.1016/j.devcel.2005.04.003 (2005).
208 Li, A. *et al.* Ciliary transition zone activation of phosphorylated Tctex-1 controls ciliary resorption, S-phase entry and fate of neural progenitors. *Nat Cell Biol* **13**, 402-411, doi:10.1038/ncb2218 (2011).
209 Yeh, C. *et al.* IGF-1 Activates a Cilium-Localized Noncanonical Gbetagamma Signaling Pathway that Regulates Cell-Cycle Progression. *Dev Cell* **26**, 358-368, doi:10.1016/j.devcel.2013.07.014 (2013).
210 Kapoor, T. M., Mayer, T. U., Coughlin, M. L. & Mitchison, T. J. Probing spindle assembly mechanisms with monastrol, a small molecule inhibitor of the mitotic kinesin, Eg5. *J Cell Biol* **150**, 975-988. (2000).
211 Howell, B. J. *et al.* Cytoplasmic dynein/dynactin drives kinetochore protein transport to the spindle poles and has a role in mitotic spindle checkpoint inactivation. *J Cell Biol* **155**, 1159-1172 (2001).
212 Lo, K. W., Kogoy, J. M. & Pfister, K. K. The DYNLT3 light chain directly links cytoplasmic dynein to a spindle checkpoint protein, Bub3. *J Biol Chem* **282**, 11205-11212, doi:10.1074/jbc.M611279200 (2007).
213 Guo, Y., Kim, C., Ahmad, S., Zhang, J. & Mao, Y. CENP-E-dependent BubR1 autophosphorylation enhances chromosome alignment and the mitotic checkpoint. *J Cell Biol* **198**, 205-217, doi:10.1083/jcb.201202152 (2012).
214 Rozier, L. *et al.* The MRN-CtIP Pathway Is Required for Metaphase Chromosome Alignment. *Mol Cell*, doi:10.1016/j.molcel.2013.01.023 (2013).
215 Starr, D. A., Williams, B. C., Hays, T. S. & Goldberg, M. L. ZW10 helps recruit dynactin and dynein to the kinetochore. *J Cell Biol* **142**, 763-774 (1998).
216 Whyte, J. *et al.* Phosphorylation regulates targeting of cytoplasmic dynein to kinetochores during mitosis. *J Cell Biol* **183**, 819-834, doi:10.1083/jcb.200804114 (2008).
217 DeLuca, J. G., Moree, B., Hickey, J. M., Kilmartin, J. V. & Salmon, E. D. hNuf2 inhibition blocks stable kinetochore-microtubule attachment and induces mitotic cell death in HeLa cells. *J Cell Biol* **159**, 549-555 (2002).

218 Maiato, H. *et al.* Human CLASP1 is an outer kinetochore component that regulates spindle microtubule dynamics. *Cell* **113**, 891-904 (2003).
219 Coquelle, F. M. *et al.* LIS1, CLIP-170's key to the dynein/dynactin pathway. *Mol Cell Biol* **22**, 3089-3102 (2002).
220 Dujardin, D. *et al.* Evidence for a role of CLIP-170 in the establishment of metaphase chromosome alignment. *J Cell Biol* **141**, 849-862 (1998).
221 Liang, Y. *et al.* Nudel modulates kinetochore association and function of cytoplasmic dynein in M phase. *Mol Biol Cell* **18**, 2656-2666, doi:10.1091/mbc.E06-04-0345 (2007).
222 Tai, C. Y., Dujardin, D. L., Faulkner, N. E. & Vallee, R. B. Role of dynein, dynactin, and CLIP-170 interactions in LIS1 kinetochore function. *J Cell Biol* **156**, 959-968, doi:10.1083/jcb.200109046 (2002).
223 Varma, D. *et al.* Development and application of in vivo molecular traps reveals that dynein light chain occupancy differentially affects dynein-mediated processes. *Proc Natl Acad Sci U S A* **107**, 3493-3498, doi:10.1073/pnas.0908959107 (2010).
224 Selvaraj, A. & Prywes, R. Expression profiling of serum inducible genes identifies a subset of SRF target genes that are MKL dependent. *BMC Molecular Biology* **5**, 13-13, doi:10.1186/1471-2199-5-13 (2004).
225 Schratt, G. *et al.* Serum response factor is crucial for actin cytoskeletal organization and focal adhesion assembly in embryonic stem cells. *The Journal of Cell Biology* **156**, 737-750, doi:10.1083/jcb.200106008 (2002).
226 Zhang, S. X. *et al.* Identification of Direct Serum-response Factor Gene Targets during Me2SO-induced P19 Cardiac Cell Differentiation. *Journal of Biological Chemistry* **280**, 19115-19126 (2005).
227 Gassmann, R. *et al.* An inverse relationship to germline transcription defines centromeric chromatin in C. elegans. *Nature* **484**, 534-537, doi:http://www.nature.com/nature/journal/v484/n7395/abs/nature10973.html#supplementary-information (2012).
228 Serebryannyy, L. A. *et al.* Persistent nuclear actin filaments inhibit transcription by RNA polymerase II. *Journal of Cell Science* **129**, 3412 (2016).
229 Wong, N. C. *et al.* Permissive Transcriptional Activity at the Centromere through Pockets of DNA Hypomethylation. *PLoS Genetics* **2**, e17, doi:10.1371/journal.pgen.0020017 (2006).
230 doi:10.1371/journal.pbio.1000350.
231 Yasuda, S. *et al.* Cdc42 and mDia3 regulate microtubule attachment to kinetochores. *Nature* **428**, 767-771, doi:http://www.nature.com/nature/journal/v428/n6984/suppinfo/nature02452_S1.html (2004).
232 Marshall, W. F. *et al.* Interphase chromosomes undergo constrained diffusional motion in living cells. *Current Biology* **7**, 930-939, doi:http://dx.doi.org/10.1016/S0960-9822(06)00412-X (1997).
233 Feric, M. & Brangwynne, C. P. A nuclear F-actin scaffold stabilizes ribonucleoprotein droplets against gravity in large cells. *Nat Cell Biol* **15**, 1253-1259, doi:10.1038/ncb2830

http://www.nature.com/ncb/journal/v15/n10/abs/ncb2830.html#supplementary-information (2013).
234 Guse, A., Carroll, C. W., Moree, B., Fuller, C. J. & Straight, A. F. In vitro centromere and kinetochore assembly on defined chromatin templates. *Nature* **477**, 354-358, doi:http://www.nature.com/nature/journal/v477/n7364/abs/nature10379.html#supplementary-information (2011).
235 Brenner, S. & Miller, J. H. *Encyclopedia of Genetics*. (Academic Press, 2001).

236 Cech, J. N. & Peichel, C. L. Centromere inactivation on a neo-Y fusion chromosome in threespine stickleback fish. *Chromosome Research*, 1-14, doi:10.1007/s10577-016-9535-7 (2016).
237 Warburton, P. E. Chromosomal dynamics of human neocentromere formation. *Chromosome Research* **12**, 617-626, doi:10.1023/B:CHRO.0000036585.44138.4b (2004).
238 Van Hooser, A. A. *et al.* Specification of kinetochore-forming chromatin by the histone H3 variant CENP-A. *Journal of Cell Science* **114**, 3529-3542 (2001).
239 Bernad, R. *et al.* Xenopus HJURP and condensin II are required for CENP-A assembly. *The Journal of Cell Biology* **192**, 569-582 (2011).
240 Bodor, D. L., Rodríguez, M. G., Moreno, N. & Jansen, L. E. T. in *Current Protocols in Cell Biology* (John Wiley & Sons, Inc., 2012).
241 Williams, J. C., Xie, H. & Hendrickson, W. A. Crystal Structure of Dynein Light Chain TcTex-1. *Journal of Biological Chemistry* **280**, 21981-21986 (2005).
242 Rapali, P. *et al.* DYNLL/LC8: a light chain subunit of the dynein motor complex and beyond. *FEBS Journal* **278**, 2980-2996, doi:10.1111/j.1742-4658.2011.08254.x (2011).
243 Mok, Y.-K., Lo, K. W. H. & Zhang, M. Structure of Tctex-1 and Its Interaction with Cytoplasmic Dynein Intermediate Chain. *Journal of Biological Chemistry* **276**, 14067-14074 (2001).
244 Chuang, J.-Z. *et al.* The Dynein Light Chain Tctex-1 Has a Dynein-Independent Role in Actin Remodeling during Neurite Outgrowth. *Developmental Cell* **9**, 75-86, doi:10.1016/j.devcel.2005.04.003 (2005).
245 Kasuboski, J. M. *et al.* Zwint-1 is a novel Aurora B substrate required for the assembly of a dynein-binding platform on kinetochores. *Molecular Biology of the Cell* **22**, 3318-3330, doi:10.1091/mbc.E11-03-0213 (2011).
246 Tanenbaum, M. E., Galjart, N., van Vugt, M. A. T. M. & Medema, R. H. CLIP-170 facilitates the formation of kinetochore–microtubule attachments. *The EMBO Journal* **25**, 45-57, doi:10.1038/sj.emboj.7600916 (2006).
247 Maiato, H. *et al.* Human CLASP1 Is an Outer Kinetochore Component that Regulates Spindle Microtubule Dynamics. *Cell* **113**, 891-904, doi:http://dx.doi.org/10.1016/S0092-8674(03)00465-3 (2003).
248 Amaro, A. C. *et al.* Molecular control of kinetochore-microtubule dynamics and chromosome oscillations. *Nat Cell Biol* **12**, 319-329, doi:http://www.nature.com/ncb/journal/v12/n4/suppinfo/ncb2033_S1.html (2010).